ADDIS ABABA INSTITUTE OF TECHNOLOGY

ENERGY CENTER

Design and Simulation of Fluidized Bed Gasifier to Improve the Quality of Synthesis Gas

A Thesis Submitted to the School of Graduate Studies of Addis Ababa Institute of Technology in Partial Fulfillment of the Requirements for the Degree of Master of Science in Energy Technology

By: Abywork Genzeb

Advisor: Dr.-Ing. Abebayehu Assefa

Co-advisor: Sileshi Kore

October, 2011

DESIGN AND SIMULATION OF FLUIDIZED BED GASIFIER TO IMPROVE THE QUALITY OF SYNTHESIS GAS

BY: ABYWORK GENZEB

A THESIS SUBMITTED TO THE SCHOOL OF GRADUATE STUDIES OF ADDIS ABABA INSTITUTE OF TECHNOLOGY IN PARTIAL FULFILLMENT OF THE REQUIREMENTS FOR THE DEGREE OF MASTER OF SCIENCE IN ENERGY TECHNOLOGY

ADDIS ABABA INSTITUTE OF TECHNOLOGY

ENERGY CENTER

ADDIS ABABA, ETHIOPIA

OCTOBER, 2011

ADDIS ABABA INSTITUTE OF TECHNOLOGY

ENERGY CENTER

DESIGN AND SIMULATION OF FLUIDIZED BED GASIFIER TO IMPROVE THE QUALITY OF SYNTHESIS GAS

By: Abywork Genzeb

Approved by Board of Examines:

Dr.-Ing. Abebayehu Assefa	_____	_____
Chairman, Department	*Signature*	*Date*
Graduate Committee		
Dr.-Ing. Abebayehu Assefa	_____	_____
Advisor	*Signature*	*Date*
Sileshi Kore	_____	_____
Co- Advisor	*Signature*	*Date*
Dr.-Ing. Demiss Alemu	_____	_____
Internal Examiner	*Signature*	*Date*
Dr.Tesfaye Dama	_____	_____
External Examiner	*Signature*	*Date*

Abstract

Biomass has emerged as one of the promising candidates for the future, in the renewable energy area. Biomass has been a major source of fuel for human from the existence of mankind. Rapid urbanization and widespread use of fossil fuels in the industrial world has related it to the status of a minor source of energy. The innovation, however, started with increasing concerns over reducing carbon footprints and also due to strong causative connections between non-renewable fossil fuels and "global warming".

Alternative energy production through biomass gasification (a thermo-chemical process of converting biomass into the producer gas or syngas) produces combustible gases, such as carbon monoxide, hydrogen, and methane. These gases can be used for generation of direct heat, electricity, or liquid fuels through the Fischer Tropsch process. However, a major limitation of the overall process is the purity of the generated synthesis gas. The tars and particulates generated in the gasification process constitute a major impediment to the commercial use of this technology because they may condense on valves, fittings, and therefore, hinder the smooth running of an engine. This research was aimed at developing a gas characterization and better understanding of the effect of various parameters on the syngas composition, and the removal of tars and particulates in the synthesis gas generated from a bubbling fluidized bed biomass gasifier. The study is primarily design of the different components of the gasifier and supplemented by the mathematical modeling that explains various steps in terms of existing scientific principles.

The study compares the experimental results sited from different literatures with the equilibrium model results and also identifies the optimum operating parameters and design criteria for better quality syngas production. Using the proposed model, the optimum compositions of carbon monoxide, methane and hydrogen with the respective values of the operating temperature, moisture content and equivalence ratio was obtained.

Acknowledgments

First of all I would like to express my sincere gratitude to Dr.-Ing. Abebayehu Assefa, (Head of Energy Center) and Sileshi Kore; for their reliable and valuable advices, constant support, guidance; and help throughout this thesis work. Discussions with them have formed the basic background for this work. Without their help, much of this thesis would have remained undone and could have never achieved its current form.

Secondly, I am very grateful to the Energy Center and Addis Ababa Institution of Technology for providing fund for this study.

Thirdly, I would like to thank the Mechanical Engineering staff members for their ideal and material support throughout this thesis work.

Finally, I would like to thank my parents for being the source of motivation and support for me throughout my entire academic career. They are always the source of my perseverance, understanding and willingness to accept the challenges I have faced.

Table of Contents

Contents **Pages**

List of Tables

List of Figures

Nomenclatures and Abbreviations

a- g	*Coefficient for Gibbs free energy empirical relation*
A	*Cross-sectional area of the reactor in m^2*
Ash	*Ash*
C, H, O	*Carbon, hydrogen and oxygen fraction in biomass (dry basis*
C, H*, O**	*Carbon, hydrogen and oxygen fraction in biomass (wet basis)*
C_{pX}	*Specific heat capacity of X species (KJ/kmol)*
C_1-C_4	*Coefficient for specific heat capacity*
Char	*Char*
C_d	*Co-efficient of discharge through orifice*
C_p	*Specific heat (related to subscript) (J/kg.K)*
C, H, O	*Carbon, hydrogen, oxygen*
d	*Screw axis diameter in m.*
D	*Screw outer diameter in m.*
d_p	*Mean particle diameter in m.*
D_r	*Internal diameter of the bed*
d_{or}	*Diameter of orifice (m)*
E_a	*Fluidization – gasification air energy in kW*
E_{SD}	*Saw dust energy in kW.*
E_{cw}	*Non- burned carbon energy loss in kW*
E_l	*Energy losses in kW*
E_g	*Produced gas energy in Kw*
E_{wall}	*Wall energy losses in kW*
E_W	*Energy contained in the wastes in kW*
E_s	*Sensible energy in the produced gas in kW*
E_u	*Useful or chemical energy in the produced gas in kW*
E_{ash}	*Loss of energy by sensible heat in the wastes in kW*
g	*Gravitational acceleration in m/s^2.*
ΔG_T	*Gibbs free energy (KJ/kmol))*

$\Delta g_{f,T,i}$	*Change in Gibbs free energy for individual gas with temperature*
h	*Fillet height (m)*
H_{bio}	*Heat of formation of biomass (kJ/kmol)*
h_{cw}	*Carbon enthalpy (to 780 ºC) (kJ/kg)*
HHV	*Higher Heating Value (related to subscript) (MJ/kg)*
H^o_f	*Enthalpy of formation (KJ/kmol)*
h_i	*Enthalpy of each component of the gas produced in kJ/kmol.*
H	*Complete fluidization height or expanded bed height in m.*
H_{mf}	*Minimum fluidization height in m*
H_t	*Overall container height in m*
K_1	*Equilibrium constant for water-gas shift reaction*
K_2	*Equilibrium constant for* $C + 2H_2 \rightarrow CH_4$
LHV_{cw}	*Carbon low heating value in MJ/kg*
LHV_g	*Produced gas low heating value in MJ/Nm^3*
LHV	*Lower Heating Value (related to subscript) (MJ/kg)*
$\dot{m}_a$	*Dry air mass flow in kg/hr*
M_{bio}	*Molecular weight of the biomass*
m	*Moisture content in biomass (% dry basis)*
m_w	*Number of moles of water vapor (dry basis)*
M	*Molar mass (kg/k mol)*
$\dot{m}_{SD}$	*Saw dust mass flow (kg/hr)*
$\dot{m}_W$	*Solid wastes mass flow (kg/hr)*
M_g	*Produced gas mass flow (kg/hr)*
M_{wa}	*Air molecular weight (kg/kmol)*
M_{wi}	*Molecular weights of the component gases of the produced gas in kg/kmol*
N	*Rotating speed of the feeding screws (rpm).*
Re	*Reynolds number.*
$(R_{A/c})_s$	*Air-fuel stoichiometric relation 9Nm^3/kg)*
$(R_{A/C})_r$	*Air-fuel real relation (Nm^3/kg)*

S	*Step screw in m*
T_{ash}	*Ashes temperature exit (Kelvin)*
T	*Temperature in Kelvin*
T^*	*Dimensionless temperature*
T_O	*Reference temperature (273.15 K)*
T_{DH}	*Threshold disengaging height in m*
U_f	*Fluidization velocity during the gasification in m/s*
U_{mf}	*Minimum fluidization velocity in m/s*
U_o	*Minimum fluidization velocity through the orifice (m/s)*
U_{or}	*Velocity of fluid through orifice (m/s)*
Ut	*Terminal particle velocity in m/s*
V_O	*Molar volume at T_O (0.0224 m^3/mol)*
V_m	*Molar volume at T (m^3/mol)*
W	*Stoichiometric coefficients of water vapor*
X, Y	*Normalized coefficient of atomic hydrogen and oxygen for biomass molecule*
x_1-x_5	*Number of moles of H_2, CO, CO_2, H_2O and CH_4 respectively*
X_g	*Number of moles of oxygen for gasification*
X	*Mass fraction of hydrogen on the biomass based on ash-free substance*
X'	*Molar fraction based on ash-free substance*
X_1	*Saw dust reaction coefficient*
Y	*Mass fraction oxygen on the biomass based on dry ash-free wood*
Y_i	*Volumetric fractions of component gases of the gas product*
Z_i	*Gasification air reaction coefficient*
$\%C$	*Carbon in the saw dust*
$\%CO$	*Carbon monoxide volumetric concentration*
$\%CH_4$	*Methane volumetric concentration*
$\%H$	*Hydrogen in the saw dust*
$\%H_2$	*Hydrogen volumetric concentration*
$\%O$	*Oxygen in the saw dust*

%S	*Sulfur in the saw dust*

Greek letters:

ε	*Particle porosity*
Ω	*Mass ratio of two gas species in the volatiles gases*
γ_i	*Mass fraction in the volatile gases*
Φ	*Sphericity or load factor (accordingly)*
μ_a	*Air viscosity to the temperature and pressure operation conditions of the gasifier*
ρ_{SD}	*Saw dust density (kg/m^3)*
ρ_a	*Air density to the temperature and pressure operation conditions of the gasifier*
ρ_g	*Produced gas density under normal conditions of temperature and pressure kg/m^3*
ρ_p	*Particle density in kg/m^3*
ξ	*Equivalence ratio*

CHAPTER 1

INTRODUCTION

1.1 Background

Renewable energy technologies are increasingly applied throughout the world to supply the demand for "clean energy" as the concerns of the impact of non-renewable energy extraction and use on the environment increases. Biomass gasification is an old concept that is starting to gain popularity. The concept has been there for the past eight decades. In Ethiopia the majority of poor people live in rural areas that are located outside the electricity grid or cannot afford presently available energy services. Most of these rural areas are endowed with biomass resources that can be used to supply rural communities with their energy demands.

Electricity generation from woody biomass grew from 59.5 to 79.6 TWh between 1990 and 2001 around the world, yielding a 2.7% average annual growth. As the second largest renewable electricity source after hydropower, solid biomass accounted for 5.6% of renewable electricity generation in 2001 [World Energy Council, 2004]. Biomass comprises unprocessed plant matter, which are wood, twigs, straw, animal dung, vegetable matter and agricultural wastes. Processed biomass includes charcoal, methane, sawdust and alcohol produced from fermentation processes. Biomass fuels can be converted to energy through thermo chemical and biological processes.

Biomass gasification has attracted the highest interest amongst the thermo chemical conversion technologies as it offers higher efficiencies in relation to combustion [Maniatis, 1999 and Costello, 1999]. The conversion efficiency of combustion processes is lowered by the converters from thermal power to electrical power. Biomass gasification also produces far much less greenhouse gases than combustion processes thereby improving the world's carbon footprint.

Biomass gasification is the conversion of wood, charcoal, sawdust and other biomass materials into a gaseous energy carrier known as syngas [Hos and Groeneveld, 1987]. Syngas is the abbreviation for Synthesis gas. This is a gas mixture that comprises of carbon

monoxide, carbon dioxide and hydrogen and is the direct end-product of the process. This is produced due to the gasification of a carbon containing fuel to a gaseous product. Though it can be used as a standalone fuel, the energy density of syngas is only about 50% that of natural gas and is therefore mostly suited for use in producing transportation fuels and other chemical products. As its abbreviated name implies, Synthesis gas is mainly used as an intermediary building block for the final production (synthesis) of various fuels such as synthetic natural gas, methanol and synthetic petroleum fuel (Dimethyl ether – synthesized gasoline and diesel fuel). While generating energy from biomass via gasification or combustion CO_2 is produced. This CO_2 is taken up by plants as a vital constituent for their growth, and thus the CO_2 remains in a closed cycle with net zero CO_2 emissions. Syngas is a mixture of carbon monoxide (approximately 22%), hydrogen (approximately 15%), methane (approximately 3%), carbon dioxide (approximately 7%), nitrogen (approximately 45%) and steam (approximately 6%) [Enger & Smith, 2002 and Li, *et al*, 2004]

Biomass is the only carbon source among all the other renewable energy sources, and as such biomass has a strong potential to be the starting material for liquid fuels and carbon-based chemicals. Gasifier efficiency is an important factor used in determining the technical and economic viability of using a gasifier system. There exist various types of biomass gasifier technologies, each designed for specific fuel types. The efficiency and effectiveness of these gasifiers is dependent on, amongst other things, the gasifier type/design. There are many types of biomass gasifiers such as fixed bed, fluidized bed and entrained flow gasifiers. Among these gasifiers, fluidized bed gasifiers achieve higher efficiencies than other gasifier types. They are not, however, preferred for electricity generation because of their high levels of tar production.

Tar formed in gasification is a mixture of organic components ranging from low molecular weight components like benzene to heavy poly-aromatic hydrocarbons. Tars are equivalent to a major economic penalty in biomass gasification. Tar aerosols and deposits lead to more frequent maintenance and repair of especially gas cleaning equipment and resultantly lower plant capacity factors. This leads to a decrease of revenues or to higher investments. The tar in the gas poses major operational challenges because it clogs in the engine valves resulting in high engine maintenance costs.

Because of the carbon dioxide emitted during conversion of biomass to electricity is matched by that sequestered during biomass growth, life-cycle CO_2 emissions from bioelectricity are very low, with net emissions resulting from use of fossil fuels for cultivation, harvesting, transport and pre-treatment and processing of the biomass fuel. CO_2 emissions from procurement of biomass fuels are also generally lower than from procurement of fossil fuels. Replacement of fossil-fuel-based electricity with bioelectricity therefore results in significant reductions in greenhouse gas emissions. The levels of emissions of other gases and particulates from biomass power plants depend on the fuel, conversion technology, plant operational characteristics and the use of emission reduction measures.

Because of the generally low level of sulphur in biomass, SO_x emissions are usually substantially reduced in bioelectricity production compared with coal or oil-based electricity. With good planning, design and management of the entire bioelectricity production chain, it is usually possible to limit any negative environmental impacts to satisfactory levels.

1.2 Overview of the Gasification Process

Various thermo chemical processes take place in a limited supply (26-33%) of the oxidizer (air or oxygen) in a specially designed reactor commonly referred to as biomass gasifier. In this reactor, the biomass particles undergo drying, pyrolysis, oxidation and char reduction reactions to generate a gaseous mixture of combustibles namely carbon-monoxide, hydrogen and methane, and diluents namely carbon dioxide and nitrogen.

In the drying zone biomass materials are dried at temperature above 100°C, carbonization takes place above the heath/combustion zone at temperature between 600°C-800°C converting biomass materials into charcoal giving off nitrogen, methane and some tar. In the oxidation zone/heath combustion of biomass takes place resulting in carbon dioxide and water vapour. Various high temperature chemical reactions take place in the reduction zone below the oxidation zone; the carbon dioxide from combustion reacts with carbon and is reduced to carbon monoxide.

The water vapour also reacts with carbon and forms carbon monoxide and hydrogen; then the hydrogen reacts with carbon dioxide and form carbon monoxide and water vapour.

The hydrogen also reacts with carbon to form methane. It is in this zone where a large proportion of syngas is formed.

1.3 Problem Statement

Small scale biomass gasification was active in Ethiopia a long time ago. These gasifiers can be traced to farms where they were used mainly for powering engines used for water pumping during the 1950s to 1970s. Currently no large scale biomass projects are taking place in the country. This research sought to revive the use of fluidized bed biomass gasifiers with the intention of employing these technologies to improve the livelihood of rural people.

The currently existing saw mills in Ethiopia operate and generate large volumes of biomass waste most of which are burned as a means for firing purpose. This biomass can be used as fuel for biomass gasifiers and generate low-cost electricity that can be used to support community based business ventures. The major problem with the available biomass gasifier systems is the high production of tar and other particulate matters. This research investigates the strategies that can be employed to bring down the high production of tar, char and other particulate matters by designing a bubbling fluidized bed gasifier with optimum design parameters and through an investigation of the selection of the best operating parameters.

1.4 Research Objectives

1.4.1 General objective

The general objective of the project is to design and simulate fluidized bed gasifier to improve the quality of synthesis gas.

1.4.2 Specific objectives

The specific objectives of the project are:

- Design of reactor subsystem, reaction chamber, air distribution plate, pre-heater bed subsystem, atmospheric emissions control subsystem, feedstock feeding subsystem and other components of the system;
- Develop a mathematical model which predicts syngas composition based on carbon, hydrogen and oxygen contents for the selected feed stock (sawdust) based on its ultimate analysis and moisture content;
- Simulation of the system to investigate the effects of operating parameters (equivalent ratio, temperature, system pressure, moisture content, and other parameters on the performance of the fluidized bed gasifiers;
- Conduct detail study on tar concentration and investigate different techniques to minimize the production of tar during gasification in order to get better quality synthesis gas;

1.5 Thesis Statement

In light of the problem and the objectives stated earlier, the thesis investigates the possibility of using biomass energy in an efficient and effective manner to improve the livelihood of the country. The high cost and high production of tar associated with biomass gasifiers can be avoided through improvement of the design of gasifier systems components and the selection of the operating parameters of the system. The efficiency of a gasifier system is the major determining factor of its cost, so is the efficiency and effectiveness of other downstream components. Therefore this research investigates the efficiency of a bubbling fluidized bed biomass gasifier and that of the cyclone dust collector used in the system. The availability and suitability of biomass feedstock for gasification using bubbling fluidized bed gasifiers will be also investigated.

1.6 Research Methods

A bubbling fluidized bed biomass gasifier consists of the feed stock feeding sub system, gas producing sub system, the purification unit, etc. The purification unit consists of the cyclone, gas scrubber/cooler, particle interference sawdust filters and engine safety filters. A study of the availability, properties and suitability of off-cuts generated by the sawmill operator and the suitability of these off-cuts for gasification using bubbling fluidized bed biomass gasifier will be investigated.

The methods to be employed to achieve the objectives of the research are:

- Literature review;
- Collection of both simulation and design datas for the analysis;
- Simulation of a bubbling fluidized bed biomass gasifier using Mat Lab or any other software that are suitable for simulation of the system;
- Design of the gasifier systems by considering all the necessary conditions;
- Investigation of different techniques to minimize the production of tar during gasification in order to get better quality synthesis gas; and
- Analysis and interpretation of the results.

1.7 Rationale of the Study

The majority of people in under-developed and developing countries such as Ethiopia live in rural areas that are located outside the national electricity grid. In some cases, they have access to electricity and other energy services. Most of these people are ranked amongst the poor with a very low level of literacy and skills that could assist them in securing employment elsewhere. In the case of such communities in Ethiopia, there are saw mills that operate and generate large volumes of biomass waste. So, it is necessary to use those waste materials for biomass gasification instead of using them for firing purpose only. The main aim of this project is to produce a tar free synthesis gas that could be used for community economic empowerment, and to establish the technical viability of biomass gasification using the fluidized bed biomass gasifier.

1.8 Chapters Overview

Chapter 2 provides basic literature review on the gasification process, various types of gasifiers and elaborated discussion about the effect of various parameters on syngas composition for different types of gasifiers. The effect are primarily discussed for updraft, downdraft and fluidized bed gasifiers which currently cover amore than 98% of the total biomass gasification market and mainly deals with fluidized bed biomass gasifiers and their system of operation.

Chapter 3 presents a thermodynamic model of the process inside the gasifier. Syngas composition is predicted assuming thermodynamic equilibrium conditions inside the gasifier. The effect of moisture content as well as temperature is determined. Based upon the results of the simulations, equations are derived to predict the syngas composition of the biomass based on their elemental composition and moisture content.

Chapter 4 deals with the optimum design of a bubbling fluidized bed biomass gasifier and it presents the effect of selected process parameters such as equivalent ratio and moisture content on syngas composition in the fluidized bed gasifier. Parts that are designed include the reactor, the air distributor plate, the plenum, the fuel feeding subsystem, the cyclone and other components. A mass and energy analysis is also done to collaborate the model results as well as to visualize the heat, and mass transfer inside the gasifier.

Conclusion and recommendations are presented in Chapter 6. The chapter covers summary of major findings of the research work. A summary of the research contributions and recommendations for further research are also presented in this chapter.

CHAPTER 2

LITERATURE REVIEW

In this chapter, various aspects of biomass gasification were reviewed. The most widely used configurations of biomass gasifiers and the effect of various operating parameters on the quality of syngas are discussed in detail.

2.1 Introduction

Biomass has evolved as one of the most promising sources of fuel for the future. This has spurred the growth of research and development efforts in both federal and private sectors throughout the world. This impetus is motivated by several factors; dwindling fossil fuels and thus an increase need of energy security, environmental concerns and promotion of socioeconomic benefits to rural areas.

Another important fact is somewhat uniformly distributed nature of biomass worldwide which means it is available locally and is helpful in reducing the dependence upon the fossil fuel [1].

The energy derived from biomass is significant and accounts for more than half of all the renewable energy generation worldwide among which, two-thirds is used for heat, power or combined heat and power (CHP).

The end-use of products from biomass conversion can be mainly in any one of heat and power applications, transportation fuels (biodiesel, bioethanol) and chemicals for subsequent process in. Up to present, the only long-term solution for the carbon based fuels and chemical is biomass and can be effectively converted into solid, liquid and gas [1]. Huber et al. [2] opine that among all the renewable energy sources, biomass is the most optimal long-term fuel for transportation. Biomass can be converted into biofuels using either thermal or chemical processes. Among thermal conversion processes, gasification has received the most attention. This is due to the higher efficiency compared to processes such as direct combustion, pyrolysis and liquefaction [1]. This industrial rate of power generation using gasification process can be expected to rise with advances in clean coal technologies and more economically feasible techniques for biomass gasification.

Different forms of thermal treatment of biomass are distinguished from each other by the amount of air supplied, residence time, temperature, and consequently the heat transfer rate in the process. Supplying excess air results in combustion while treatment without air/oxygen results in pyrolysis products [1].

Gasification is the conversion of biomass into the mixture of combustible and non-combustible gases (referred as syngas hereafter) by partial oxidation at high temperature around 800-900˚C in the presence of a gasifying medium such as air, oxygen or steam. Syngas from biomass is a mixture of carbon monoxide (CO), carbon dioxide (CO_2), hydrogen (H_2), water (H_2O) and a small amount of methane (CH_4). The use of syngas for power generation is widely accepted and considered mature technology [1].

The main steps of the gasification process can be schematically described by the figure shown below.

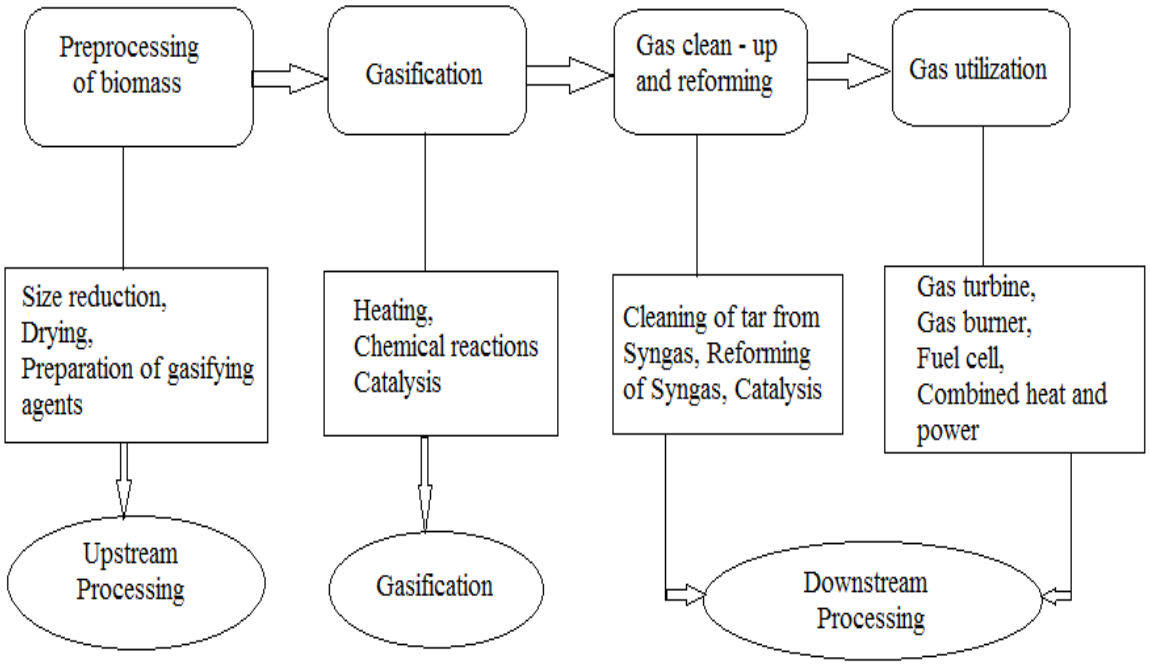

Figure 2.1 Block diagram of the gasification process

2.2 Gasifier Types and Processes

Gasification is a form of incomplete combustion; heat from the burning solid fuel creates gases which are unable to burn completely, due to insufficient amounts of oxygen from the available supply of air. By weight, syngas from gasification of wood contains approximately 15-21% hydrogen (H_2), 10-20% carbon monoxide (CO), 11-13% carbon dioxide (CO_2), and 1-5% of methane (CH_4), all of which are combustible plus nitrogen (N_2) (Heesch *et al*., 1999).
The nitrogen is not combustible; however, it does occupy volume and dilutes the syngas as it enters and burns in an engine. A generalized reaction describing biomass gasification is as follows (Dayton, 2002):

$$Biomass + \ air\ (or\ H_2O) \rightarrow \ CO, CO_2, H_2O, H_2, CH_4, and\ N_2 + \ tars \ + \ particulates$$

The actual biomass syngas composition depends on the gasification process, the gasifying agent, and the feedstock composition [Beenackers and van Swaaij, (1984); Hos and Groeneveld, (1987)]. Various gasification technologies have been under investigation for converting biomass into a gaseous fuel. A characteristic of the various gasifiers is the way in which the fuel is brought into contact at the gasification stage.

Warnecke [3] has classified the gasifiers in four categories which are based on the fluid and/or solid movement inside the reactor.

i. Quasi non-moving or self-moving feedstock
ii. Mechanically-moved feedstock such as downdraft, updraft and cross-draft gasifiers
iii. Fluidically-moved feedstock like bubbling fluidized bed (BFB), circulating fluidized bed (CFB) gasifier and entrained bed gasifier
iv. Special reactors including spouted bed gasifier and cyclone gasifier

Among those listed above, downdraft, updraft, and BFB and CFB gasifiers are the most common as shown by studies. Figures 2.2-2.5 show schematics of various gasifiers that are widely used in the commercial market. Commercially, about 75% of the gasifiers sold are downdraft gasifiers, 20% fluidized bed, 2.5% updraft, and 2.5% of the other types [1].

The updraft gasifier is popular for application choice when the primary purpose of gasification is heating only (below 10 MW) due to its high thermal efficiency and ability to handle feedstock with wide variation in size and moisture content as high as 50% [1].

Downdraft gasifiers are preferred for small scale power generation due to low amount of tar content in the syngas. The problem with fixed-bed gasifiers is their inability to maintain uniform radial temperature which results in local slag, bridging and clinkering problems. Lack of uniform radial temperature is one of the reasons why this kind of gasifier cannot be scaled up rendering them inflexible and of limited use [1].

Fluidized bed gasifier provides higher throughput than those with a fixed bed. Fluidization enhances mass and heat transfer from the fuel thereby increasing heating value of the output and higher efficiency rendering it excellent for low-rank coal and biomass gasification. Entrained bed gasification is similar to fluidized bed gasification except for the operation temperature range which is usually higher than 1900^{o}C. This type can have even higher throughput capacity but is limited to coal use only due to the particle size constraint on the feedstock (less than 0.15 mm).

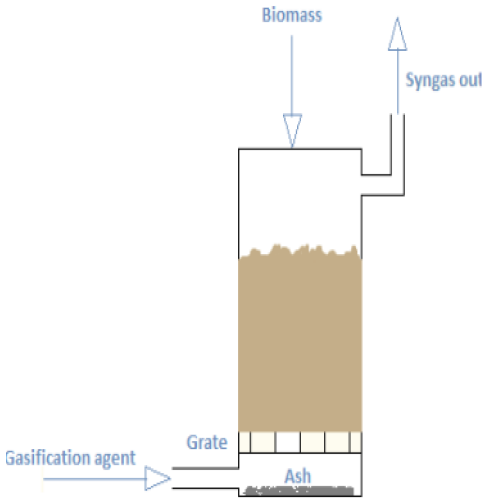

Figure 2.2 Up-draft gasifier

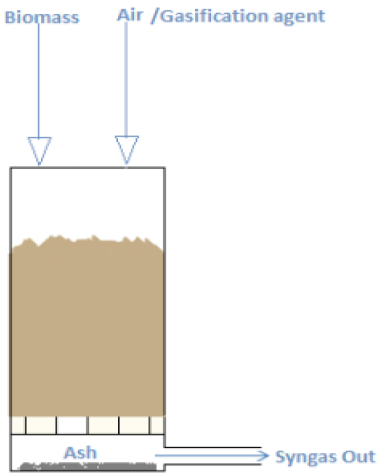

Figure 2.3 Downdraft gasifier

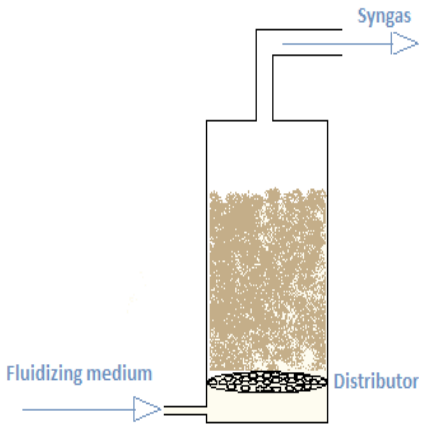

Figure 2.4 Bubbling bed fluidized gasifier

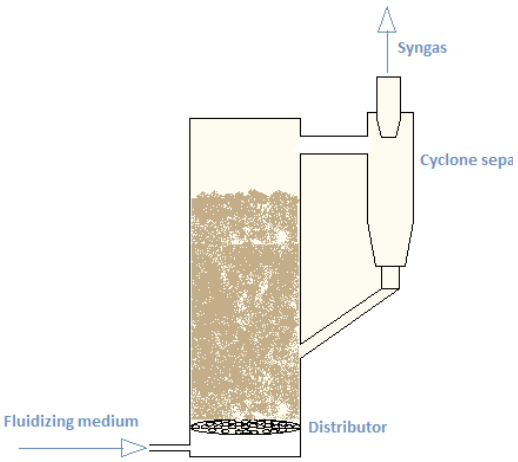

Figure 2.5 Circulating fluidized bed gasifier

The various types of gasifiers shown in figure 2.2 - 2.5 are discussed in the sections below. BFB and CFB gasifiers are discussed in a single section as fluidized gasifier due to minor differences between them.

2.2.1 Updraft Gasifier

The movement of the feedstock and the gasifying agent are in opposite directions in this kind of gasifier (also called a counter-current gasifier). Since the syngas formed is not forced to pass through the hot high temperature zone, the tar content is high in the syngas from this gasifier. On the other hand, the temperature of syngas exiting from this gasifier is lower around (200-300 ^{o}C) and hence the thermal efficiency of this kind of gasifier is high. Due to high tar content in the syngas, a subsequent tar cleaning system is needed, which can become a major investment if the end-process requires tar-free syngas.

2.2.2 Downdraft Gasifier

In a downdraft gasifier, the feedstock and gasifying agent both move in the same direction. The gases have to pass through the high-temperature. So, the amount of tar here is significantly lower than that in an updraft gasifier. The particulate content is however higher for downdraft gasifier

and the thermal efficiency are lower since syngas draws an appreciable amount of energy while passing through the high-temperature zone inside the gasifier.

2.2.3 Fluidized Gasifiers

Most biomass gasifiers under development employ one of two types of fluidized bed configurations: bubbling fluidized bed and circulating fluidized bed.

2.2.3.1 Bubbling Fluidized Bed

A bubbling fluidized bed consists of fine, inert particles of sand or alumina, which have been selected for size, density, and thermal characteristics. As gas (oxygen, air or steam) is forced through the inert particles, a point is reached when the frictional force between the particles and the gas counterbalances the weight of the solids. At this gas velocity (minimum fluidization), bubbling and channeling of gas through the media occur, such that the particles remain in the reactor and appear to be in a “boiling state”. The fluidized particles tend to break up the biomass fed to the bed and ensure good heat transfer throughout the reactor.

The advantages of bubbling fluidized-bed gasification are [2]:

- Yields a uniform product gas
- Exhibits a nearly uniform temperature distribution throughout the reactor
- Able to accept a wide range of fuel particle sizes, including fines
- Provides high rates of heat transfer between inert material, fuel and gas
- High conversion possible with low tar and unconverted carbon

2.2.3.2 Circulating Fluidized Bed

Circulating fluidized bed gasifiers operate at gas velocities higher than the minimum fluidization point, resulting in entrainment of the particles in the gas stream. The entrained particles in the gas exit the top of the reactor, are separated in a cyclone and returned to the reactor.

The advantages of circulating fluidized-bed gasification are [2]:

- Suitable for rapid reactions
- High heat transport rates possible due to high heat capacity of bed material

- High conversion rates possible with low tar and unconverted carbon

The disadvantages of circulating fluidized-bed gasification are [2]:

- Temperature gradients occur in direction of solid flow
- Size of fuel particles determine minimum transport velocity; high velocities may result in equipment erosion
- The heat exchange capacity is less efficient than bubbling fluidized-bed

2.3 Chemical Reactions in Biomass Gasification Process

Gasification is a highly complex chemical process. Bridgewater described the gasification sequence as drying and evaporating processes of biomass followed by pyrolysis, and finally oxidation and reduction. However, the overall process can be reasonably described by the reactions described below [4].

$$Biomass \rightarrow gases\,(CO, CO_2, H_2, light\ HC's) + pyrolyzed\ vapors + char \quad (2.1)$$

$$Pyrolyzed\ vapor \rightarrow gases\,(CO, CO_2, H_2, light\ HC's) \quad (2.2)$$

$$C + O_2 \rightarrow CO_2\ , \Delta H = -393.5\ \frac{kJ}{mol} \quad (2.3)$$

$$C + \left(\frac{1}{2}\right) O_2 \rightarrow CO, \Delta H = -110.5 \frac{kJ}{mol} \quad (2.4)$$

$$C + CO_2 \rightarrow 2CO, \Delta H = 172.4 \frac{kJ}{mol} \quad (2.5)$$

$$C + H_2O \rightarrow H_2 + CO, \Delta H = 131.3 \frac{kJ}{mol} \quad (2.6)$$

$$C + 2H_2 \rightarrow CH_4, \Delta H = -74.8 \frac{kJ}{mol} \quad (2.7)$$

$$CO + H_2O \rightarrow H_2 + CO_2, \Delta H = -41.1 \frac{kJ}{mol} \quad (2.8)$$

$$CO + 2H_2 \rightarrow CH_4 + H_2O, \Delta H = 206.1 \frac{kJ}{mol} \quad (2.9)$$

Among the reactions described above, the char-oxidation (eqn. 2.3) and partial-oxidation (eqn. 2.4) reactions are slowest, and consequently the rate controlling factor in the overall gasification process. Pyrolysis also results in liquid which is resistant to the cracking due to temperature increase though most of the pyrolyzed liquid does so at higher temperature. This requires subsequent cleaning set-up for the tar, which can be a substantial investment in many cases [4].

2.4 Effect of Various Parameters in the Gasification Process

Syngas composition varies widely and mostly depends upon the gasifier type, feedstock, feedstock pre-treatment, gasifying medium and operating parameters like temperature, pressure, and nature of interaction between reactants in the gasification process [1]. The effects of major parameters affecting the quality of syngas are discussed in the sections below.

2.4.1 Moisture Content

Biomass contains moisture in both ways: intrinsically by its nature, and extrinsically wherein moisture is absorbed from the surrounding atmosphere. Moisture content in the biomass, during gasification, increases CO_2 concentration by the water-shift reaction which consumes CO and liberates H_2 [1]. While the equilibrium constant for water-shift reaction varies little over a wide range of temperatures, the direction tends to reverse at higher temperature. Since more heat is required for moisture evaporation than the small amount of heat gained due to the exothermic behavior of the water-shift reaction, thermal energy inside the gasifier reduces when gasifying biomass with higher moisture content [4]. Thus, the decrease in temperature further exacerbates the scenario and forms more CO_2 since the water-shift reaction is improved at lower temperature. The overall effect is the reduction in calorific value of syngas because, the small increase in H_2 is not sufficient to compensate the loss of significant amount of CO with increase in moisture content [5]. However, the negative effect of moisture content on the calorific value of syngas is lower at lower equivalence ratio (ER). Roy et al. [5] have observed that, in a downdraft gasifier, when the moisture content is increased from 0 to 40%, heating value of syngas decreases by 8.72% at ER of 0.45 while the decrease was of 4.7% when the ER used was 0.29. This result was reported from their equilibrium model and thus is applicable to any gasification process.

Table 2.1 Summary of the effect of moisture content in three common gasifier types

Parameter	***Gasifier type***	***CO***	***H_2***	***CH_4***	***Maximum limit (% w.b)***
Moisture content [MC]	*Updraft*	*Decrease with [MC]*	*Increase in some extent*	*Has no effect*	< 50 [1]
	Downdraft	*Decrease with [MC]*	*Increase in some extent*	*Has no effect*	< 40 [6]
	Fluidized	*Decrease with [MC]*	*Increase in some extent*	*Has no effect*	< 10 [1]

A limiting condition called auto-thermal limit is reported as 65% moisture content in literature beyond which self-sustaining gasification is not possible due to an enthalpy deficiency for vaporization. In fact, supplemental fuel is required for most of the combustor when the moisture content is greater than 50% on a wet basis [6]. Moisture content up to 30% (wet basis) can be used for downdraft gasifier. When air is used as the gasification agent, the amount of methane produced is small and stays almost constant with change in moisture content. Thus the temperature decrease inside the gasifier due to moisture also results lower mass conversion efficiency and increases tar content. Sheth et al. [7] report the decrease in biomass consumption rate with increase in moisture content which is due to the higher amount of heat necessary for drying those wood chips inside the reactor before they can be pyrolysis. However, some moisture content is always desirable since it enhances steam reforming and helps to crack tar, and at higher temperature, also enhances other reactions such as char gasification. Steam injection is widely used in industrial applications to adjust syngas composition in the gasification process but often, in the presence of higher temperature provided by some external source [1].

2.4.2 Equivalence Ratio

Equivalence ratio (ER) is the most influential parameter in any gasification process and often has significant impact on syngas composition. Increase in ER increases the temperature inside the gasifier while increase in ER decreases char formation inside the gasifier. As can be seen from

figure 2.6, all combustible products reduce with an increase in ER with the formation of higher amount of CO_2 as well as total gas yield greatly diminishing the heating value of the final syngas.

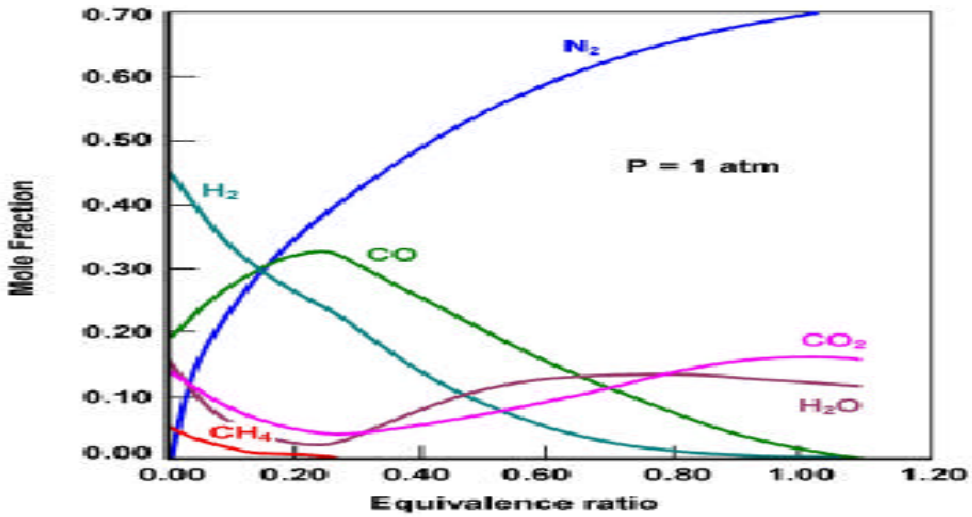

Figure 2.6 Effect of ER upon syngas composition

The optimum equivalence ratio is necessary for accelerating gasification and drying rate due to conduction and convection process which also increases the biomass consumption rate [7].

Both Skoulou et al. [8] and Sheth et al. [7] report an optimal equivalence ratio of 0.2 for downdraft gasification of olive kernels and olive tree cutting and furniture wood. The optimum equivalence ratio varies for different biomass due to the amount of oxygen elementally present in the biomass as well as the ash content. The existing literature shows that equivalence ratio should be around 0.2-0.4 for the successful gasification. Table 2.2 shows the optimal equivalence ratio for selected feed stocks. Optimal equivalence ratio for an updraft gasifier is not shown in the table due to the limitations of available literature for updraft configuration.

Table 2.2 Optimal ER for some feed stocks in downdraft and fluidized bed gasifiers

Gasifier type	***Feedstock***	***Optimal ER***
Downdraft	Furniture wood + charcoal	0.38
	Furniture waste	0.2
Fluidized bed	Rice husk	0.2-0.55
	Saw dust	0.2-0.45

In this research, determination of the best optimal value of the ER for the fluidized bed gasifier by using saw dust as feedstock will take place. The effect of equivalence ratio for each syngas composition will also be analyzed with an expected optimal equivalence ratio of between 0.2 and 0.35 which is the maximum range for the successful gasification of biomass.

2.4.3 Temperature

Increase in temperature reduces the tar content as well as decreases char inside the gasifier [8]. Gas yield increases due to higher tar cracking. One of the means of increasing temperature is by internal recirculation of syngas. Tar cracking temperatures are often reported to be around 1000-1100^{o}C with some dependency on gasifier design [9]. Other methods of tar cracking are also employed such as multi-stage gasifiers [1]. Multi-stage gasifiers have separated pyrolysis and gasification zones and make use of partial oxidation of pyrolysis gas obtained in the pyrolysis zone for tar cracking and thus, tar content can be reduced as low as 15mg/Nm^3 (Nm^3 –volume at STP) [1]. CO content increases with increase in temperature because endothermic reactions are more favored at higher temperature. Mass conversion efficiency decreases with decrease in temperature. An oxidation zone below a temperature of 725^{o}C gives significantly lower mass conversion efficiency.

Uniformity of temperature in a radial as well as in axial direction inside the reactor is very important for efficient mixing in a fluidized bed. Generally, less than 100^{o}C difference in total riser height is acceptable. Heating value as well as syngas yield is found to increase due to increase in combustibles, particularly at temperatures above 800^{o}C with an increase in operating temperature driven by an external supply of heat in the gasifier for constant ER [1]. However, this is different when the temperature is increased due to increase in ER inside the reactor which actually reduces the combustibles [1]. Temperature control cannot be independent in any gasification process with the exception of small lab-scale or pilot plants which can be heated with external heat. The temperature of the reactor is dependent on various factors such as moisture content of the fuel, ER, heat losses from the system, and amount of steam added [1]. Thus, the temperature inside the gasifier should represent an optimal compromise with ER.

The best approach is the proper insulation of the reactor and using waste heat. Higher temperature also reduces tar content significantly due to thermal cracking. In addition, Riley et al. [11] report higher reduction in tar with same increase in top part of reactor than in bottom section. However, Drift et al. [10] suggest that the tar that is cracked due to temperature is mostly the heavy tar while light tar is not decomposed. Heavy tars are the product of pyrolysis process which has not gone through cracking while light tars are the cracking products of heavy tar. In certain cases, light tar seems to increase due to the subsequent breakdown of heavy tar into light tar and other compounds.

Typical temperatures suggested for biomass gasification in a fluidized bed are around 650-950^{o}C by various studies [1]. Although, high temperature increases carbon conversion efficiency of the overall gasification system, consideration should be given to prevent the formation of ash-melt, made not to form ash-melting, especially when used to gasify biomass material with high ash content like rice husk [9].

2.4.4 Biomass Type

Biomass elemental composition has a significant effect on syngas composition. The release of pyrolysis gas is highly dependent on hydrogen/carbon ratio as well as oxygen/carbon ratio and increases when these ratios increase, especially with an increase in Hydrogen/Carbon ratio [6]. A higher oxygen concentration in biomass needs lower ER for gasification because of its inherent oxygen that will also be available for gasification [1].

Another important factor is the ash content of the feedstock. Although formation of clinkers can cause problems for the gasifier operation with biomass having ash-content above 5%, successful gasification with ash-content up to 25% is reported. Higher ash content causes slugging, and consequently ash agglomeration due to fusion, the rate of which is dependent upon the ash content in biomass and ash composition [6].

In this research, the effect of ash content on the syngas composition and on the performance of the gasifier is ignored because the ash content in the saw dust is small and the presence of ash in biomass can be controlled by controlling the operating temperature of the system.

Thus, the operating temperature should be neither high enough to fuse minerals as the ash forming a barrier to further gasification by formation of clinkers, nor too low leading to unburnt carbon resulting in lower carbon conversion efficiency.

2.4.5 Particle Size

Fixed bed gasifiers have lower biomass feedstock size restrictions compared to fluidized bed gasifiers. Usually, feed size less than 51 mm and 6 mm is recommended for fixed bed and fluidized bed, respectively. Use of larger size feedstock has been tried and reported by several authors. Saravanakumar et al. [12] have successfully gasified long sticks with length of 68 cm and diameter of 6 cm successfully in a top-lit updraft gasifier. Bridgewater et al [4] reported that the maximum particle size suggested for a conventional downdraft gasifier with throated design is one-eighth of the reactor throat diameter. The larger particles form bridges preventing the efficient flow of biomass inside a gasifier while smaller particles interferes with the air/gasifying agent passage creating high pressure drop and consequently can result in gasifier shut-down [4].

Enden [13] reports increase in the temperature of oxidation and reduction zone with decrease in particle size of the biomass feedstock in a downdraft gasifier. Decrease in particle size reduces the heat loss due to radiation and enhances the thermal conductivity in the oxidation and reduction zones. On the other hand, decrease in particle size increases pressure drop inside the gasifier. Burning rate and thus the char oxidation period of fuel particles decrease with increase in bulk density and particle size [4]. Biomass consumption rate is inversely related to particle size. In other words, higher residence time is recommended for larger biomass particle size. Decrease in CO with increase in CO_2 concentration is observed. Bridgewater et al. [4] reported that the composition of CO decrease from 18% to 13.5% when the size of wood cubes used in the experiments were increased from 10 mm to 35 mm. Their model predicts a decrease in CH_4 and an increase in H_2 with increase in size of biomass particles. Also, the temperature gradient decreases thus increasing time taken for diffusion of heat. This will result in poor temperature distribution which is also one of the reasons for the increase in CO_2 concentration with increase in particle size.

Carbon conversion efficiency is not strongly affected by particle size except the lower biomass size increases tar concentration because of high entrainment susceptibility during fluidization. This is because particles can be easily transported to the upper part of the reactor, leaving little time for tar cracking. Multi-staging can prevent this as demonstrated the novel concept developed by Kersten et.al [16] using a gasifier design consisting of several cone shaped structures welded together with the base of each connected to the next tubes of equal diameters. On the other hand, the axial temperature drop increases significantly with decrease in size. This is due to the easy passage of feed particles from the feed point and thus little or no reaction taking place below the feed point. Thus, the homogeneity of the bed material cannot be maintained throughout the reactor. Wiman and Almstedt [17] report increase in gas-particle interactions with decrease in particle size in a fluidized bed reactor.

2.4.6 Pressure

High-pressure gasification reduces the size of the reactor for the same amount of feedstock and can act to reduce the need for further compression when the gasification products are intended for subsequent use in Fischer-Tropsch process or other chemical synthesis which requires high pressure. Pressure drop across the gasifier increases with smaller particle size due to increased porosity. Increase in pressure in a fluidized bed increases turbulence and thus increase in gas particle interaction. Increase in pressure also results in bubble instability and bubble splitting in fluidized bed [1].

Valin et al. [16] have studied the effect of pressure upon syngas composition with pressure from 2 to 10 bars in fluidized bed with wood sawdust as a feedstock. With increase in pressure, an increase in CO_2, CH_4 and H_2 were observed, while CO decreased. By using steam and N_2 as the gasification medium, with increase in pressure from 2 to 10 bars, an increase of 16%, 53% and 38% of H_2, CO_2 and CH_4, respectively and decrease of CO by 33% was also reported by Valin. Overall, increase in dry gas yield increase is reported to be 20% with increase in pressure from 2 to 7 bars after which the gas yield remains constant. The increase in various gases and total gas yield is due to the increase in char hold-up rate which increases catalytic activity of char as well as improved reaction kinetics due to high pressure.

Altafini *et al* [2003] carried out simulations to establish the impact of pressure on gas compositions through the equilibrium model. He reported that the increase in pressure results in reduced hydrogen and carbon monoxide volumes. They also established that very low pressures (10.13kPa) results in an increase in the yield of H_2, however the increase was found to be negligible (less than 0.2%). Low pressure does not provide substantial improvements and high pressure reduces H_2 yield. They also conclude that atmospheric pressure is the best condition for fluidized bed gasifiers. By comparing the above negative and positive effects of the pressure content and from the conclusion of Altafini, for this research atmospheric pressure is used as a gasifying pressure. Table 2.3 shows the simulation results obtained by Altafini *et al* [2003].

Table 2.3 Equilibrium gas moles at various gasification pressures [Altafini *et al*, 2003]

P (KPa)	***CO***	***CO_2***	***H_2***	***CH_4***	***Remark***
10.13	0.746	0.253	1.303	$1.61* 10^{-5}$	Low pressure system
50.66	0.745	0.253	1.302	$4.0* 10^{-4}$	
101.3	0.744	0.254	1.301	$1.6* 10^{-3}$	High pressure system
1013.25	0.633	0.286	1.09	$8.* 10^{-2}$	
2533.125	0.491	0.326	0.897	$1.8* 10^{-1}$	

2.4.7 Gasification Medium and Secondary Air

Biomass gasification can be done with any of the following medium: Air, Oxygen or Steam. Gasification with air results in syngas with low higher heating value (HHV) due to inherent dilution with N_2 present in the air. Conversely, gasification with oxygen yields syngas with a heating value of 10-12 MJ/Nm^3 and steam gasification results in syngas with heating value even higher, 15-20 MJ/Nm^3 [4].

Secondary air reduces the tar content in the syngas due to partial combustion of syngas. This in turn establishes local high temperature zone due to exothermic reactions. Thermal cracking of tar is thus due to these high temperature zones in the periphery of the secondary air.

2.4.8 Tar

Any compound with molecular weight greater than that of benzene is called tar [9]. The reduction of tar in biomass gasification has been the subject of a great number of studies [1, 2]. Tar elimination approaches can be classified into two categories: primary measures and secondary treatments.

Primary removal techniques refer to techniques that reduce the tar content in the syngas and are employed inside the gasifier without the need of a secondary reactor. Primary measures for tar control can be achieved by the control of operating parameters and novel design of gasifiers, and more effectively by the addition of catalysts in the gasifier [32]. The in-bed catalysts could play important roles not only in increasing the gasification reaction rate at a lower gasifier temperature, but also facilitating conversion of tar into valuable combustible gases [32].
Numerous studies have shown that the gasification operating parameters, primarily gasification temperature, ER, type of gasifying agent, total gasifying agent to biomass ratio, and feed rate are effective in reducing the amount of tar in the syngas. Tar concentration decreases with increase in ER. Thus, at some point between the applicable ranges (0.15 - 0.4), a shift between types of tar is also reported. Light tar increases while heavy tar decreases. Corella et al. [9] suggests an equivalence ratio above 0.36 for pine saw dust in a fluidized bed to reduce the tar content below 2 g/m^3. In an air-blown fluidized bed gasifier, typical tar contents in the producer gas have been reported as between 0.5 to 100 g/m^3. Formation of tar not only results in a lower heating value of the fuel gas produced, but also causes some operating issues such as downstream fouling due to condensation of the tars at temperatures below 350^oC. For many applications, with the exception of direct and immediate syngas combustion for heat or electricity production, these tar levels must be reduced, often to below 50 g/m^3 [2].

Secondary tar removal techniques use a separate reactor to destruct and reform the tar content below acceptable level in the product gas. Secondary treatments include cold-gas mechanical methods to remove tar from the cooled producer gas (using filter, scrubbers, etc.) and hot-gas catalytic processes to crack tar into gaseous products at a high temperature in a down-stream

reactor [2]. Although secondary treatments proved to be effective for removing tar from biomass gasification, primary measures (i.e., treatments inside the gasifier) were found to be more economically viable in terms of capital/operating costs [2].

2.4.9 Bed Material

Proper consideration of bed material in a fluidized bed is important for achieving proper homogenization of feed particles and efficient heat transfer so that minimum temperature gradient is realized within the riser. In many cases, bed material can itself act as a catalyst facilitating efficient tar cracking [8]. Skoulou et al. [8] compared the effect of olivine over silica sand, latter of which is reported to have adverse effect upon effective fluidization due to agglomeration and tar formation when operating at the temperature below 800^{o}C. He was also studied in-bed catalysts in a dual bed fluidized bed reactor with Ni/olivine as the catalyst and observed significant tar reduction. And he reported that use of catalyst for tar cracking is itself a vast subject.

CHAPTER 3

ESTIMATION OF SYNGAS COMPOSITION USING EQUILIBRIUM MODELING

3.1 Introduction

Among various biomass conversion technologies within thermo-chemical and biochemical platforms, this study is focused on a biomass gasification process for syngas production. Biomass gasification has received the highest interest among various biomass conversion technologies because it is almost feedstock-agnostic and can be used to produce electricity and liquid fuels such as "green" gasoline and diesel using the Fisher- Tropsch process.

The product gas (synthesis gas or syngas) from the biomass gasification is a mixture of carbon dioxide (CO_2), carbon monoxide (CO), hydrogen (H_2), methane (CH_4), water (H_2O) and nitrogen (N_2) if air is used as a gasifying agent. Syngas has been mostly accepted for power generation and is considered to be more mature technology compared to other biomass conversion processes.

Most of the time, syngas composition is unknown until the gasification work is conducted. Experimental work is often resource-intensive (time and money) and a mathematical model predicting syngas composition (concentration of H_2, CO, CH_4 and CO_2) using elemental analysis of biomass would be helpful.

There are several models such as thermodynamic equilibrium, kinetics-free, steady-state, semi-transient and transient that can be used to determine the syngas composition [17]. Among these techniques, the thermodynamic equilibrium model is the simplest of all type and gives syngas composition for various biomass types at selected gasification temperatures with reasonable accuracy. A system is said to be in thermodynamic equilibrium when it is in thermal, mechanical and chemical equilibrium. Chemical equilibrium is the state of minimum Gibbs free energy and maximum system entropy. Mechanical equilibrium occurs when the system is not performing or

receiving any work. Thermodynamic equilibrium modeling provides a closer prediction when the reaction temperature is sufficiently higher [1]. Equilibrium conditions are difficult to achieve in practical operating conditions and results obtained from thermodynamic equilibrium modeling can serve as the maximum limit on syngas composition. A few studies have been conducted to determine syngas composition and heating value of syngas using thermodynamic equilibrium modeling on limited biomass types [1]. The study found the best prediction for entrained bed gasifier with a lower degree of accuracy in predicting syngas composition from fluidized bed and moving bed gasifiers. Jarungthammachote and Dutta [19] and Melger et al. [20] have predicted syngas composition from various biomass types using thermodynamic equilibrium modeling at a fixed equivalence ratio. The present study predicts gasification temperature through an iterative process and the syngas composition at various equivalence ratios and moisture contents.

3.2 Methodology

3.2.1 Model Formulation

Although there are several factors affecting syngas composition from biomass, it mainly depends on the gasifier type, feedstock and feedstock pre-treatment, gasifying medium and operating parameters such as temperature, moisture content and equivalence ratio.

In this study, the main features and assumptions of the thermodynamic model can be summarized as follows:

1) All carbon content in biomass is converted into gaseous form and the residence time is high enough to achieve thermodynamic equilibrium. This might not be true in an actual gasification process; however the degree of error introduced by this assumption is acceptable and the applicability of this assumption is confirmed in literature [1, 20]. The products taken into account are CO, CO_2, H_2, CH_4, N_2 and water. These are the major gaseous compounds formed during the gasification process. Hydrocarbons other than CH_4 were assumed negligible in syngas and were not taken into account.

2) Ash in the feedstock was assumed inert in all gasification reactions although it holds true typically only for reaction temperatures less than 700^{o}C. Herbaceous biofuels contain

silicon and potassium as the major mineral content which lowers ash fusion temperature below 700^{o}C whereas gasification generally occurs at temperatures higher than 700^{o}C. Therefore, the relations derived in this study cannot be used effectively for biomass with high mineral content.

3) All the gaseous products are assumed to behave as ideal gases. This will lead to insignificant errors because the gasification in fluidized bed gasifiers is conducted at high temperature.

4) The process is completely adiabatic so that no heat losses occur from the gasifier. The amount of air is varied to achieve the desired reaction temperature in the gasifier.

5) Output from the gasification is assumed only to be permanent gases free of oxygen which is true because the oxygen supplied is far less than that needed for combustion in a gasification process. Sulfur and chlorine content in biomass were also neglected since they are less than 0.6% in most biomass feed stocks.

The chemical composition of biomass is taken to be in the form CH_XO_Y and the global reaction can be written as follows:

$$CH_XO_Y + a(O_2 + 3.76N_2) \rightarrow CO_2 + H_2O + 3.76 * a * N_2 \qquad (3.1.a)$$

Where: a is the stoichiometric value of air required for gasification

$$CH_XO_Y + m_wH_2O + X_g\,(O_2 + 3.76N_2) \rightarrow X_1H_2 + X_2CO + X_3CO_2 + X_4H_2O + X_5CH_4 + 3.76X_gN_2 \qquad (3.1.b)$$

Where: X_g is the actual fuel to air ratio and m_w is the amount of water per kmol of biomass and the value of m_w in eqn. (3.1.b) can be calculated using the following relations. Moisture content of the feedstock is stated as:

$Moisture\ content = \frac{\text{Amount of water per kmol of biomass} * \text{Molecular mass of water}}{Mass\ of\ feedstock * Molecular\ mass\ of water}$ and from this equation the amount of water per kmol of biomass can be derived as follows.

$$m_w = \frac{(Mbio * m)}{18(1-m)} \quad (3.2)$$

The major reactions that occur inside the fluidized bed reactor are as follows:

$$C + CO_2 \rightarrow 2CO \quad (3.3)$$

$$C + H_2O \rightarrow H_2 + CO \quad (3.4)$$

The two reactions shown above can be combined into one single reaction eqn.3.5 known as water-gas shift reaction [6, 8]:

$$CO + H_2O \rightarrow H_2 + CO_2 \quad (3.5)$$

The other reaction that is prominent in the gasification process is formation of methane as Shown below:

$$C + 2H_2 \rightarrow CH_4 \quad (3.6)$$

Eqns. (3.5) and (3.6) are the two major reactions that occur in the gasification process [20]. The equilibrium constant for these two above equations (3.5) and (3.6) as the function of their molar composition can be written as follows:

$$k_1 = \frac{P_{CH_4}}{(P_{H_2})^2} = \frac{X_5}{{X_1}^2} \quad (3.7)$$

$$k_2 = \frac{P_{CO_2}.P_{H_2}}{P_{CO}.P_{H_2O}} = \frac{X_3 * X_1}{X_2 * X_4} \quad (3.8)$$

Gibbs free energy is used in determining the value of K_1 and K_2 as presented in eqn. (3.9). For the given ideal gas, the Gibbs free energy is a strong function of the reaction temperature and a weak function of pressure [23].

$$Ln\,K\,(T) = \frac{-\Delta GT}{RT} \quad (3.9)$$

$$\Delta GT = \sum_i Xi\,\Delta g^{-o} f, T, i \quad (3.10)$$

Where, $\Delta g^{-o} f, T, i$ is empirically calculated according to the Eqn. (11).

$$\Delta g^{-o}{}_{f,T,i} = H^{-o}{}_{f,T,i} - aTlnT - bT^2 - \frac{c}{2T3} - \frac{d}{3T4} + \frac{e}{2T} + f + gT \qquad (3.11)$$

Eqns. *(3.12-3.14)* can be written by balancing carbon, hydrogen and oxygen moles, respectively as shown below.

$$C: 1 = X_2 + X_3 + X_5 \qquad (3.12)$$

$$H: 2m_w + X = 2X_1 + 2X_4 + 4X_5 \qquad (3.13)$$

$$O: 2 * X_g + Y + m_w = X_2 + 2X_3 + X_4 \qquad (3.14)$$

Solving the simultaneous sets of equations

From eqn. (3.12) $X_5 = 1 - X_2 - X_3$ and from eqn. (3.13) $X_4 = m_w + 0.5 * X - X_1 - 2X_5$

Using x_5 from eqn. (3.12) and substituting to eqn. (3.13), then the following result is obtained.

$$X_4 = -X_1 + 2X_2 + 2X_3 + m_w - 2 + \frac{X}{2} \qquad (3.15)$$

From eqn. (3.7) and from eqn. (3.12), we get $X_1{}^2 K_1 + X_2 + X_3 = 1$ *(3.16)*

Substituting value of x_4 from the eqn. (3.15) to eqn. (3.14) and then following equation is generated.

$$-X_1 + 3X_2 + 4X_3 = 2X_g + 2 + Y - \frac{X}{2} \qquad (3.17)$$

Substituting x_4 from *eqn. (3.15) to eqn. (3.8)* and it leads to the following equation

$$X_1 * X_3 = K_2 X_2 \left| - X_1 + 2X_2 + 2X_3 + m_w - 2 + \frac{X}{2} \right] \qquad (3.18)$$

Multiplying eqn. *(3.16) by (-4)* and solve eqn. *(3.16) and (3.17)* simultaneously

$\begin{Bmatrix} -4*(X_1{}^2*K_1+X_2+X_3=1) \\ (-X_1+3*X_2+4*X_3=2*X_g+1.955) \end{Bmatrix}$ *and solve for* x_2

$$X_2 = -4 * X_1{}^2 * k_1 - X_1 - 1.025 * E_R + 2.045 \qquad (3.19)$$

Multiplying eqn. *(3.16) by (-3)* and solve eqn. *(3.16)* and *(3.17)* simultaneously

$$\left\{\begin{matrix}-3*\left({X_1}^2*K_1+X_2+X_3=1\right)\\(-X_1+3*X_2+4*X_3=2*X_g+1.955)\end{matrix}\right\}$$ *and solve for* x_3

$$X_3 = 3 * {X_1}^2 * k_1 + X_1 - 2 * 1.025 * E_R + 2.045 \qquad (3.20)$$

Substitute eqn. (3.19) and eqn. (3.20) in to eqn. (3.18) and solve for x_1

$$\left[X_1 * \left(3{X_1}^2 k_1 + X_1 - 2X_g + 2.045\right) = [k_2\left(-4{X_1}^2 k_1 - X_1 - 3.2X_g + 2.045\right)] * \{-X_1 + 2 - 4X12k1 - X1 - 3.2Xg + 2.045) + 2*(3*X12*k1 + X1 - 2*Xg + 2.045) + mw - 1.255)\}\right.$$

(3.21)

After multiplication and rearrangement of eqn. (3.21), the following forth degree polynomial equation is generated

$$\left\{\left(8{k_1}^2 k_2\right){X_1}^4 + \left(3k_1 * (2 * k_2 - 1)\right){X_1}^3 + (k_2 k_1 * (1.24 - 4) * \left(X_g - m_w\right){X_1}^2 - k2*mw + 1.72X1 - 4*1.54*Xg + 1.4832* k2 = 0\right.$$

(3.22)

From the above polynomial function, we can find its possible roots which are the values of x_1 and solve for other unknown from their respective relations with x_1.

Now, there are five equations (3.7), (3.8), (3.12) and (3.14), and six unknowns (x_1 - $x_5$and X_g). The final equation can be obtained by an enthalpy balance inside the gasifier. Total enthalpy content in any chemical species is the sum of its chemical enthalpy and sensible enthalpy and can be written as follows:

$$\begin{aligned} H^o_{f-biomas} &+ m_w\left(H^0_{fH_2O(l)} + H^0_{fH_2O(vap)}\right) + X_g(H^0_{fO_2} + 3.76H^0_{fN_2}) \\ &= X_1\left(H^0_{fCO} + \int_{298}^{Tg} C_{PCO}\,dT\right) + X_2\left(H^0_{fH_2} + \int_{298}^{Tg} C_{PH_2}\,dT\right) \\ &+ X_3\left(H^0_{fCO_2} + \int_{298}^{Tg} C_{PCO_2}\,dT\right) + X_4\left(H^0_{fH_2O} + \int_{298}^{Tg} H_2O\,dT\right) \\ &+ X_5\left(H^0_{fCH_4} + \int_{298}^{Tg} C_{PCH_4}\,dT\right) + \left(3.76 * X_g \int_{298}^{Tg} C_{PN_2}\,dT\right) \end{aligned} \qquad (3.23)$$

Zainal et al. [24] have used HHV for predicting syngas composition from biomass. However, the use of LHV for finding heat of formation is also common [1]. In this study, LHV is used for evaluating heat of formation of biomass. Heat of formation of biomass is calculated by using following equation [1]:

$$H^0_{f-biomass} = LHV + \sum_{i=1}^{n} n_i\, p_i \qquad (3.24)$$

LHV is calculated in dry basis of biomass using the following equation [18]:

$$LHV = 4.187 * (81\,C + 300H - 26\,(O - S) - 6 * (9H + m))\ kJ/kg \qquad (3.25)$$

The above equation (*eqn. 3.23*) can be reduced to the following form since $H^0_{fN_2}$, $H^0_{fH_2}$ and $H^0_{fO_2}$ are zero at the reference temperature and pressure of 298.15 K and 1 atm respectively.

$$\begin{aligned} H^o_{f-biomas} + m_w \left(H^0_{fH_2O(l)} + H^0_{fH_2O(l)}\right) &= X_1 \left(H^0_{fCO} + \int_{298}^{Tg} C_{PCO}\, dT\right) + X_2 \left(H^0_{fH_2} + \int_{298}^{Tg} C_{PH_2}\, dT\right) \\ &+ X_3 \left(H^0_{fCO_2} + \int_{298}^{Tg} C_{PCO_2}\, dT\right) + X_4 \left(H^0_{fH_2O} + \int_{298}^{Tg} C_{PH_2O}\, dT\right) \\ &+ X_5 \left(H^0_{fCH_4} + \int_{298}^{Tg} C_{PCH_4}\, dT\right) + \left(3.76 * X_g \int_{298}^{Tg} C_{PN_2}\, dT\right) \end{aligned} \qquad (3.26)$$

Eqn. (*3.26*) acts as the constraint for the gasification process and forms the basis for adjusting the amount of air to be supplied. The amount of air is adjusted in such a way that total enthalpy of the reactants is equal to that of products in gaseous form. Cp can be determined using an empirical relation that holds for a wide range of temperature.

$$C_P\,(T) = C_1 + C_2T + C_3T^2 + C_4T^3 \left(\frac{kJ}{kg}\right) \qquad (3.27)$$

The sensible heat of each gas species was found by integrating eqn. (*3.26*) from the ambient temperature to gasification temperature. The value of C_1-C_4 is taken as reported by Reid et.al.

Table 3.1 Coefficients of specific heat capacity for various gases

Species	C_1	C_2	C_3	C_4
N_2	31.2	-1.36×10^{-2}	2.68×10^{-5}	-1.17×10^{-8}
CO_2	19.8	7.34×10^{-2}	-5.60×10^{-5}	1.72×10^{-8}
H_2	29.1	-1.92×10^{-3}	4.00×10^{-6}	-8.70×10^{-10}
CO	30.9	-1.29×10^{-2}	2.79×10^{-5}	-1.23×10^{-8}
CH_4	19.3	5.21×10^{-2}	1.20×10^{-5}	-1.13×10^{-8}
H_2O(g)	32.2	1.92×10^{-3}	1.06×10^{-5}	-3.60×10^{-9}

Similarly, the change in Gibbs free energy for an individual gas is given by:

$$\Delta g^{-o}{}_{f,T,i} = H^{-0}{}_{f,T,i} - aTlnT - bT^2 - \frac{c}{2}T^3 - \frac{d}{3}T^4 + \frac{e}{2T} + f + gT \qquad (3.28)$$

The values of a-g are taken from Probstein and Hicks [20] and are shown in table 3.2.

Table 3.2 Enthalpy of formation and constant coefficient

Species	***a***	***b***	***c***	***d***	***e***	***f***	***g***
CH_4	-4.6×10^{-2}	1.3×10^{-5}	1.3×10^{-8}	-6.6×10^{-12}	-4.89×10^{2}	14.1	-0.223
CO	5.6×10^{-3}	-1.2×10^{-5}	6.4×10^{-9}	-1.8×10^{-12}	-4.89×10^{2}	0.868	-0.0613
CO_2	-2×10^{-2}	3.2×10^{-5}	2.5×10^{-8}	7×10^{-12}	-4.89×10^{2}	5.27	-0.121
H_2O	-8.9×10^{-3}	-3.7×10^{-6}	5.21×10^{-9}	-1.5×10^{-12}	0	2.87	-0.0172

Generating the Equilibrium Constant equation from the general equations:

Standard Gibbs Function:

$$\Delta G^o = J - RT\left(\Delta A\, lnT + \frac{\Delta B}{2}T + \frac{\Delta C}{6}T^2 + \frac{\Delta D}{2}T^2 + I\right) \qquad (3.29)$$

Heat of Formation:

$$\Delta H^o = \frac{J}{R} + \left(\Delta A\, lnT + \frac{\Delta B}{2}T^2 + \frac{\Delta C}{3}T^3 - \frac{\Delta D}{2}T\right. \qquad (3.30)$$

Equilibrium Constant:

$$LnK = -\frac{J}{RT} + (\Delta A\ lnT\ + \frac{\Delta B}{2}T + \frac{\Delta C}{6}\ T^2 + \frac{\Delta D}{2}T^2 + I) \qquad (3.31)$$

The values for J and I are determined by substituting the constants A,B,C and D, and the values of standard Gibbs and heat of formation at 298.15K. These values are tabulated as follows.

Table 3.3.Standard Gibbs free energy and heat of formation at 298.15K

Component	***Condition***	***ΔG298.15(kJ/kmol)***
H_2O	l	-237129
H_2O	g	-228572
CO_2	g	-394359
CO	g	-137169
CH_4	g	-50460
H_2	g	0
N_2	g	0

Component	***A***	***B***	***C***	***D***
CH_4	1.702	9.08E-03	-2.164E-06	
H_2	3.249	4.22E-04		8300
CO_2	3.376	5.57E-04		-3100
CO	5.457	1.05E-03		-115700
N_2	3.280	5.93E-04		4000
H_2O	3.470	1.45E-03		12100

Source: Z.A.Zainal et al., Energy Conversion and Management, 2001.

The following intermediate values have been generated to derive the final equilibrium constant equation. *R (kJ/kmol.K) = 8.314 and T (Kelvin) = 298.15*

Table 3.4 Intermediate values to derive the final equilibrium constant equation

For k_1		***For k_2***	
ΔA	-6.567	ΔA	-2.302
ΔB	7.47E-03	ΔB	-1.52E-03
ΔC	-2.16E-06	ΔC	0
ΔD	70100	ΔD	116400
ΔH	-74520	ΔH	-41166
ΔG	-50460	ΔG	-28618
ΔH/R	-8963.19	ΔH/R	-4951.41

Alfa (lumped constant)	-1880.35	Alfa (lumped constant)	-1118.73
J	-58886.80	J	-31864.89
Gamma (lumped constant	-35.941	Gamma (lumped constant	-12.730
I	32.541	I	-18.007
Lambda(lumped constant)	7082.85	Lambda(lumped constant)	5870.53
ΔA	-6.5670	ΔA	-2.302
ΔB/2	3.73E-03	ΔB/2	-2.7E-04
ΔC/6	-3.61E-07	ΔC/6	0
ΔD/2	35050.00	ΔD/2	58200

Substituting the above calculated values, the following sets of equilibrium constant equations are formed:

$$lnk_1 = \left[\frac{7082.848}{T} - 6.567\, lnT + \frac{7.466*10^{-3}}{2}T - \frac{2.164*10^{-6}}{6}T^2 + \frac{0.701*10^{-5}}{2*T^2} + 32.541\right| \quad (3.32)$$

$$lnk_2 = \left[\frac{5870.53}{T} + 1.86lnT - 2.7*10^{-4}T - \frac{58200}{T^2} - 18.007\right| \quad (3.33)$$

The values of X and Y in the Gasification Reaction is determined using the Sawdust elemental composition from literature and shown below.

Table 3.5 Saw dust elemental composition from its Ultimate and Proximate analysis (wt. %)

Feed Stock	***Ultimate analysis, (Wt. %)***			***Proximate analysis (wt. %)***			
Saw dust	*C*	*H*	*O*	*Moisture content*	*Volatile Matter*	*Ash content*	*fixed carbon (FC)*
	44-51	*5.5-6.7*	*41-50*	*0-50*	*74.6*	*0.6-3.47*	*15.82*

$$Normalization\ of\ C\ =\ elemental\ composition\ of\ \frac{C}{12};$$

$$Normalization\ of\ H\ =\ elemental\ composition\ of\ \frac{H}{1.008}$$

$$Normalization\ of\ C\ =\ elemental\ composition\ of\ \frac{O}{16}$$

X = Normalization H/ Normalization C and Y= Normalization O/ Normalization C

The operating temperature of the system can be determined using the following general equation.

$$T_2 = T_1 + \frac{\left\{\begin{matrix}\{H^0_{f-biomas} + m_w\left(H^0_{fH20(l)} + H^0_{fH20(vap)}\right) + H^0_{fO_2} + 3.76X_g H^0_{fN_2} + \Delta T'\left(X_g\, C_{PO_2} + 3.76X_g C_{PN_2}\right)\} \\ -x_1 H^0_{fH20(l)} + x_2 H^0_{fCO} + x_3 H^0_{fCO_2} + x_4 H^0_{fH20(vap)} + x_5 H^0_{fCH_4}\end{matrix}\right\}}{\{x_1 C_{PH_2} + x_2 C_{PCO} + x_3 C_{PCO_2} + x_4 C_{PH20(vap)} + x_5 C_{PCH_4} + 3.76X_g C_{PN_2}\}}$$

(3.34)

A sample of the predicted synthesis gas composition at gasifier operating temperature of 780 ^oC and equivalence ratio of 0.26 in the dry basis is summarized in table 3.6.

Table 3.6 Sample of the predicted synthesis gas composition from the equilibrium model

Gas components	***Variables***	***Predicted values***	***Mole fraction***	***Percentage (%)***
H_2	*X_1*	*0.7344*	*0.1956*	*19.56*
CO	*X_2*	*0.6474*	*0.1724*	*17.24*
CO_2	*X_3*	*0.6170*	*0.1642*	*16.42*
H_2O	*X_4*	*0.3199*	*0.0852*	*8.52*
CH_4	*X_5*	*0.0835*	*0.0224*	*2.24*
N_2	*3.76*X_6*	*1.3525*	*0.3602*	*36.02*
Total		*3.7547*	*1.0000*	*100.00*

Moisture content can be accounted in above correlation by using the following values of C, H and O if the data for ultimate analysis are based on wet basis [1]:

$$C^* = \frac{C}{(1+0.01m_w)}$$

$$O^* = \frac{(O+0.889m_w)}{(1+0.01m_w)}$$

$$H^* = \frac{(H+0.111m_w)}{(1+0.01m_w)} \qquad (3.35)$$

Air mass flow: From the fluidization parameters previously established, the air mass flow necessary for the process can be determined through the expression [26]:

$$\dot{m}a = 3600 * (U_f * A * \rho_a) + 0.648 * Y \qquad (3.36)$$

With this value, the reaction coefficient related to the air necessary for gasification was obtained:

$$Z_i = \frac{\dot{m}a}{4.76.Mwa} \qquad (3.37)$$

Saw dust mass flows: Based on the stoichiometric balance previously made, the saw dust mass flow was calculated:

$$\dot{m}_{SD} = 3.6 * R + 0.648 * X \qquad (3.38)$$

Equivalence ratio: The equivalence ratio of the gasification process is one of the most important parameters for the adjustment of the operating conditions [26]. Its value is defined as:

$$\xi = \frac{\left(R_{A/C}\right)r}{\left(R_{A/C}\right)s} \qquad (3.39)$$

where, the air-fuel actual ratio is calculated from the expression:

$$\left(R_{A/C}\right)r = \frac{\dot{m}a}{1.292\ .\dot{m}_{SD}} \qquad (3.40)$$

The air-fuel stoichiometric ratio is calculated from the expression (Sánchez, 1997):

$$\left(R_{A/C}\right)s = 8.89 * (\%\,C + 0.375 * \%\,S) + 26.5 * \%\,H - 3.3 * \%O \qquad (3.41)$$

3.2.2 Mass and Heat Transfer

When the solid saw dust particles enter the hot bed of sands, they are subject to fast pyrolysis. The rate of temperature increase in the saw dust particles is important in calculating the final yield of different gases. In the range of particle sizes of this study (less than 1 mm) the internal heat transfer limitation is negligible. Moreover, the yield of the different products in gasification of biomass in fluidized bed has been shown to be independent of particle size in the range of 4 μm to 2 mm [27]. This eliminates the possibility of secondary reactions between the evolving vapor products and tar with char and the consequent thermal impact (endothermic or exothermic) of those reactions on particle temperature. In this condition, the heat balance for a single particle can be expressed as follow:

$$(\rho_p * C_p * V_p)\frac{dT}{dt} = h_{conv} * A * (T_b - T_p) + \sigma_{rad} * \varepsilon_{rad} * A * ({T_b}^4 - {T_p}^4) \qquad (3.42)$$

The convection heat transfer coefficient is calculated by the Ranz–Marshall correlation and given as follows.

$$\frac{h_{conv} * dp}{K_g} = \left(2 + 0.6 * Re^{1/2} * Pr^{1/3}\right) \qquad (3.43)$$

The effective emissivity in the condition of fluidized bed is calculated according to the correlation developed by Linjewile:

$$\varepsilon_{rad} = \frac{1}{\varepsilon p} + \frac{1}{\varphi\left(\frac{1}{\varepsilon_{fb}} - 1\right)} \; And \; \varphi = \left(1 + np\frac{di}{da}\right)^2 \qquad (3.44)$$

Table 3.7 Input data's for the determination of heat transfer

Parameters	***Value***
Wood specific heat	Cp =1112.0 + 4.85(T - 273)J/(kg K)
Density of the wood	360, kg/m^3
ε_p for wood particles	0.95
Effective emissivity, ε_{fb}	0.8
Parameter in Eq. 52, n_p	5.0
Stephan–Boltzmann constant, σ	5.67 *10^{-8} W m^{-2} K^{-4}

Where ε_p is the emissivity; ε_{fb} is the effective emissivity of the fluidized bed; and *di* and *da* are the diameters of the inert (sand) and active particles (sawdust), respectively. Thermal properties of wood particles can be found in table 3.7.

3.2.3 Heating Values of Feed Stock and Syngas

HHV of the biomass was calculated by Dulong and Petit's Formula given in eqn. *(3.45)* using results from ultimate analysis.

$$HHV_{biomass} = \left(33823 * C + 144249 * \left(\frac{8*H-O}{8}\right) + 9418 * S\right) \frac{kJ}{kg} \qquad (3.45)$$

where: C, H, O and S are the carbon, hydrogen, oxygen and sulfur content of biomass in dry basis.

The higher heating value of the syngas is the main parameter to be analyzed and to be compared with the experimental values sited from different literatures. The volumetric content of syngas constituents multiplied by their individual higher heating value *(HHV)* gave the overall higher heating HHV of the syngas as shown in eqn. (*3.46*).

$$HHV_{syngas} = y_{H_2} HHV_{H_2} + Y_{CO} HHV_{CO} + y_{CH_4} HHV_{CH_4} \quad (3.46)$$

In above equation, HHV_{syngas} is the heating value of syngas while HHV_i and y_i are higher heating value and volumetric fraction of syngas constituents (i = H_2, CO,CH_4). The HHV of H_2, CO and CH_4 *are 12.76 MJ/m*^{3}*, 12.63 MJ/m*^{3} *and 39.82 MJ/m*^{3}, respectively [1]. Then eqn. (*3.46*) can be rewrite as:

$$HHV_{syngas} = \frac{12.76*H_2 + 12.63*CO + 39.82*CH_4}{100} MJ/Nm^3 \quad (3.47)$$

This equation was derived based on the heat of combustion of different gases. The gas concentration in *eqn. (3.47*) is in mol.

3.3 Composition of Tar and Char in the Syngas

The major challenge of biomass gasification is related to the formation of tar, a highly variable mixture of condensable aromatic hydrocarbons in the syngas which condense inside the gasifier or in the equipment used for handling the product stream to its end use. It is a generic term used for all organic compounds found in the product gas with the exception of gaseous hydrocarbons. Removal of tar is one of the biggest technical challenges facing the commercialization of gasification technology. The high-temperature product gas from a gasifier contains tar. If not removed, the tar condenses on the wall of the downstream equipment such as heat exchangers, combustion engine, reactors or fuel cells.

3.3.1 Composition of Tar

In this study, the correlation of Samolada and Vasalos [2] can be used for the determination of the composition of tar and char for gasification of saw dust in a bubbling fluidized bed gasifier. This correlation is described below.

$$Y_{tar} = \frac{-2.8025}{(1-1112.345*ln(-912*0.08*(T-273.15)))} + 45.698lnZ \qquad (3.48)$$

where: $Z = \frac{(T-833)}{160}$ is a dimensionless temperature and T the temperature of the reactor

The carbon, hydrogen and oxygen contents in tar seem to vary with temperature and the variation is shown below.

$$X_C, tar = \frac{54.5}{\{1 + \exp[-54.5 * 0.0024 * (T - 273.15)]\}} \qquad (3.49)$$

$$X_H, tar = 6.5 * \exp\{-0.0077 * (T - 273.15)\} \qquad (3.50)$$

$$X_O, tar = 39 * \exp\{-0.0012 * (T - 273.15)\} \qquad (3.51)$$

3.3.2 Composition of Char

The amount of char formed during gasification seems to decrease exponentially when the surrounding temperature increases.

$$Y_{char} = \frac{5}{\{1 - 1.25 * \exp[-5 * 0.0002 * (T - 273.15)]\}} \qquad (3.52)$$

The carbon, hydrogen and oxygen contents in the char of a given biomass can be calculated with:

$$X_C, cha = \frac{98}{\{1 + \exp[-98 * 0.0035 * (T - 273.15)]\}} \qquad (3.53)$$

$$X_H, char = 53 * \exp\{-0.00177 * (T - 273.15)\} \qquad (3.54)$$

$$X_O, char = 25 * \exp\{-0.0027 * (T - 273.15)\} \qquad (3.55)$$

CHAPTER 4

BASIC DESIGN OF BUBBLING FLUIDIZED BED GASIFIER FOR SAW DUST

4.1 Introduction

Gasification is defined as a thermo chemical conversion process whereby biomass is heated in a sub-stoichiometric oxygen, air or steam to produce gaseous fuel. There are various types of gasifiers and the design is specified by the feedstock type, preparation and end-use of product gas. For instance, fluidized bed gasification is originally developed to overcome the operational problems with fixed bed gasification of fuels with high ash content, but is very suitable for the larger capacities (larger than 10 MWT) in general. Compared to fixed bed gasifier, the gasification temperature is relatively low 650^{o}C - 950^{o}C (Mckendry, 2002). The fuel is fed into a hot (sand) bed which is in a state of bubbling. The bed behaves more or less like a fluid and is characterized by high turbulence. Fuel particles mix very quickly with the bed material, resulting in a fast pyrolysis and a relatively large amount of pyrolysis gases.

For this study, the fluidized bed gasifier is selected due to:

- The characteristic of the feedstock and the ease of control in terms of handling of feedstock in the gasifier.
- Uniform particle mixing**:** due to the intrinsic fluid-like behavior of the solid material, fluidized beds do not experience poor mixing as in packed beds. This complete mixing allows for a uniform product that can often be hard to achieve in other reactor designs. The elimination of radial and axial concentration gradients also allows for better fluid-solid contact, which is essential for reaction efficiency and quality.
- Uniform temperature gradients: many chemical reactions require the addition or removal of heat. Local hot or cold spots within the reaction bed, often a problem in packed beds, are avoided in a fluidized situation such as an FBR. In other reactor types, these local temperature differences, especially hotspots, can result in product degradation. Thus

FBRs are well suited to exothermic reactions. Researchers have also learned that the bed-to-surface heat transfer coefficients for FBRs are high.

- Ability to operate reactor in continuous state: the fluidized bed nature of these reactors allows for the ability to continuously withdraw product and introduce new reactants into the reaction vessel. Operating at a continuous process state allows manufacturers to produce their various products more efficiently due to the removal of startup conditions in batch processes.

4.2 Design Methodology for Fluidized Bed Gasifier

The design methodology uses a two step approach whereby the thermodynamic and process parameters are obtained from the predicted value of synthesis gas composition as a function of gasification temperature, ER and moisture content from the previous chapter. These values are used as inputs for the basic design and sizing of the fluidized bed gasifier for sawdust gasification.

Sawdust is chosen as the biomass fuel in this project because compared to other materials sawdust is easily and abundantly available as waste and generally used as firing purpose. In addition, it is locally available at the surrounding areas of the university especially at the furniture industrial areas. Sawdust is readily available in dry pulverized form which can be used directly with or without pretreatment process. The use of sawdust from wood based industries must be carefully analyzed to offer the best technical, economic and environmental alternative. The characterization (quantity, type, chemical and energetic analysis) of the residues generated is essential to determine which technology is more suitable.

For the design calculations, the physical properties of the sawdust and the inert material (common sand) composing the bed were determined. The values of these properties for both materials appear in table 4. 1 (Martinez, 2005)

Table 4.1 Sand and sawdust properties

Property	***Sand***	***Sawdust***
Mean particle size, dp (μm)	*385*	*578*
Apparent density, ρ_p (kg/m^3)	*2,650*	*716*
Porosity, ε	*0.46*	*0.67*
Sphericity, φ	*0.78*	*0.46*
Density of gasifying medium, ρ_a (kg/m^3)	*1.171*	

The gasifier design was made according to information available in the literature with innovative reforms implemented by the past researchers especially basic design of a fluidized bed gasifier for rice husk on a pilot scale done by Latin American applied researcher. The calculation model was developed separately for each one of the seven parts or subsystems in which the gasifier equipment was divided.

4.2.1 Reactor Subsystem

Reactor subsystem is made up of the reaction chamber, external heat insulation, an air distribution plate and a plenum.

4.2.1.1 Reaction Chamber

Based on references of previous researches of vegetal biomass gasification on pilot scale (Natarajan *et al.*, 1998 and Sánchez, 1997), a 0.4m internal diameter fluidized bed zone was considered (inferior module of the reaction chamber). From this data the gasifier height was determined, involving additionally the following hydro dynamical parameters:

a) Minimum fluidization velocity*:* The lower limit of the superficial velocity of the gas that will flow through the particle bed was calculated separately for the sand and the saw dust using the expression in Eqn. (1) (Kunii and Levenspiel, 1991)

$$U_{mf} = \frac{dp^2.(\rho p - \rho a).g}{150.\mu a} * \frac{\varepsilon^3.\ \varphi^2}{1-\varepsilon} \qquad (4.1)$$

$$U_{mf(sand)} = \frac{(385*10^{-6})^2*(2650-1.171)*9.81}{150*4.014*10^{-5}} * \frac{0.46^3.\ 0.78^2}{1-0.46} = 0.07 m/s$$

$$U_{mf(SD)} = \frac{(578*10^{-6})^2*(716-1.171)*9.81}{150*4.014*10^{-5}} * \frac{0.67^3.\ 0.46^2}{1-0.67} = 0.075 m/s$$

b) Terminal velocity of the particle: The maximum value of the superficial velocity of the gas was determined for both materials of the bed depending of the Reynolds number *(for 0.4 < Re < 500) of the particle (Souza - Santos, 1996):*

$$U_t = d_p x \left[\frac{4*(\rho_p-\rho_a)^2}{225*\rho_a*\mu_a} g^2\right]^{1/3} \quad (4.2)$$

$$U_{t(sand)} = 385 * 10^{-6} * \left[\frac{4*(2650-1.171)^2}{225*1.171*4.014*10^{-5}} * 9.81^2\right]^{1/3} = 2.44 m/s$$

$$U_{t(SD)} = 578 * 10^{-6} * \left[\frac{4*(716-1.171)^2}{225*1.171*4.014*10^{-5}} * 9.81^2\right]^{1/3} = 1.53 m/s$$

c) Fluidization velocity during the gasification*:* The superficial velocity of the gas to be used during the gasifier operation was established considering the relation between the expanded and minimum heights of the fluidized bed (Chatterjee *et al.*, 1995):

$$\frac{H}{H_{mf}} = 1 + \frac{10.978(U_f-U_{mf})^{0.738} * \rho_p{}^{0.376} * d_p{}^{1.006}}{U_{mf}{}^{0.937*}\ \rho_a{}^{0.126}} \quad (4.3)$$

For the bubbling fluidized bed the restriction suggested in *eqn. (4.4)* was used (Kunii and Levenspiel, 1991):

$$1.2 < \frac{H}{H_{mf}} < 1.4 \quad (4.4)$$

For the design, the average value of the two (1.3) was selected for the *eqn. (4.4),* and *the eqn. (4.3)* was solved to determine the value of U_f.

$$1.3 = 1 + \frac{10.978\left(U_f - 0.075\right)^{0.738} * \ 716^{0.376} * (578 * 10^{-6})^{1.006}}{0.075^{0.937} * \ 1.171^{0.126}}$$

$$\Longrightarrow U_f = 0.34 m/s$$

The fluidization velocity finally considered corresponded to 0.6 m/s.

d) Overall height of the reaction chamber

. The sizing of the fluidized bed is established via several sets of assumption and equations. These assumptions are important to enable a practical design of the gasifier.

i) The air flow (and the gas flow) through the bed is assumed to be well distributed and homogeneous mixture of product gas is obtained at averaged bed temperature of 800^{o}C.

ii) The minimum fluidization void age (ε_{mf}) of the bed is assumed 0.66 (ranging 0.5 to 0.85).

iii) The fluidized bed is assumed to be operated with common sand which has a particle density (ρ_p) of 2650 kg/m^3 and average particle diameter (d_p) of 385 microns.

iv) The bed operates at atmospheric pressure due to the air delivered by the blower is nearly the same as atmospheric pressure

The first step in sizing activity is the determination of the fluidized bed diameter, which uses the following correlation:

$$\dot{m}_{air} = \frac{\rho air * (\pi * Dr^2) * Us}{4} \qquad (4.5)$$

$$= \frac{1.171 * (\pi * 0.4^2) * 0.15}{4} = 0.025 kg/s$$

The air flow rate ($\dot{m}_{air}$) through the bed is given as a function of bed diameter *(D_r)* and the gas superficial velocity *(U_s).* The following sets of equations are required to determine the superficial velocity [24], which necessitates the information on the bed minimum fluidization velocity *(U_{mf}).*

$$U_s = 2 * U_{mf} \qquad (4.6)$$

$$= 2 * \frac{0.075m}{s} = \frac{0.15m}{s}$$

Using the superficial value calculated from the above equations, the bed diameter is determined, whereby the air flow rate had already been established in previous section. The next step will require the determination of bed dynamic height *(H_B)*, which is the section of the bed where the fluidized particles (including sawdust) will rise when air is injected for reaction. This is determined using the relationship between bed residence time *(t) and* U_{mf}. The overall reaction bed height (H) is the sum of the height of sawdust feeding point *(H_f)* and dynamic bed height *(H_B)*.

$$H_B = t * U_{mf} \qquad (4.7)$$

The residence time for most fluidized bed reactor is in the range of 2 to 6sec. Hence, there is a need to take the average value of the two ranges (4sec).

Therefore, H_B*=4s*0.075m/s = 0.3m*

$$H = H_B + H_f \qquad (4.8)$$

The location of the feedstock feeding point with respect to the bed height has visible effect on the process of fluidization. When the feeding point is either at the bottom or top of the reaction bed height, it leads for poor fluidization of the bed material and the feedstock with the gasifying medium. So, it is better to fix the location of the feedstock feeding point to be on the midpoint of the overall reaction bed height. Thus, the height of sawdust feeding point (H_f) *is 0.3m*. So, the overall reaction bed height *(H)* will be *H = 0.3 + 0.3 = 0.6m*

$$H_t = T_{DH} + H \qquad (4.9)$$

The maximum expanded height of the bed was assumed as 0.3 m, being 0.75 times the internal diameter of reactor, with the purpose of diminishing the slugging phenomena.

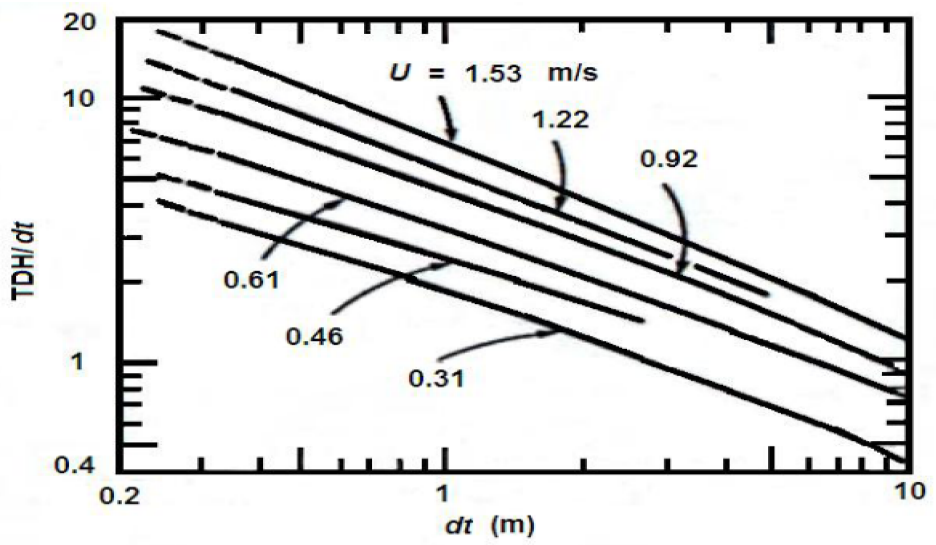

Figure 4.1 Zens and Weil correlations to TDH calculation

The calculation of the threshold disengaging height (T_{DH}) was made in agreement with the graphical correlations shown in the Fig.4.1 (Kunii and Levenspiel, 1991) based on the internal diameter (0.4 m) and the fluidization velocity (0.34 m/s). Because the height of the upper module of the reaction chamber was extended to 0.25 m to avoid excessive particles drag by the expected increase of the gas volume within the reactor, the final T_{DH} corresponded to an average value which is 0.875m. And then the overall height of the reaction chamber *(H_t)* will be

$$H_t = 0.875m + 0.6m = 1.475m$$

Table.4.2 shows the values used for the parameters previously described.

Parameter		***Selected value to the design***	***Obtained value of the calculation model***
Fluidization velocity (m/s):-	Sand	0.5	0.5
	sawdust	0.6	0.34
Overall height of the reaction chamber (m)		1.5	1.475

Fluidization will be considered to begin at the gas velocity at which the weight of the solids gravitational force exerted on the particles equals the drag on the particles from the rising gas. All parameters at the point where these two forces are equal will be characterized by the subscript "m_f," to denote that this is the value of a particular term when the bed is just beginning to become fluidized. The combination [g (ρp– ρa) occurs very frequently, and this grouping is termed [η].

$$\eta = \left(g * (\rho_p - \rho_a)\right) = 9.81 * (716 - 1.171) = 7012$$

$$\frac{\Delta P}{H} = \frac{2}{9} * H * g * \eta * (1 - \varepsilon_{mf}) \qquad (4.10)$$

Then the Ergun Equation, can be written in the form

$$\Delta P = \left(H * \rho_g * U_f\right) * \left[\frac{150(1-\varepsilon)}{Red*\varphi} + 7/4\right] * \left[\frac{(1-\varepsilon)*\varphi 2}{\varphi * dp * \varepsilon^3}\right] \qquad (4.11)$$

$$\Delta P = 0.625 * 1.171 * 0.342 * \left[\frac{150(1-0.46)}{5.7*0.78} + 7/4\right] * \frac{1}{4}\left[\frac{(1-0.46)*0.78^2}{0.78*385*10^{-6}*0.46^3}\right] = 3.7\text{Kpa}$$

Where $R_{ed} = \frac{\rho_a * U_{mf} * d_p}{\mu_a}$

$$= \frac{1.171*0.075*578*10^{-6}}{4.014*10^{-5}} = 5.7$$

At the point of minimum fluidization, the weight of the bed just equals the pressure drop across the bed

$$W_s = \Delta P * A_C = 0.1256 * 3.6 = 0.452\ N$$

where A_C Cross-sectional area of the bed and given by:

$$A_C = \frac{\pi}{4} * D^2 = \frac{\pi}{4} * 0.4^2 = 0.1256 m^2$$

$$g(1 - \varepsilon)\left(\rho_C - \rho_g\right) * A_C = \rho_g * {U_f}^2 \left[\frac{150(1-\varepsilon)}{Red*\varphi} + \frac{7}{4}\right] * \left[\frac{(1-\varepsilon)*Ac}{\varphi * dp * \varepsilon^3}\right] \qquad (4.12)$$

$$For\ R_{ed} < 10,\ \left(R_{ed} = \frac{\rho_a d_p U_f}{\mu a}\right)$$

Reynolds numbers less than 10 represents the usual situation, in which fine particles are fluidized by a gas. Sometimes, higher values of the Reynolds number do exist at the point of incipient fluidization, and then the quadratic equation (12) must be used.

Two dimensionless parameters in these two equations for u_{mf} deserve comment. This first is φ, the "sphericity," which is a measure of a particle's nonideality in both shape and roughness. It is calculated by visualizing a sphere whose volume is equal to the particles, and dividing the surface area of this sphere by the actually measured surface area of the particle. Since the volume of a spherical particle is

$$V_p = \frac{\pi}{6} * {d_p}^3 = \frac{\pi}{6} * (578 * 10^{-6})^3 = 1.02 * 10^{-10} m^3$$

and its surface area is

$$\mathrm{A_S} = \pi\left[(6\mathrm{Vp}/\pi)^{1/3}\right]^2$$
$$= \pi\left[(6 * 1.02 * 10^{-10}/\pi)^{1/3}\right]^2 = 1.06*10^{-6} m^2$$

φ, The shape factor of catalyst particle, sometimes called the sphericity can be determined as

$$\varphi = \frac{As}{Ap} = \frac{\pi(6V_p\,\pi)^{2/3}}{Ap} \qquad (4.13)$$

Measured values of this parameter range from 0.5 to 1, with 0.6 being a normal value for a typical granular solid. The second parameter of special interest is the void fraction at the point of minimum fluidization, $\varepsilon_{mf.}$ It appears in many of the equations describing fluidized bed characteristics. There is a correlation that apparently gives quite accurate predictions of measured values of ε_{mf} (within 10%) when the particles in the fluidized bed are fairly small:

$$\varepsilon_{mf} = 0.586 * \varphi^{-0.72} * \left[\frac{\mu^2}{\rho_a * \eta * {d_p}^3}\right]^{0.029} \left[\frac{\rho_a}{\rho_p}\right]^{0.021} \qquad (4.14)$$

$$= 0.586*0.46^{-0.72}* \left[\frac{(4.014*10^{-5})^2}{1.171*7012*(578*10^{-6})^3}\right]^{0.029} \left[\frac{1.171}{716}\right]^{0.021} = 0.733$$

Another correlation commonly used is that of Wen and Yu

$$\varepsilon_{mf} = \left[\frac{0.071}{\varphi}\right]^{1/3} = \left[\frac{0.071}{0.46}\right]^{1/3} = 0.536 \qquad (4.15)$$

So, it is better to take the average of the two correlations which is $\varepsilon_{mf} = 0.634$. When the particles are large, the predicted ε_{mf} can be too small. If a value of ε_{mf} below *0.40* is predicted, it should be considered suspect. Kunii and Levenspiel state that ε_{mf} is an easily measurable value. However, if it is not convenient to do so, equation *(4.14)* should suffice. Values of ε_{mf} around 0.5 are typical. If the distribution of sizes of the particles covers too large a range, the equation will not apply because smaller particles can fill the interstices between larger particles [31].

If the gas velocity is increased to a sufficiently high value, however, the drag on an individual particle will surpass the gravitational force on the particle, and the particle will be entrained in a gas and carried out of the bed. The point at which the drag on an individual particle is about to exceed the gravitational force exerted on it is called the maximum fluidization velocity. When the upward velocity of the gas exceeds the free-fall terminal velocity of the particle, U_t, and the particle will be carried upward with the gas stream. For fine particles, the Reynolds numbers will be small, and two relationships presented by Kunii and Levenspiel are:

$$U_t = \frac{\eta * {d_p}^2}{18\mu_a} \qquad Red < 0.4$$

$$U_t = d_p x \left[\frac{4*(\rho p - \rho a)^2.}{225.\rho a.\mu a} g^2\right]^{1/3} \qquad (0.4 < Red < 500)$$

In this study the second case is applied because *Red = 5.7* is between 0.4 and 500.

$$U_t = 578 * 10^{-6} * \left[\frac{4*(716-1.171)^2.}{225*1.171*4.014*10^{-5}} * 9.81^2\right]^{\frac{1}{3}} = 1.53 m/s \qquad (4.16)$$

We now have the maximum and minimum superficial velocities at which we may operate the bed. The entering superficial velocity, U_o, must be above the minimum fluidization velocity but below the slugging U_{ms} and terminal, U_t, velocities.

$U_{mf} < U_o < U_t \; and \; U_{mf} < U_o < U_{ms}$, both of these conditions must be satisfied for proper bed operation.

- Bubble Velocity

From experiments with single bubbles, Davidson and Harrison found that the velocity of rise of a single bubble could be related to the bubble size by:

$$U_{br} = 0.71 * (g * d_p)^{0.5} \qquad (4.17)$$

$$= 0.71 * (9.81 * 0.08505)^{0.5} = 0.6485 m/s$$

When many bubbles are present, this velocity would be affected by other factors. The more bubbles that are present, the less drag there would be on an individual bubble; the bubbles would carry each other up through the bed. The greater number of bubbles would result from larger amounts of gas passing through the bed (i.e., a larger value of (U_o). Therefore, the larger the value of U_o, the faster should be the velocity of a gas bubble as it rises through the bed. Other factors that should affect this term are the viscosity of the gas and the size and density of the solid particles that make up the bed. Both of these terms also affect the minimum fluidization velocity, and so this term might well appear in any relationship for the velocity of bubble rise; the higher the minimum fluidization velocity, the lower the velocity of the rising bubble.

Adopting an expression used in gas-liquid systems, Davidson and Harrison proposed that the rate of bubble rise in a fluidized bed could be represented by simply adding and subtracting these terms:

$$U_b = U_{br} + \left(U_o - U_{mf}\right) = U_o - U_{mf} + 0.71 * (g * d_p)^{0.5} \qquad (4.18)$$

$$= 0.67 - 0.075 + 0.71 * (9.81 * 0.08505)^{0.5} = 1.2435 \frac{\mathrm{m}}{\mathrm{s}}$$

- Bubble Size

The equations for the velocity of bubble rise, equations (17) and (18) are functions of the bubble diameter, an elusive value to obtain. As might be expected, it has been found to depend on such factors as bed diameter, height above the distributor plate, gas velocity, and the components that affect the fluidization characteristics of the particles. Unfortunately, for predictability, the bubble diameter also depends significantly upon the type and number of baffles, heat exchangers tubes, and so forth, within the fluidized bed (sometimes called "internals"). The design of the distributor plate, which disperses the inlet gas over the bottom of the bed, can also have a pronounced effect upon the bubble diameter [31].

Studies of bubble diameter carried out thus far have concentrated on fluidized beds with no internals and have involved rather small beds. Under these conditions the bubbles grow as they rise through the bed. The best relationship between bubble diameter and height in the column at this writing seems to be that of Mori and Wen, who correlated the data of studies covering bed diameters of 7 to 130 cm, minimum fluidization velocities of 0.5 to 20 cm/s, and solid particle sizes of 0.006 to 0.045 cm. Their principal equation was

$$\frac{d_{bm} - d_b}{d_{bm} - d_{bo}} = e^{-0.3 * \frac{h}{Dr}} \qquad (4.19)$$

In this equation, *db* is the bubble diameter in a bed of diameter D_r, observed at a height *H* above the distributor plate; *dbo* is the diameter of the bubble formed initially just above the distributor plate and *dbm* is the maximum bubble diameter attained if all the bubbles in any horizontal plane coalesce to form a single bubble (as they will do if the bed is high enough). The maximum bubble diameter, *dbm* has been observed to follow the relationship

$$d_{bm} = 0.652\left[A_C * \left(U_0 - U_{mf}\right)\right]^{0.4} \qquad (4.20)$$

$$= 0.652 * \left[0.1256 * \left(0.67 - 0.075\right)\right]^{0.4} = 0.23$$

For all beds, the initial bubble diameter depends upon the type of distributor plate. For porous plates, the relationship

$$d_{bo} = 0.00376 * \left(U_O - U_{mf}\right)^2 \quad (4.21)$$

$$= 0.00376 * \left(0.67 - 0.075\right)^2 = 1.331 * 10^{-3}$$

For perforated plates, the relationship

$$d_{bo} = 0.347 * \left[A_c(U_0 - U_{mf})/nd\right]^{0.4} \quad (4.22)$$

$$= 0.347 * \left[0.1256 * (0.67 - 0.075)/40\right]^{0.4} = 0.0281$$

Appears to be valid, in which *nd* is the number of perforations. Werther developed the following correlation based on a statistical coalescence model.

$$d_p = 0.853 \sqrt[3]{1 + 0.272\left(U_0 - U_{mf}\right)} * [1 - 0.0684 * H]^{1.21} \quad (4.23)$$

$$= 0.853 * \sqrt[3]{1 + 0.272 * (0.67 - 0.075\ )} * [1 - 0.0684 * 0.625]^{1.21}$$

= 0.08505cm

e) Determination of the wall thickness of the reaction chamber

Treating the reaction chamber as thick pressure vessels, then try to determine the thickness of the reaction chamber using different techniques. The reason for assuming the reaction chamber as thick pressure vessel is to avoid explosion and burning of the chamber with the reaction temperature during gasification.

From the material property table, there is a need to select metals for the design of the reaction chamber, because metals are locally available, have high fire and other internal and external damage resistance property and have long service duration.

Table 4.3 Common candidate materials for the design of reaction chamber

Name of Materials	***Mild Steel***	***St-34***	***St-37***	***St-42***	***Steel - Carbon Alloy***
δ_u (MPa)	360	340	370	420	286
δ_y (MPa)	-	210	220	240	105
Availability	Moderate	Moderate	High	Low	Low
Corrosion resistance	Moderate	Moderate	High	High	medium
Load carrying capacity	Medium	Medium	High	High	low
Weld ability	Low	Medium	Medium	High	low
cost	Low	Low	Medium	High	low

Based on the above design matrix, there is a need to select St-37, because it is locally available, has high strength and has relatively low cost.

$St-37:\ \sigma e = 200MPa, \quad \sigma y = 220MPa, \sigma u = 370MPa, \quad \rho = 1750kg/m3$

Assuming factor of safety to be 2

- Culverins equation

It develops an equation to determine the thickness of pressure vessels with closed ends and made of ductile materials.

$$t = R_i * [\sqrt{(\sigma_{all} + (1-2\mu) * \frac{p_i}{\sigma_{all}} - (1+\mu) * p_i)} - 1]$$

Where: R_I is internal radius of the reaction chamber and take μ =0.3 for ductile materials.

$$\sigma_{all} = \frac{\sigma_y}{F_s} = \frac{220}{2} = 110MPa \qquad R_i = \frac{Dr}{2} = \frac{400}{2} = 200mm$$

Based on the above known data's and assumption's we will have the following dimensions. The internal height of the reaction chamber =1.475m

The internal diameter of the reaction chamber = 0.4m

Now let us determine the thickness of the reaction chamber

$$t = R_i * \sqrt{\frac{1}{2} * [(\sigma_{all} + (1 - 2\mu) * \frac{p_i}{\sigma_{all}} - (1 + \mu) * pi\ ) - 1]}$$

$$t = 200 * \sqrt{\frac{1}{2} * [(110 + (1 - 2 * 0.3) * \frac{0.115}{110} - (1 + 0.3) * 0.115\ ) - 1]}$$

$$t = 3.507mm\ and\ take\ it\ to\ be\ t\ =\ 4mm$$

4.2.2 Air Distribution Plate

A Tuyer type air distributor plate was selected, consisting of a plate with vertical nozzles with lateral perforations through which passes the air that is distributed uniformly into the reactor. This alternative was selected due to its convenience for use with high temperatures and its advantage of reducing the backflow of bed material toward the plenum. The sphericity, φ, and void age at minimum fluidization velocity, ε_{mf}, corresponding to sand particle size of 0.385 mm are taken as 0.78 and 0.46 respectively. In addition the following data is used for design of the air distributor plate [27]. Calculation of Reynolds number for the total flow approaching the plate and select the corresponding value of Cd.

$$Red_{mf} = \frac{(\rho_a * U_{mf} * d_p)}{\mu_a}$$

$$= \frac{1.171 * 0.07 * 385 * 10^{-6}}{4.014 * 10^{-5}} = 11.23$$

Red_{mf} is Reynolds number for minimum fluidization

$$C_d = \frac{24}{Red_{mf}} \quad for\ low\ Red_{mf}$$

$$Cd\ =\ 0.44 \quad for\ Red_{mf}\ \geq\ 10^3$$

Hence it is better to use $C_d = \frac{24}{Red_{mf}}$ because Red_{mf} is less than 10^3

Therefore, $C_d = \frac{24}{11.23} = 2.14$

Minimum fluidization velocity is calculated from the relation

$$U_{mf} = \frac{\pi * dor^2 \times Uo \times N_{or}}{4} \quad (4.24)$$

$$Red_{mf} = \frac{Ar}{150 * \frac{1-\varepsilon_{mf}}{\varepsilon_{mf}^3} + \sqrt{1.75 * \frac{Ar}{\varepsilon_{mf}^3}}} \quad (4.25)$$

where: $Ar = \frac{dp^2 * \rho a * g\,(\rho p - \rho a)}{\mu a^2}$ Archimedes number

$$L_{mf} = \frac{\{(1-\varepsilon) * Ls}{(1-\varepsilon_{mf})} \quad (4.26)$$

where: $\varepsilon_{mf} = (\frac{0.071}{\varphi})^{1/3} = \left(\frac{0.071}{0.78}\right)^{1/3} = 0.45$

$$L_{mf} = \frac{(1-0.46) * 0.1}{(1-0.45)} = 0.04\text{m}$$

$$L_s = 0.1\,m \quad assumption$$

Pressure drop across the bed at minimum fluidization is given as:

$$\Delta P = L_{mf} * (1 - \varepsilon_{mf}) * (\rho_p - \rho_a) * g \quad (4.27)$$

$$= 0.04 * (1 - 0.45) * (2650 - 1.171) * 9.81 = 0.572Kpa$$

Pressure drop across the distributor plate at minimum fluidization is given as:

$$\Delta pd = 0.1 * \Delta p \quad (4.28)$$

$$\Delta pd = 0.1 * 0.572 = 0.0572Kpa$$

• Determination of velocity of fluid through orifice using:

$$U_{or} = C_d * \left[\frac{2*g*\Delta pd}{\rho a}\right]^{1/2} \quad (4.29)$$

$$= 2.14 * \left[\frac{2*9.81*0.0572}{1.171}\right]^{1/2} = 2.1m/s$$

Nor, number of orifices per unit area of distributor is decided and the corresponding orifice diameter is calculated as:

$$U_o = C_d * \left[\frac{2*\Delta pd}{\rho a}\right]^{1/2} \quad (4.30)$$

$$= 2.14 * \left[\frac{2*0.0572}{1.171}\right]^{1/2} = 0.67m/s$$

Assume the number of orifices per square meter is 320. So, the number of orifices per the area of the distributor plate is 40.

$$d_{or} = \frac{4Uo}{\pi * Uor * Nor}$$

$$= \frac{4*0.67}{\pi*2.1*40} = 0.01m$$

Since there is a need to have a gap between those orifices the above calculated value of the orifice diameter have been taken as $d_{or} = 0.006m$

$$\text{Area of vessel} = \frac{\pi*dor^2}{4} = \frac{\pi*0.006^2}{4} = 0.0003 \text{ m}^2$$

Table 4.4 Operating conditions for the air distributor plate of fluidized bed gasifier

Parameters	***Sand***
Air flow rate, L/s	3.12-18.47
Superficial velocities in the vessel, U_{ms} in m/s	0.18-1.05
Superficial velocities in Disengagement section, U_0 in m/s	0.04-0.26
Void age at minimum fluidization state, εmf	0.46

Pressure drop at minimum fluidization, $(\Delta p)_{mf}$ in N/m^2	572
Static bed height of inert particles, L_s in mm	100
Minimum fluidization velocity, U_{mf} in m/ s	0.07
Bed height at minimum fluidization, L_{mf} in mm	40

Table 4.5 Design parameters and calculated results for the air distribution plate

Parameter	***Value***
Fluidization velocity (m/s)	0.34
Minimum fluidization velocity (m/s)	0.07
Minimum fluidization height (m)	0.47
Particle density (kg/m^3)	2,650
Mean particle size (μm)	385
Bed porosity	0.46
Bed zone diameter (m)	0.4
Number of tuyer lateral orifices	4.0
Pressure drop in the bed (kPa)	3.6
Tuyer orifice diameter (mm)	2.38
Pressure drop in the distributing plate (kPa)	1.1
Tuyer internal diameter (mm)	10
Air velocity for the orifice (m/s)	18
Total number of tuyers	40
Tuyer height (mm)	6

4.2.3 Plenum

Plenum is used to collect the air from blower and to pass the air equally into the gasifier through the nozzles in the distributor plate. The height of the frustum is 22 mm, with 400 mm bigger diameter and 76 mm smaller diameter. Air is fed from the blower into the plenum with the 76 mm diameter pipe fitted at 76 mm diameter of the frustum. This plenum is welded at the extreme bottom of the gasifier to form a leak proof space between the distributor plate and the cone.

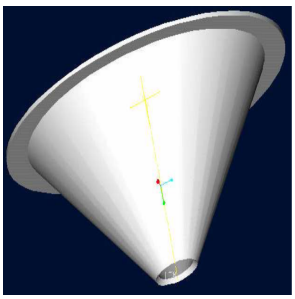

Figure 4.2 Plenum model

4.2.4 Preheating Bed Subsystem

For the reaction chamber preheating, a natural gas burner connected to the entrance of the plenum was selected. The combustion gases generated by the burner crossed through the sand of the bed warming it up to around 400°C. At this temperature the fluidized bed temperature ensured the saw dust self-ignition giving start to the autonomy of the combustion and gasification reactions.

Based on the heat transfer equations presented in literature (Howard, 1989), it was determined the minimum power required of the burner to preheat the bed with 30 kg of sand in a period of one hour, considering a temperature of 850ºC for the combustion gases of the burner. Equally, from the mass and energy balances established, the natural gas and air mass flows for the burner were calculated. Table 4.6 presents the data used for the calculations as well as the results obtained. For the design parameters, verifications of the gas velocity in the distributing plate

orifices (< 70 m/s) and in the bed zone (> 0.07 m/s) were made. Both verifications were satisfactory.

Table 4.6 Data and results for the preheating bed subsystem

	Parameter	***Value***
Data	Preheating time (h)	1
	Combustion gases temperature (°C)	830
Results	Natural gas flow (ml/min)	62
	Air flow (l/min)	780

4.2.5 Atmospheric Emissions Control Subsystem

This subsystem consisted of a high efficiency cyclone which is intended to collect the particulate material that could be released during the gasification process. Based on the literature information (Ashbee and Davis, 1992), a cyclone with the geometric relations presented by Stairmand was designed. Table 4.7 shows the considerations made in the design.

Table 4.7 Particle separator design considerations

Parameter	***Value***
Gas inlet velocity (m/s)	15-27
Pressure drop (kPa)	<2.5
Collection efficiency (%)	>85

The raw gas is passed through the cyclone, which removes the coarse carbon particles from the raw gas. When operating at full gasifier/engine power, the conventional fixed cyclone removes about 80% of the carbon particles and soot, or about 4g/m^3 of gas, leaving the remaining about 20% fine carbon and soot particles or about 1g/m^3 of gas and this is carried through the gas scrubber/cooler. If the power output is reduced, the cyclone starts to lose efficiency [Johansson, 2002]. This is basically because of the reduced centrifugal forces as explained later in this section.

Typically, a particulate-laden gas enters tangentially near the top of the cyclone. The gas flow is forced into a downward spiral simply because of the cyclone's shape and the tangential entry. Centrifugal forces and inertia cause the particles to move outward, collide with the outer wall, and then fall downward to the bottom of the device. Near the bottom of the cyclone, the gas reverses its downward spiral and moves upward in a smaller inner spiral. The cleaned gas exits from the top through a vortex finder tube, and the particles exit from the bottom of the cyclone through a pipe sealed by a spring-loaded flapper valve or rotary valve. The clean gas exiting the cyclone is termed the overflow while the retained particles collected at the bottom are termed the underflow.

The collection efficiency of cyclones vary with particle size and cyclone design. The efficiency of particle collection is generally good for particles that are larger than 5 microns. Other cyclones have collection efficiency greater than 98% for particles larger than 5 microns and others do achieve efficiencies of 90% for particles larger than 15-20 microns [Cooper and Alley, 1986 and Gradon *et al*, 1998]. Three categories of cyclones are available and these are the high efficiency, conventional and high throughput. The high efficiency attains a higher efficiency followed by the conventional and high throughput respectively.

1) Standard Cyclone Dimensions

Extensive work has been done to determine in what manner dimensions of cyclones affect performance. In some classic work that is still used today, Shepherd and Lapple (1939, 1940) determined "optimal" dimensions for cyclones. Subsequent investigators reported similar work, and the so-called "standard" cyclones were born. For the best efficiency of the cyclone, the body diameter of the cyclone should be in the range of *100mm to 200mm*. So, it is better to use the average of the two end values which is *D =150mm*

All dimensions are related to the body diameter of the cyclone so that the results can be applied generally. The next table summarizes the dimensions of standard cyclones of the three types mentioned in the previous section [Manphweli, 2009].

Table 4.8 Standard Dimensions of the common cyclones

Cyclone Type	***Body Diameter D/D***	***Height of Inlet, H/D***	***Width of Inlet, W/D***	***Diameter of Gas Exit, De /D***	***Length of Body, Lb/D***	***length of Cone, Lc/D***	***Diameter of dust Outlet, Dd /D***
High efficiency	*1.0*	*0.5*	*0.2*	*0.5*	*1.5*	*2.5*	*0.375*
conventional	*1.0*	*0.5*	*0.25*	*0.5*	*1.75*	*1.75*	*0.25*
High Throughput	*1.0*	*0.75*	*0.375*	*0.75*	*1.5*	*2.5*	*0.375*

Source: Stairmand, 1951

2) Particle Collection Efficiency of Cyclone

A model can be used to determine the effects of both cyclone design and operation on collection efficiency. In this model, gas spins through a number of revolutions N_e in the outer vortex is considered and its value can be approximated by [Cooper and Alley, 1986] as follows.

$$N_e = \left(\frac{2*Lb+Lc}{2*H}\right) \qquad (4.31)$$

$$= \left(\frac{2*285+475}{2*95}\right) = 5.5$$

N_e = number of effective turns, H = height of inlet duct (m), L_b = length of cyclone cylindrical body (m), L_c = length (vertical) of cyclone cone (m).

Figure.4.3 shows the various parts of the cyclone for better understanding of the equations.

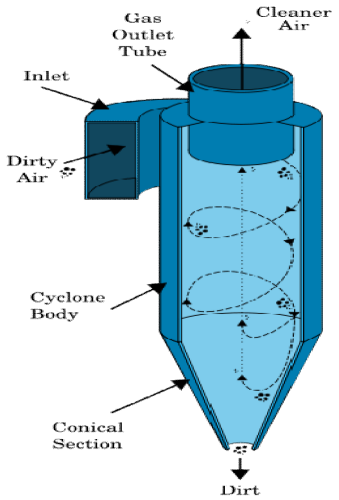

Figure 4.3 Various parts of the cyclone

To be collected, particles must strike the wall within the amount of time that the gas travels in the outer vortex. The gas residence time in the outer vortex is:

$$\Delta t = \frac{\pi DNe}{Vi} \qquad (4.32)$$

$$= \frac{\pi * 0.190 * 5.5}{21} = 1.5633\ sec.$$

where: $\Delta t = time\ spent\ by\ gas\ during\ spiraling\ descent\ (sec)$

$$D = cyclone\ body\ diameter\ (m)\ , V_i = \frac{Q}{(W*H)},\ gas\ inlet\ velocity\ \left(\frac{m}{s}\right)$$

$$Q = volumetric\ inflow\ of\ the\ gas\ \left(\frac{m^3}{s}\right)$$

$$Q = V_i * W * H = 21\ \frac{m}{s} * 0.095 * 0.038 = 0.07581\ \frac{m^3}{s}$$

The maximum radial distance travelled by any particle is the width of the inlet duct (W). The centrifugal force quickly accelerates the particle to its terminal velocity in the outward (radial) direction, with the opposing drag force equaling the centrifugal force. The terminal velocity V_t of the particle in a radial direction that will just allow a particle initially at distance (W) away from the wall to be collected in time Δt is:

$$V_t = \frac{W}{\Delta t} \qquad (4.33)$$

$$= \frac{0.038m}{1.5633sec} = 0.243m/s$$

Assuming Stokes' regime flow (*drag force* = $3\pi\mu dpV_t$) and spherical particles subjected to a centrifugal force F.

$$F = \frac{m*Vi^2}{r} \qquad (4.34)$$

Where: m = mass of particle in excess of mass of gas displaced

V_i = *velocity* of inlet flow, and $r = \frac{D}{2} = radius$

We obtain:

$$V_t = \frac{\left(\rho_p - \rho_g\right)\ {d_p}^2\ {V_i}^2}{9*D*\mu} \qquad (4.35)$$

$$= \frac{(1600-1.171)\ (4.865*10^{-6})^2\ \ 21^2}{9*0.19*4.014*10^{-5}} = \ 0.243m/s$$

The density and viscosity values of air and syngas are similar, since most of syngas constituents are similar to air (CO, N_2, and to a lesser extent CO_2). Only the hydrogen portion is substantially great in syngas.

3) Wall Thickness of the Cyclone

For the design of the cyclone the same material as the reaction chamber was used and it is steel – 37 with the following properties.

$$\sigma e\ = 200MPa, \sigma y\ =\ 220MPa,\ \sigma u = 370MPa,\ \rho\ = 1750\ \frac{kg}{m^3}, F.S = 2$$

$$\sigma_{all}\ = \frac{\sigma y}{Fs} = \frac{220}{2} =\ 110\ MPa\ ,\ R_i\ = \frac{Dr}{2} = \frac{190}{2} =\ 95mm$$

Now let us determine the thickness of the cyclone

$$t\ =\ R_i * \sqrt{\frac{1}{2} * [(\sigma_{all} + (1-2\mu) * \frac{p_i}{\sigma_{all}} - (1+\mu) * pi\ ) - 1]} \qquad (4.36)$$

$$= 95 * \sqrt{\frac{1}{2} * [(110 + (1 - 2 * 0.3) * \frac{0.114}{110} - (1 + 0.3) * 0.114\ ) - 1]}$$

$$t = 3.062 \text{ mm and take it to be 4 mm}$$

Note that the thickness of all the cyclone parts will be the same as the thickness of the main body of the cyclone for the purpose of consistency. The cyclone performance is rated in terms of particle cut diameter (d_P) or cut size. The impact of particle size on collection efficiency is quantified in the following section. Substitution of equation 4.32 into the 4.33 eliminates *Δt*. Then, equating 4.34 and 4.35 and rearranging to solve for particle diameter, then the following result can be obtained.

$$d_p = \left(\frac{9*\mu*w}{\pi N_e V_i(\rho_p - \rho_g)}\right)^{0.5} \qquad (4.37)$$

$$= \left(\frac{9*4.014*10^{-5}*0.038}{\pi*5.5*21(1600-1.171)}\right)^{0.5} = 4.865 * 10^{-6}\, m$$

It is worth noting that in this expression, d_p is the size of the smallest particle that will be collected if it starts at the inside edge of the inlet duct. Thus, in theory, all particles of size d_p or larger should be collected with 100% efficiency [Cooper and Alley, 1986]. In equation 4.34, increasing the velocity of the particle (V) and/or decreasing the radius of the vortex flow (r) can increase the efficiency of separation [Holley *et al*, 2006]. However care should be taken when decreasing the size of the vortex finder as this might results in low gas flow rates impacting negatively on the efficiency of the engine as it will have to apply more power in sucking the gas.

The preceding equation shows that, in theory, the smallest diameter of particles collected with 100% efficiency is directly related to gas viscosity and inlet duct width, and inversely related to the number of effective turns, inlet gas velocity, and density difference between the particles and the gas. Lapple (1951) developed a semi-empirical relationship to calculate a "50% cut diameter" d_{pc}, which is the diameter of particles collected with 50% efficiency. The expression is:

$$d_{pc} = \left(\frac{9*\mu*w}{2\pi N_e V_i(\rho_p - \rho_g)}\right)^{0.5} \qquad (4.38)$$

$$= \left(\frac{9*4.014*10^{-5}*0.038}{\pi*2*5.5*21(1600-1.171)}\right)^{0.5} = 3.44 * 10^{-6}\, m$$

$Particle\ density\ (\rho p) = 1600\,\frac{kg}{m^3}$

Where: d_{pc} is the diameter of particle collected with 50% efficiency. Note the similarity between the last two equations. The only difference is a factor 2 in the denominator. Lapple then developed a general curve for standard conventional cyclones to predict the collection efficiency for any particle size (see the following figure).

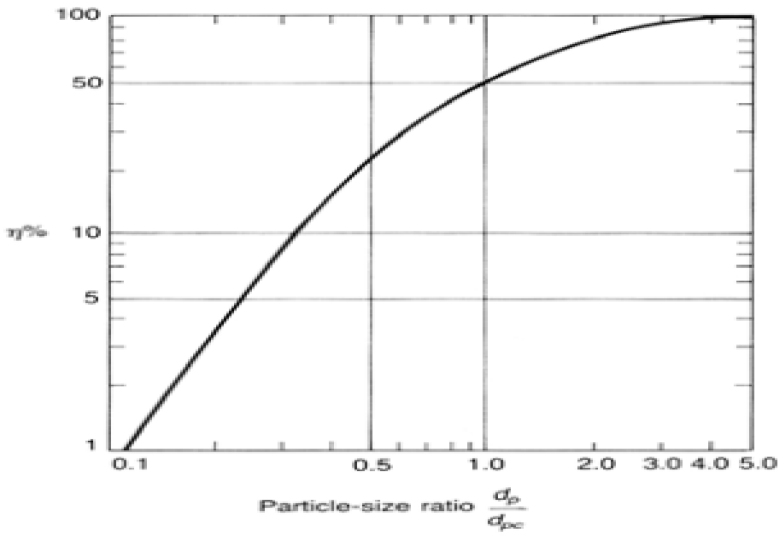

Figure 4.4 Particle collection efficiency versus particle size ratio for standard conventional cyclones

If the size distribution of particles is known, the overall collection efficiency of a cyclone can be predicted by using the above figure. Theodore and DePaola (1980) then fitted an algebraic equation to the curve, which makes Lapple's approach more precise and more convenient for application to computers.

The efficiency of collection of any size of particle is given by:

$$\eta_j = \frac{1}{1+(d_{pc}/d_{pj})^2} \qquad (4.39)$$

$$= \frac{1}{1+(3.14/4.885)^2} = 0.967$$

where: η_j = collection efficiency of particles in the j^{th} size range *(0 < η_j < 1)*

d_{pj} = characteristic diameter of the j^{th} particle size range (in μm).

The overall efficiency, called performance, of the cyclone is a weighted average of the collection efficiencies for the various size ranges, namely

$$\eta = \frac{1.5*\sum \eta_{j*} m_j}{M} \qquad (4.40)$$

$$=1.5 * (0.427 * 0.10 + 0.656 * 0.30 + 0.854 * 0.30 + 0.945 * 0.14 + 0.979 * 0.05 + 0.994 * 0.01) = 0.987$$

where: η = overall collection efficiency $(0 < \eta < 1)$

m_j = mass of particles in the j^{th} size range and *M* = total mass of particles

Table 4.9 Data's for the determination of overall collection efficiency of the cyclone

Size Range of dp (in μm)	***Average Size dp (in μm)***	***Collection Efficiency η***	***Mass Fraction m/M***	***Contribution to Performance η x m /M***
0-2	*1*	*2.9%*	*0.01*	*0.029%*
2-4	*3*	*21.1%*	*0.09*	*1.903%*
4-6	*5*	*42.7%*	*0.10*	*4.268%*
6-10	*8*	*65.6%*	*0.30*	*19.678%*
10-18	*14*	*85.4%*	*0.30*	*25.613%*
18-30	*24*	*94.5%*	*0.14*	*11.953%*
30-50	*40*	*97.9%*	*0.05*	*4.897%*
50-100	*75*	*99.4%*	*0.01*	*0.994%*
			1.00	70.6%

The pressure drop is an important variable to evaluate the performance of the cyclone. The pressure drop was defined as the different between the mean total pressure at the inlet and outlet. About 80% of pressure drop caused by pressure losses inside the cyclone due to rotational turbulent flow and the remaining 20% are caused by contraction of the fluid flow at the outlet, expansion at the inlet and fluid friction on the cyclone wall surface. There is a pressure drop of 100 to 460 Pa in the cyclone depending on the geometry of its outlet pipe (Frederickson, 1999). The desire to minimize the pressure drop is conflicts with the wish to maximize the separation efficiency. The lower the pressure drop, the lower the separation efficiency. Based on this idea, the pressure drop in the cyclone can be taken as the maximum value of the two ranges. This estimation is done in order to maximize the separation efficiency of the cyclone.

Table 4.10 Particle separator dimensional and operational characteristics

Parameter	***Value***
Cyclone diameter (mm)	*150*
Cyclone gas exit diameter (mm)	*75*
Width of Inlet duct (mm)	*112*
height of inlet duct (mm)	*75*
Cyclone body cylindrical height (mm)	*262.5*
Vertical length of cyclone cone (mm)	*262.5*
Cyclone total height (mm)	*530*
Cyclone solids exit diameter (mm)	*54*
Separation efficiency (%)	*98.7*
Pressure drop (kPa)	*0.46*

From the mass flow of the product gas in the gasification process (mass balance), and its density, the gas volumetric flow at the cyclone inlet for the operating conditions of the gasifier (approximately 772 ºC and 101,325 kPa) was calculated.

4.2.6 Fuel Feeding Subsystem

This subsystem is made up of a hopper for the saw dust storage and a feeding assembly composed of a dosing screw and a feeding screw of similar dimensions. The feeding screw has a cooling device that prevents saw dust pyrolysis and carbonization before entering the reactor. The dosing screw (located in the hopper base) supplies saw dust to the feeding screw (located in the fuel supply point) at a programmed rate. The two screws are driven by a motor with a variable frequency drive as a speed controller. The feeding screw introduces the saw dust to the reaction chamber and operates at a greater speed than the dosing screw, to avoid fuel accumulation which causes system blockages.

A) *Screw sizing:* The relation between the saw dust flow with the diameter, pitch, fillet height and revolutions of the screw, is given by the expression in *eqn. (4.41)* (Olivares, 1996):

$$\dot{m}_{SD} = 60 * S * \phi * n * \rho_{SD} * (D * h - h^2) \qquad (4.41)$$

$$n = \frac{25.0385}{(60*0.64*0.25*716*(0.038*0.011 - 0.0112))} = 15rpm$$

The selected outer diameter of the screws was 38mm. A value of 0.25 for the load factor was selected, in agreement with information found in literature (Olivares, 1996). Additionally, the screws' pitch was established being 1.5 times its outer diameter. The fillet height, the outer diameter and the axis internal diameter, were related by the following expression [27]:

$$d = D - 2h \qquad (4.42)$$

$$h = \frac{D-d}{2} = \frac{38-16}{2} = 11mm$$

The selected axis internal diameter was 16mm. Based on the mass balance made for the system and the previous considerations, a 15 rpm value for the shaft of the dosing screw speed were calculated.

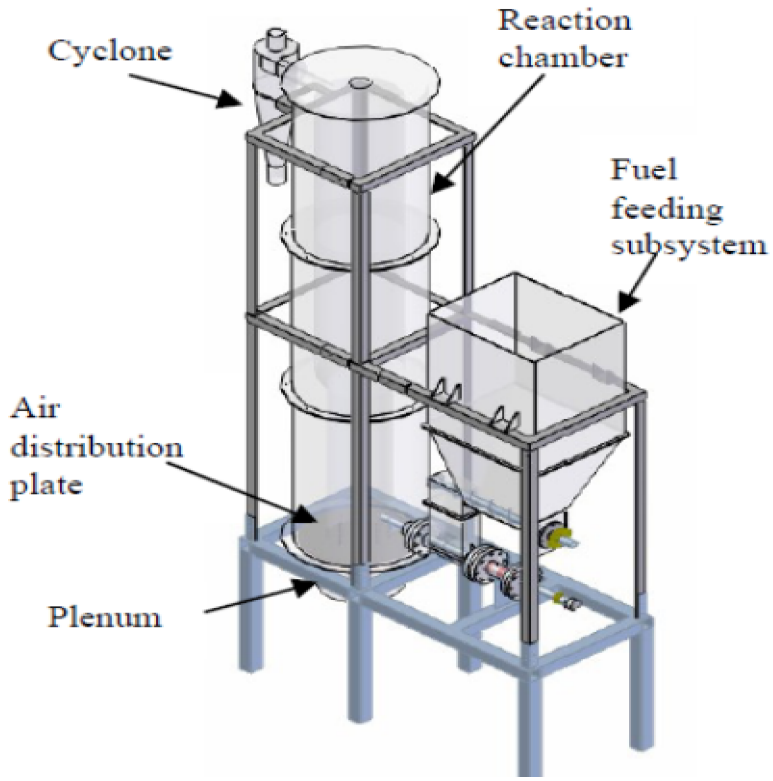

Figure 4.5 3D-assembly drawing of fluidized bed gasifier for saw dust

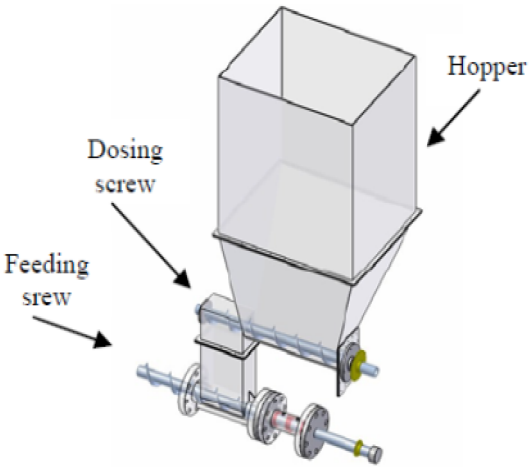

Figure 4.6 Fuel feeding subsystem

B) Determination of the wall thickness of the fuel feeding subsystem

- Material selection

Since there is no high load that applied on the feeding subsystem, the material to be selected is Steel-32 with the following properties. Assuming F.S = 2

$$\sigma_y = 196.2Mpa\,;\sigma_{ult} = 318.24Mpa$$

$$\sigma_{all} = \frac{\sigma_y}{F_S} = \frac{196.2}{2} = 98.1Mpa$$

The section modules of the selected material is given by $S = b * \frac{t^3}{12}$ and from the material property table the section modulus for selected material for rectangular cross section is 256 mm^3 Assuming the width of the top face of the fuel storage is 420mm and its height to be 500mm.

$$t = \sqrt[3]{256 * \frac{12}{420}} = 2.74mm\ take\ it\ to\ be\ t = 3mm$$

$$\rho_{SD} = 716\frac{kg}{m^3},\ d_{SD} = 578 * 10^{-6}\,m,$$

Volume occupied by the feed stock on the fuel storage tank can be determined by multiplying the area occupied by the saw dust particles and the height of the storage tank.

$$A = \frac{\pi}{4} * {d_{SD}}^2 = \frac{\pi}{4} * (578 * 10^{-6}m)^2 = 2.624 * 10^{-7}m^2 \qquad (4.43)$$

$$V = A * h = 2.624 * 10^{-7}m^2 * 0.500m = 1.312 * 10^{-7}m^3$$

Mass of a single fuel particle $= \rho_{SD} * V = 716\frac{kg}{m^3} * 1.312 * 10^{-7}m^3 = 9.4 * 10^{-5}kg$

Since the numbers of particles are not known, let assume the storage tank can store 50 kg feed stock which is its maximum storage capacity. So, the force applied on the storage tank is the weight of the feed stock which is:

$$W_1 = m * g = 50kg * 9.81\ \frac{N}{kg} = 490.5N \qquad (4.44)$$

Assuming the mass of the temporary storage, the bolts, the bearing and all other components and the mass of the screw feeder are cumulatively to be 45 kg and its weight to be

$$W_2 = 45kg * 9.81\frac{N}{kg} = 441.45N$$

$$W_t = W_1 + W_2 = 490.5N + 441.45N = 931.95N$$

Analysis of buckling of the columns on which both the reaction chamber and the feed stock storage are located is stated below. Each column is assumed to behave like a simple beam with two pin jointed supports, subjected to the breaking force F_b in its longitudinal direction.

C) Determination of the thickness of the columns and the beams

- Stresses due to buckling ($\sigma_{c\,induced}$)

Applying Rankine-Gorden formula for short column

$$\sigma_{c\,induced} = \left(\frac{Fb}{A}\right) * (1 + a * \left\{\frac{Lk}{K}\right\}^2 \qquad (4.45)$$

The length of the bottom stand *is* L_k = 40 mm

$K = \frac{\sqrt{I}}{A}$, *slenderness ratio and* $I = L_k * \frac{w^3}{12}$; $A = h * w$ *and* $\frac{I}{A} = \frac{\left(L_k * \frac{w^3}{12}\right)}{(L_k * w)} = \frac{w^2}{12}$

$K = \frac{w}{12^{0.5}}$, for w = 8mm, $K = \frac{8}{3.464} = 2.31$ and $a = \frac{1.45}{25000}$ for one end fixed and the other imperfectly fixed.

The critical load applied on the bottom stands include all the loads imposed on all of the six stands.

$$Fb = 9.81\frac{N}{kg} * \left(m_{rc} + m_{Cy} + m_{sand} + m_{dp} + m_{plenum}\right) \qquad (4.46)$$

Assuming the mass of the distributor plate and plenum cumulatively to be 15kg

$$D_{ro} = D_{ri} + 2 * t = 400mm + 2 * 6mm = 412mm$$

$$V_{rc} = \left(\frac{\pi}{4} * {D_{ro}}^2 * H - \frac{\pi}{4} * {D_{ri}}^2 * H\right)$$

$$= (196.64 * 10^6\, mm^3 - 185.35 * 10^6 mm^3) = 11.292 * 10^6 mm^3$$

$$m_{rc} = V_{rc} * \rho_{s-37} = 11.292 * 10^6 mm^3 * 1750\frac{kg}{m^3} = 19.761\, kg$$

$$V_{cy} = \frac{\pi}{4} * {D_{cyo}}^2 * H - \frac{\pi}{4} * {D_{cyi}}^2 * H$$

$$= \frac{\pi}{4} * 1902 * 762 \; - \frac{\pi}{4} * 1742 * 762 \; = \; 3.4855 * 10^6 mm^3$$

$$m_{\,cy} = \; V_{cy} \; * \rho_{s-37} \; = \; 3.4855 * 10^6 mm^{\,3} * 1750 \; \frac{kg}{m^3} = \; 6.10 \, kg$$

The mass of the bed material (sand) is known to be 30 kg taken.

$$Fb \; = 9.81 \; \frac{N}{kg} * \; (19.761 + 6.10 \; + 30 + \; 15) kg \; = \; 696N$$

$$\sigma_{c\,induced} = \; \left(\frac{Fb}{A}\right) * \; (1 + a \; \left[\frac{Lk}{K}\right]^2 = \; (\frac{695}{(40 \, * 8)}) * \; (1 + \frac{1.45}{25000} * \left\{\frac{40}{2.31}\right\}^{\,2} = \; 40.71 MPa$$

The permissible buckling resistance for steel – 37 is 140N/mm^2

Since, $\delta_{c\,induced} = \; 40.71 MPa \; < \; \delta all \; = \; 140 MPa$*. So, the design is safe for buckling.*

- Stresses due to bending ($M_{induced}$)

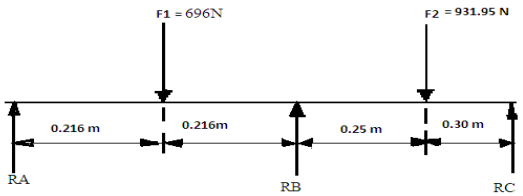

Figure 4.7 Free body diagram of the force applied on the beams

$$M_A = 0 \quad F_1 * 0.216 \; - \; F_2 * 0.682 \; + R_B * 0.432 \; + \; R_C * 0.982 \; = \; 0 \qquad (4.47.a)$$

$$R_B = \; (931.95 * 0.682 - \; 696 * 0.216 \; - \; 0.982 * R_C)/0.432$$

$$\Sigma F_Y = 0 \quad R_A \; + \; R_{\,B} + \; R_C = \; 931.95 \; + 696 \; = \; 1627.95N$$

$$M_c = 0 \qquad 696 * 0.766 - \; 931.95 * 0.3 \; + R_B * 0.55 - \; R_A * 0.982 \; = \; 0 \qquad (4.47.b)$$

$$R_B \; = \frac{0.982 * R_A - 253.551}{0.55}$$

$$M_B = 0 \qquad F_1 * 0.216 \; - \; F2 * 0.766 \; + R_A * 0.432 \; + \; R_C * 0.55 \; = \; 0 \qquad (4.47.c)$$

$$R_{\,C} = \frac{563.5377 - R_A * 0.432}{0.55}$$

Substituting the value of R_C from eqn. (4.47.c) to eqn. (4.47.a) and then substituting the value of R_A to eqn. (4.47.b). So, the value of R_B = 443N, R_A = 745N and R_C = 439N. Since it has six columns, the load can divide to six equal parts. The maximum induced bending moment is takes place or located at the middle of the beam.

$$M_{induced} = R_A * 0.491 - F_2 * 0.241$$

$$= 745 * 0.491 - 931.95 * 0.241 = 141.2Nm$$

From the material property table there is:

$$\delta_y = \frac{220N}{cm^2}, S = 187mm^3 \quad Then \quad M_{all} = \delta_y * S = \frac{220N}{mm^2} * 187mm^3 = 142.4\,Nm$$

Since $M_{all} > M_{induced}, 142.4Nm > 141.2Nm$ and the design is safe for bending.

From this value of section modulus we can get the thickness of the column

$S = \frac{M}{\delta y} = \frac{1}{6} * b * t^2 = 187mm^3$ And then,

$$t = \left(6 * \frac{S}{b}\right)^{1/2} = \left(6 * \frac{1247mm^3}{40mm}\right)^{\frac{1}{2}} = 3.058mm$$

For more safety say, t = 4mm

So, the column can support the whole weight of the mechanism and the design of the column is safe.

D) Design of the Screw Feeder

The screw feeder is the main rotary part of a machine that is used for power and torque transmission. For this design, the power transmission is based on the power transmitted by the motor.

Power transmitted by motor = 1.5kw, Assume Speed of the screw feeder = 20rpm

Outer diameter of the screw feeder = 38mm

Now the speed of the screw feeder shaft is calculated as

$V = \pi * D * \frac{N}{60}$ Where N = number of revolution of the screw

D = the outer diameter of output screw feeder =38mm

$$V = \pi * 0.038 * \frac{20}{60} = 0.04 \frac{m}{s}$$

Torque transmitted by the screw to be design

$$T = 60 * \frac{P}{(2*\pi*N)} = 60 * \frac{1.5KW}{(2*\pi*20rpm)} = 42.97\ Nm$$

Since the screw feeder shaft and the dosing screw shaft for this design are integral, the power transmitted by the screw feeder shaft is transmitted to the driving pulley of the dosing screw with some slip losses.

- Material Selection

The material of the screw feeder to be select should have the following properties: good strength, malleable and ductile, easily and locally available, cost effective and high corrosion resistance. Based on the above criteria, there is a need to select steel-37 because it fulfills all criteria.

Now let determine the loads applied on the screw feeder and calculate the bending of the screw.

The force applied on the screw shaft is the total load applied on the dosing screw.

$$F = (55kg + 45) * 9.81 = 981N$$

The weight of the machine applied between the two bearings is assumed to be 15Kg *9.81 = 147.15N by assuming the mass of the machine on the dosing screw is 15Kg.

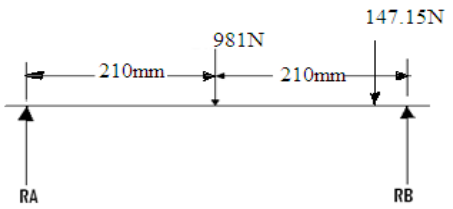

Figure 4.8 Force Moment Diagram

Now let calculate the two reactive forces RA & RB by taking zero moment at one point.

$$\Sigma M_A = 0, R_B * 420 = 981 * 210 - 147.15 * 410 \qquad (4.48)$$

$$R_B = 346.85N$$

$$Then \uparrow + \Sigma Fy = 0, \quad R_A = 981 + 147.15 - R_B = 781.3N$$

Now let us determine the moment at each point where the load is applied.

At point A, $M_A = 0$

At point B, $M_B = 981 * 0.21 = 206\ Nm$

At point C, $M_C = 981 * 0.21 - 147.15 * 0.41 = 145.68\ Nm$

At point D, $M_D = 145.68\ Nm - 346.85 * 0.42 = 0Nm$

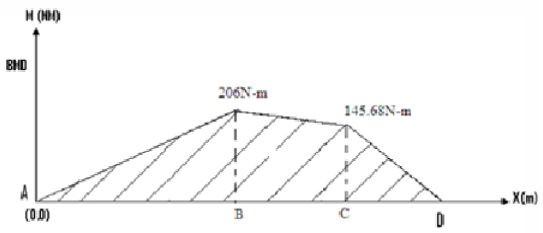

Figure 4.9 Bending moment diagram

$$M_{max} = 206\ Nm$$

Based on the maximum shear stress theory (MSST), let determine the effective torque of the shaft. Factor of safety is assumed to be 2.

$$T_e = \sqrt{\left(M_{max}{}^2 + T_{max}{}^2\right)} = \sqrt{(206^2 + 42.97^2)} = 210\ Nm$$

But $T_e = \frac{(\pi * \tau_{all} * ds^3)}{16}$, $ds^3 = 16 * \frac{Te}{(\pi * \tau_{all})}$

Where, $\tau_{all} = \frac{\tau_y}{Fs} = \frac{\delta y}{(2*Fs)}, \frac{\delta_y}{2} = \tau_y$

$$\tau_{all} = \frac{Te}{(2*Fs)} = \frac{210MPa}{(2*2)} = 52.5MPa$$

$$ds^3 = 16 * \frac{Te}{(\pi * \tau_{all})} = \frac{(16*210)}{\left(\pi * 52.5 * 106 \frac{N}{m^2}\right)}$$

$$d_s = 34.58mm$$

By considering the clearance and allowance of machining process, it has been taken to D_s = 38mm.

4.2.7 Selection of Bearing

Bearing is an element that is used for rotating of the shaft easily and smoothly. According to the function and shape there are many different types of bearings such as ball bearings, thrust bearings, tapered bearings etc.

Table 4.11 Design matrix for selection of bearing

Types of bearing	***Supported load***	***Cost***	***Availability***
Ball bearing	Radial	Low	High
Thrust bearing	Axial	Medium	Medium
Tapered bearing	Both	High	Medium

Based on the above design matrix and for this design the load applied on the bearing is radial, the ball bearing is selected .All dimensions of the bearing is selected from the standard table based on the internal diameter of the screw (d = 18mm) and those dimensions are stated below.

The bore diameter of the bearing = 38mm, external diameter of the bearing = 85mm and width of the bearing = 16mm. Based on the bore diameter of the bearing from standard table the rated capacity of the bearing is 2.5KN.

The total radial load applied on the bearing is the sum of the load of the component and the damaging force of the belt.

Fr = 1128.15N = 1.12815KN.

L_R =life corresponding to rated capacity is $9*10^7$ revolution. From standard table, the design life of the ball bearing of a machine that give a 24hr service and support relatively medium load application is in the range between $(30-40)$ thousands of hours .To be more safe we have to select the minimum value (30000 hours).

$$L = life\,required\,by\,the\,application = speed\,of\,the\,shaft * design\,life * 60\frac{min}{hour}\ \ rpm * 30000\,hours * 60\frac{min}{hour} = 27 * 106rpm = 3.4\,years\,and\,take\,L = 3\,year$$

The required rated capacity of the bearing (Creq) is given by:

$$C_{req} = F_r * \left(\frac{L}{LR}\right)^{0.3} = 1.12815 * \left(27 * \frac{106}{(90*106)}\right)^{0.3} = 0.786KN$$

Since, $C > Creq\ i.e.\ 2.5KN > 0.786KN$. So, the selection of bearing is safe

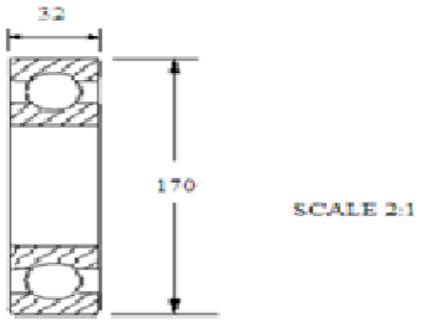

Figure 4.10 Simple representation of ball bearing

4.3 Mass and Energy Balance

4.3.1 Mass Balance

For the development of the mass balance of the process, data reported in literature referring to typical concentrations of carbon monoxide (CO), hydrogen (H_2) and methane (CH_4) of the energetic gas produced were used (Sanchez, 1997). Also, the results of the hydrodynamics parameters and the saw dust elemental analysis showed in table 4.12 were considered. Table 4.13 shows the values of typical volumetric concentrations expected for carbon monoxide, hydrogen and methane in a fluidized bed gasifier by using saw dust as fuel and air as the gasifying agent.

Table 4.12 Saw dust elemental analysis (dry basis)

Parameter	***Value***
Carbon	47.5
Hydrogen	6.10
Oxygen	45.5
Ash	0.89

Table 4.13 Expected concentrations of the energetic compounds in the fuel gas (% volumetric)

Energetic gas	***Value***
CO	22.0
H_2	20.0
CH_4	4.5

In addition to the compounds referred in table 4.11, the fuel gas will contain typical products of combustion, with the exception of oxygen which will be present in an insignificant amount. The CO_2, H_2O and N_2 proportions in the fuel gas will depend on the fuel chemical composition and the amount of air in the reaction. According to this, the following global reaction of the gasification process was raised.

$$X_1 * (3.96C + 6.05H + 2.84O) + X_2 * (O2 + 3.76N_2) + XH_2O + YH_2O$$

$$\longrightarrow X_6 * (22CO + 23H_2 + 3CH_4 + X_3H_2O + X_4CO_2 + X_5N_2) \qquad (4.49)$$

The water contents in the saw dust and the air were obtained by means of the saw dust immediate analysis shown in table.4.14, and the local atmospheric air average psychometrics properties presented in Table 4.15.

Table 4.14 Saw dust immediate analysis (%, dry basis)

Parameter	***Value***
Moisture content	6.11
Fixed carbon	15.82
Volatile matter	74.6
Ash	0.89

Table 4.15 Atmospheric air psychometrics properties in Addis Ababa

Parameter	***Value***
Saturation pressure at room	
temperature (kPa)	3,168
Atmospheric pressure (kPa)	101,325
Relative humidity (%)	60.74

Air flow: From the fluidization parameters previously established, the air mass flow necessary for the process was determined through the expression:

$$\dot{m}a = \frac{3600*(Uf*A*\rho a)}{3.14} + (0.648 * b) \qquad (4.50)$$

$$= \frac{3600*(0.34*0.1256*1.171)}{3.14} + (0.648 * 0.72) = 62.25\ \frac{kg}{hr}$$

With this value, the reaction coefficient related to the air necessary for gasification was obtained.

$$X_2 = \frac{\dot{m}a}{4.76.Mwa} \qquad (4.51)$$

$$= \frac{62.25}{4.76*137.28} = 0.095$$

Air-flow rate was calculated assuming that the source of nitrogen was from air only and thus atmospheric mass proportion of nitrogen was utilized for the calculation.

Global gasification reaction coefficients: From the molar balances for each element in eqn. (4.52), the global gasification reaction coefficients were obtained:

$$8.1(3.96C + 6.05H + 2.84O) + 13(O_2 + 3.76N_2) + 1.54H_2O + 0.72H_2O$$

$$\longrightarrow 0.696 * (22CO + 23H_2 + 2.75CH_4 + 10H_2O + 21CO_2 + 49N_2) \qquad (4.52)$$

Saw dust, produced gas and ash mass flows: Based on the stoichiometric balance previously made, the saw dust mass flow was calculated:

$$\dot{m}_{SD} = 3 * R + 0.648 * a \qquad (4.53)$$

$$= 3 * 8.1 + 0.648 * 1.54 = 25.3 \frac{kg}{hr}$$

For the calculation of the total amount of solid wastes resulting from the gasification process, a value of 20% of residual carbon not converted (Barriga, 2002) was added to the ash content presented in table 4.10, obtaining the following relation:

$$\dot{m}_w = 0.22 * \dot{m}_{SD} \quad (4.54)$$

$$= 0.22 * 25.3 = 5.566 \frac{kg}{hr}$$

Therefore, the fuel gas mass flow produced was determined from the mass balance. Table 4.16 shows a summary of the obtained results.

$$\dot{m}_g = \dot{m}_{SD} + \dot{m}_a - \dot{m}_w \quad (4.55)$$

Table 4.16 Mass flows of the saw dust gasification.

Parameter	***Value (kg/hr)***
Saw dust mass flow	25.3
Air mass flow	62.25
Solid wastes mass flow	5.566
Produced gas mass flow	81.984

Equivalence ratio: The equivalence ratio of the gasification process is one of the most important parameters for the adjustment of the operating conditions [27]. Its value is defined as:

$$\xi = \frac{(RA/C)\, r}{(RA/C)\, s} \quad (4.56)$$

where, the air-fuel real relation is calculated from the expression:

$$\left(\frac{RA}{C}\right) r = \frac{\dot{m}_a}{2.192 * \dot{m}_{SD}} \quad (4.57)$$

$$= \frac{62.25}{2.192 * 25.3} = 1.122$$

The air-fuel stoichiometric relation was calculated from the expression (Sánchez, 1997):

$$\left(\frac{RA}{C}\right) s = 8.89 * (\%\, C + 0.375 * \%\, S) + 26.5 * \%H - 3.3 * \%O \quad (4.58)$$

$$= 8.89 * (47.5\% + 0.375 * 0\%) + 26.5 * 6.10\% - 3.3 * 45.5\%) = 4.4$$

So, from Eqn. (49), the equivalence ratio will be: $\xi = \frac{1.122}{4.4} = 0.255$

In agreement with the established mathematical model, an equivalence ratio of 0.25 was obtained.

4.3.2 Energy Balance

The energy balance of the gasification process was established by *eqn. (4.59):*

$$E_{SD} + E_a = E_g + E_l \quad (4.59)$$

E) Saw dust and fluidization-gasification air energy:

From the saw dust's lower heating value (*12.28 MJ/kg dry bases*) and its mass flow, the energy available in the Saw dust was obtained:

$$E_{SD} = \frac{\dot{m}_{SD} * LHV_{SD}}{3600} \quad (4.60)$$

$$= \frac{25.3 * 12.28}{3600} = 86.3 \text{ KW}$$

Because the atmospheric air entering the reactor is considered to be at the same reference temperature (25°C), the fluidization-gasification air energy is nil.

Produced gas energy or gas power: The energy contained in the synthesis gas produced by the process was obtained by means of the following expression.

$$E_g = E_u + E_s \quad (4.61)$$

$$= 53 + 14.25 = 67.25\ Kw$$

Where the useful energy corresponds to the chemical energy of the energetic gaseous mixture is:

$$E_u = \frac{\dot{m}_g * LHV_g}{8.6 * \rho_g} \quad (4.62)$$

$$= \frac{81.984 * 6.335}{8.6 * 1.171} = 53\ KW$$

Where:

$$LHV_g = 0.1263 * (\%CO) + 0.358 * (\%CH_4) + 0.1079 * (\%H_2) \quad (4.63)$$

$$= 0.1263 * (22\%) + 0.358 * (3\%) + 0.1079 * (23\%) = 6.335 \frac{MJ}{Nm^3}$$

The other term, the sensible energy of the produced gas, incorporates the enthalpy of each component of the synthesis gas at its exit temperature.

$$E_s = \frac{\dot{m}_g.\Sigma(y_i.h_i)}{3{,}600\ .\Sigma(y_i\ .Mw_i)} \qquad (4.64)$$

$$= \frac{\left|81.984\left|\left(0.03\left(-74.8\right)+0.065\left(-393.5\right)+0.22\left(-110.5\right)\right)\right|\right|}{3{,}600\left(0.03\ 16+0.065\ 44+0.22\ 28\right)} = 14.25\ KW$$

Energy losses: The energy losses in the solid wastes and to the atmosphere closed the energy balance:

$$E_{\ l} = E_{wall} + E_W \qquad (4.65)$$

The energy contained in the wastes is given by the expression:

$$E_W = E_{cw} + E_{ash} \qquad (4.66)$$

$$= 14.5 + 3.14 = 17.64\ Kw$$

Where, considering the previously presented value of 20% of residual carbon in the solid wastes (Barriga, 2002):

$$E_{cw} = \frac{0.20.\dot{m}_w.(LHV_{cw}+h_{cw})}{3{,}600} \qquad (4.67)$$

$$= \frac{0.20\ 5.566\ (11.6+35.32))}{3{,}600} = 14.5KW$$

On the other hand, the energy loss by sensible heat in the ashes was calculated from the following expression (Sanchez, 1997):

$$E_{ash} = \frac{((0.80.\dot{m}_w).(820+1.67.(T_{ash}-273)))}{3{,}600} \qquad (4.68)$$

$$= \frac{((0.80\ 5.566\ )\ (820+1.67\ (1301-273)))}{3{,}600} = 3.14\ KW$$

4.4 Gasification Efficiency

The gasifier efficiency is expected to be 76 %, and complete gasification of sawdust fed is anticipated. Also, since the sawdust obtained from the saw mill is expected to be wet, it is pre-dried to a value below 10 % wt moisture on a wet basis, to allow proper gasification with good heating value of product gas.

Table 4.17 Inputs parameters for the determination of the performance of the gasifier

Design Parameters	***Value***	***Unit***
Heating value of gas, H_g	6763.80	$kJ/(Nm^3)$
Gas volumetric flow, Q_g	0.0641	$(Nm^3)/s$
Gas density, ρg	0.2816	kg/m^3
Gas Specific Heat, cp	1.391	$kJ/(kg^oC)$
Heating value of Solid, H_s	15127	kJ/kg
Solid Fuel Consumption, M_s	30.105	kg/hr
Solid Fuel Inlet Temp, T_{is}	25	o_C
Gas Outlet Temp, T_{os}	750	o_C
Air volumetric flow, Qa	0.033	$(Nm^3)/s$

$$\eta_{Gas} = \frac{661*[(H_g*Q_g)+(Q_g*\rho_g*C_p*\Delta T)]}{(H_S*M_S)} \qquad (4.69)$$

The higher heating value (HHV) for the predicted composition of product gas is calculated using the mole fraction and individual HHV. This value is subsequently converted to lower heating value (LHV) of gas using the rule of thumb that LHV is approximately 90 % of the HHV for gas eous combustibles. Using the input parameters from table 4.16, the gasification efficiency can be determined as follows.

$$\eta_{Gas} = \frac{661*[(6763.80*0.0641) + (0.0641*0.2816*1.391*(750-27)]}{(15127*25.3)} = 78\%$$

The calculated value of the efficiency of the gasifier is similar to the expected value with greater than by two percent.

CHAPTER 5

RESULT AND DISCUSSION

5.1 Comparison of Experimental and Model Results

Table 5.1 shows the comparison between the experimental results available from literature and predicted values from the model. Results are compared with the corresponding references [1, 2]. H_2 and CO composition as reported by Bilbao et al. [29], is the average of 57 test runs with the temperature around 700-900^oC for most of the experimental duration. They used powdery cellulose and pine sawdust as their feedstock with equivalence ratio between 0.268-0.43. H_2 and CO data from Bilodeau et al. [22] is from experiment conducted in the bubbling fluidized bed gasifier with capacity of 25-50 kg/hr and equivalence ratio of 0.247. Comparison for both Bilbao et al. [29] and Dutta et al. [19] was done with syngas composition at temperature close to this model.

Table 5.1 Comparison between the experimental results available from literature and predicted values from the model

Moisture Content, (wet basis)	***Ultimate Analysis, wt.% (dry basis)***			***H2, % vol. (moisture free basis)***		***CO, % vol. (moisture free basis)***		***CH_4, % vol. (moisture free basis)***	
	C	H	O	Mod	Expt.	Mod	Expt.	Mod	Expt.
0	47.5	6.11	45.5	27.46	16.05	11.9	10.04	12.45	6.81
6.7	47.5	6.11	45.5	22.15	15.07	25.96	24.1	3.25	3.15
12	47.5	6.11	45.5	21.5	18.3	23.8	20.2	2.50	2.23
20	47.5	6.11	45.5	16.5	14.2	19.1	18.23	1.702	1.52

As can be seen from table 5.1, the predicted result is in good agreement with the experimental results obtained from the specified literature. But the composition of syngas predicted by the model is generally higher than the concentration obtained from experiments for many cases.

5.2 Effect of Equivalence Ratio on Syngas Composition

Figure 5.1 show the effect of ER, on H_2, CO, CO_2 and CH_4. The figure shows higher ERs imply less oxygen entering the gasifier for the reaction $C + \frac{1}{2}O_2 \rightarrow CO$; thus, there are more C atoms available to react with the steam to produce H_2 via the reaction $C + H_2O \rightarrow CO + H_2$. The CO produced by the reactions of C with steam and C with oxygen reacts with the remaining steam to produce more H_2 and CO_2 (shift reaction). More C atoms consumed by the shift reaction $(CO + H_2O \rightarrow CO_2 + H_2)$ that implies less C atoms leaving as CO. The CO mole fraction increases with increased ER until ER = ~0.25 beyond which it starts to decrease. The lowest value of CO is reached at ER = 1.0 (stoichiometric reaction) while the maximum (~25.96 %) is attained at *ER =~2.5*.

The concentration of H_2 decreases monotonically and it crosses the CO curve at ER of 0.32. At ER < 0.32, increased ER decreases very strongly the concentration of H_2 but at ER > 0.32, the effect of the ER on the fraction of H_2 is rather weak. At ER < 0.27, the CO_2 decreases with increased ER whereas at ER > 0.27 increasing ER produces mixtures rich in CO_2. This is because of the higher steam concentration in the reactor, which favors the reaction of CO with steam (shift reaction) to produce more H_2 and CO_2. As shown in figure 5.1, more available *H* atoms in the gasifier lead to *CH_4-rich* concentrations and it is evident that at *ER < 0.23*, the concentration of CH_4 is decreases very strongly and beyond that the production of CH_4 nearly constant and a weak function of ER. In general, these results show that at *ER < 0.25* (increased oxygen through air), the concentration of CO increases and that the concentration of CO_2 and H_2 decrease with increased ER.

Being typical for the saw dust gasification, as expected, for the whole range of ERs considered, the yields of CH_4 (1.2-12.6 mol/kg - biomass) was much lower than that of CO (8-26 mol/kg-biomass) and H_2 (9-28 mol/kg - biomass).

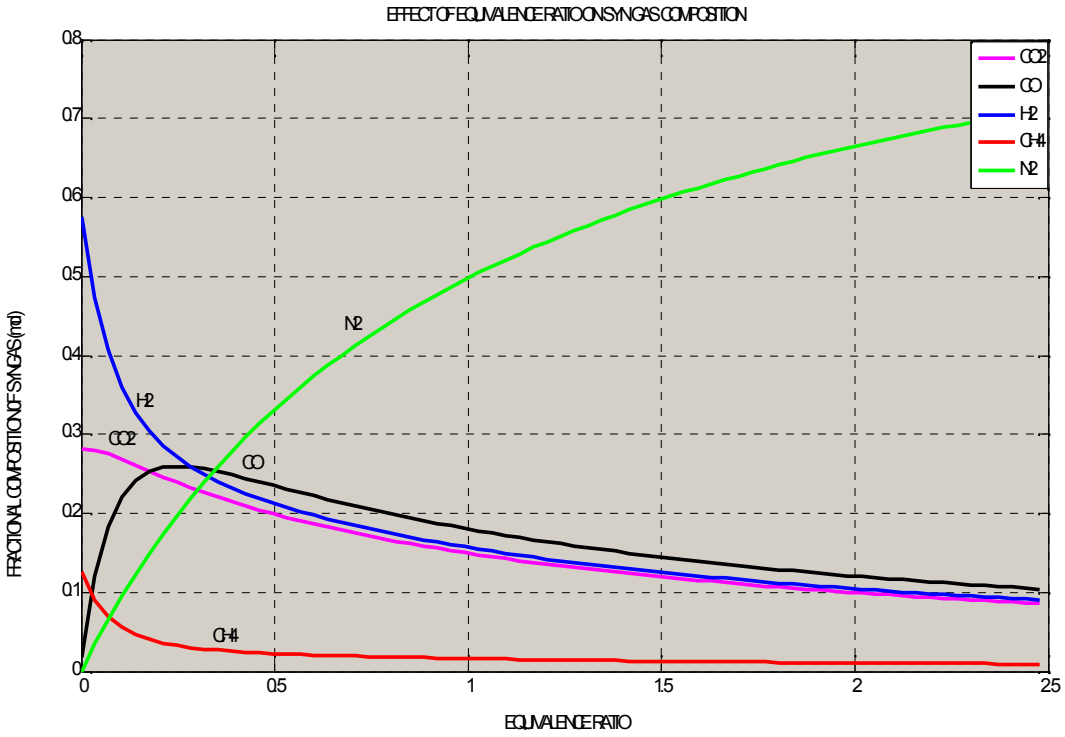

Figure 5.1 Effect of equivalence ratio on syngas composition

A further increase in ER brings about a decrease in the concentration of CO and a substantial increase in CO_2 concentration in dry gas product. This is because of the increasing role of the char combustion in the bed compared to its gasification reaction, which results in lower concentration of combustible gases and higher CO_2. These results are in agreement with the previous result published by Gil. Lim reported the same trend of gas composition changes with air ratio (ratio of actual air to stoichiometric required air) in a circulating fluidized.

5.3 Effect of Temperature on Syngas Composition

Figure 5.2 shows the increase in volumetric fraction of CO with increase in temperature up to its maximum level and then its volumetric fraction decreases with increase in temperature. The lowest value of CO is reached at the temperature of 592°C while the maximum (~25.96 %) is attained at the temperature of 772.5 °C.

The concentration of CH_4 and H_2 decreases with the gasification temperature. This decrease is due to the increase in dilution by N_2 at higher temperature because the equivalence ratio adjusts itself to meet the adiabatic condition.

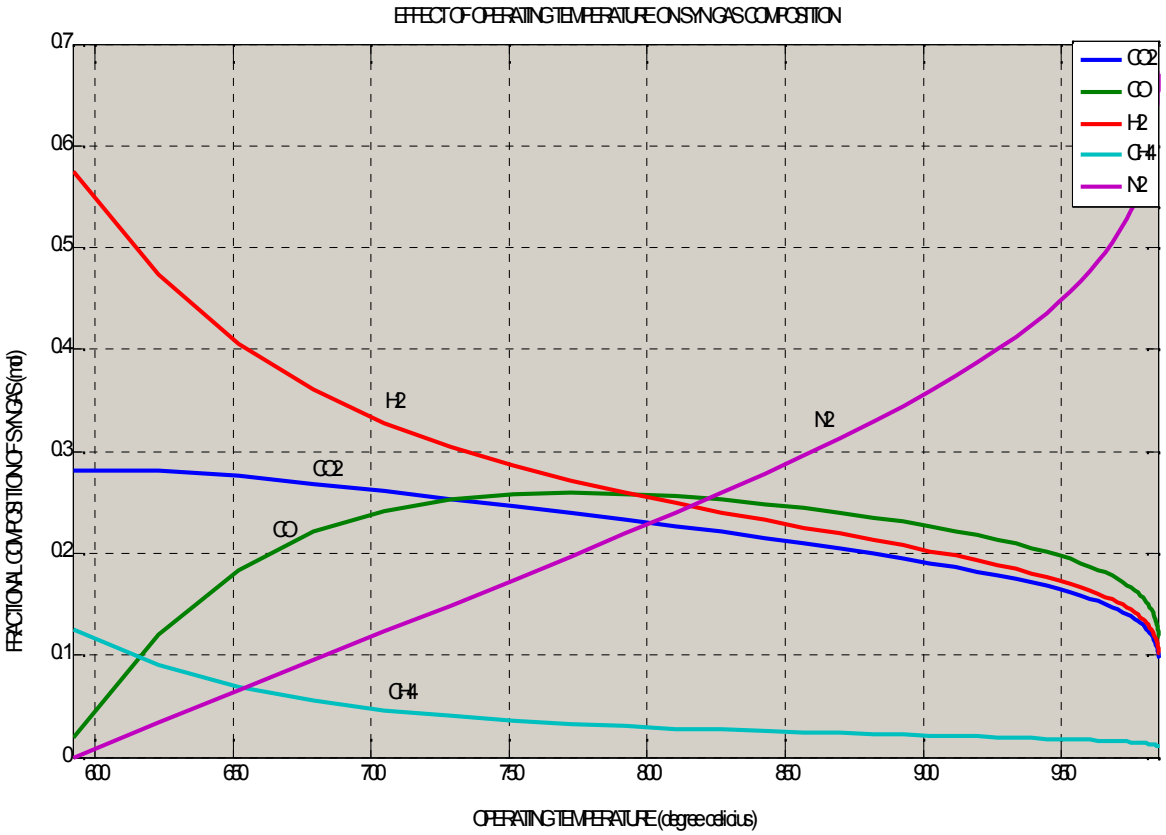

Figure 5.2 Effect of temperature on syngas composition

5.4 Effect of Equivalence Ratio on the Operating Temperature

As shown from figure 5.3, as the equivalence ratio increase the operating temperature of the system increases exponentially up to the maximum operating temperature of the system and beyond which its values becomes constant and the effect of the ER on the operating temperature of the system is rather weak.

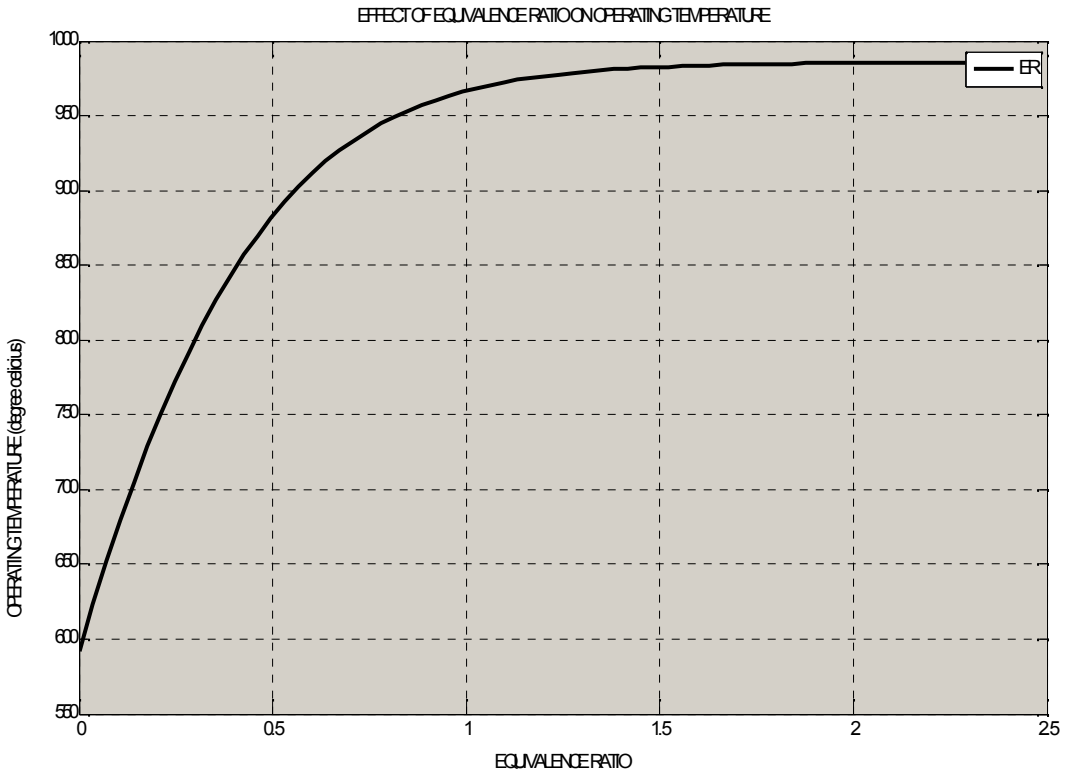

Figure 5.3 Effect of equivalence ratio on the operating temperature of the system

5.5 Effect of Moisture Content on Syngas Composition

Figure 5.4 shows the effect of moisture content on the syngas composition. The concentration of CO increased from 11.9 vol. % to 25.96 vol. % with the change in moisture content from 0 to 6.7 wt. % and started decreasing thereafter with further increase in moisture content. The concentration of H_2 decreased monotonically with increase in moisture content. H_2 decreased from 57.46 vol. % to 9.01 vol. % with an increase in moisture from 0 to 41.86 wt. %. The concentration of CH_4 decreased from 12.45 vol. % to 3.25 vol. % with the change in moisture content from 0 to 6.7 wt. % and then after its concentration decreased insignificantly with further increase in moisture content.

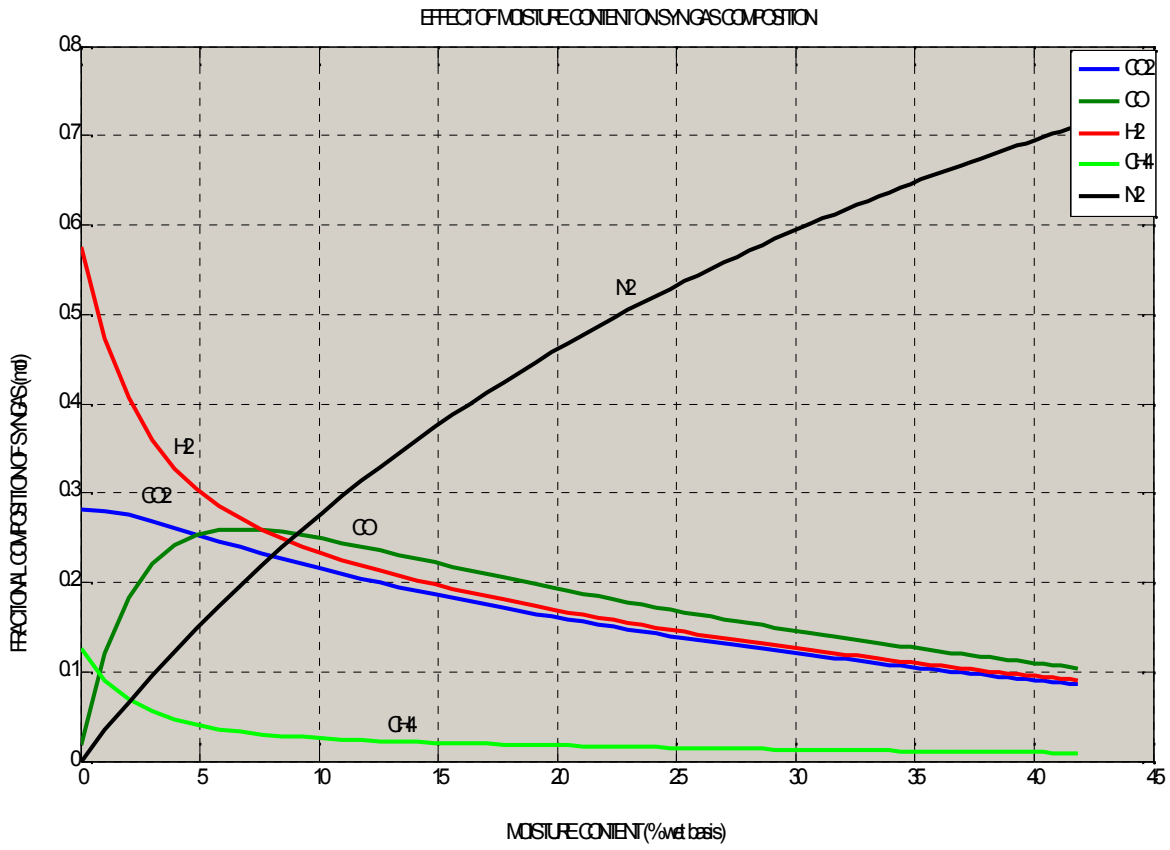

Figure 5.4 Effect of moisture content on the syngas composition

5.6 Effect of Equivalence Ratio on the HHV of Syngas

As shown from figure 5.5 the heating value of the product gas decreases by increasing ER because of the larger contribution of CO_2 in the yield of gaseous product. This, in turn, is a result of a higher contribution of combustion (of char, tar, and other combustible gases) and a lesser contribution of gasification in the overall reactions with increasing ER. The dilution of the product gas by N_2 also contributes to the lower HHV at higher ER.

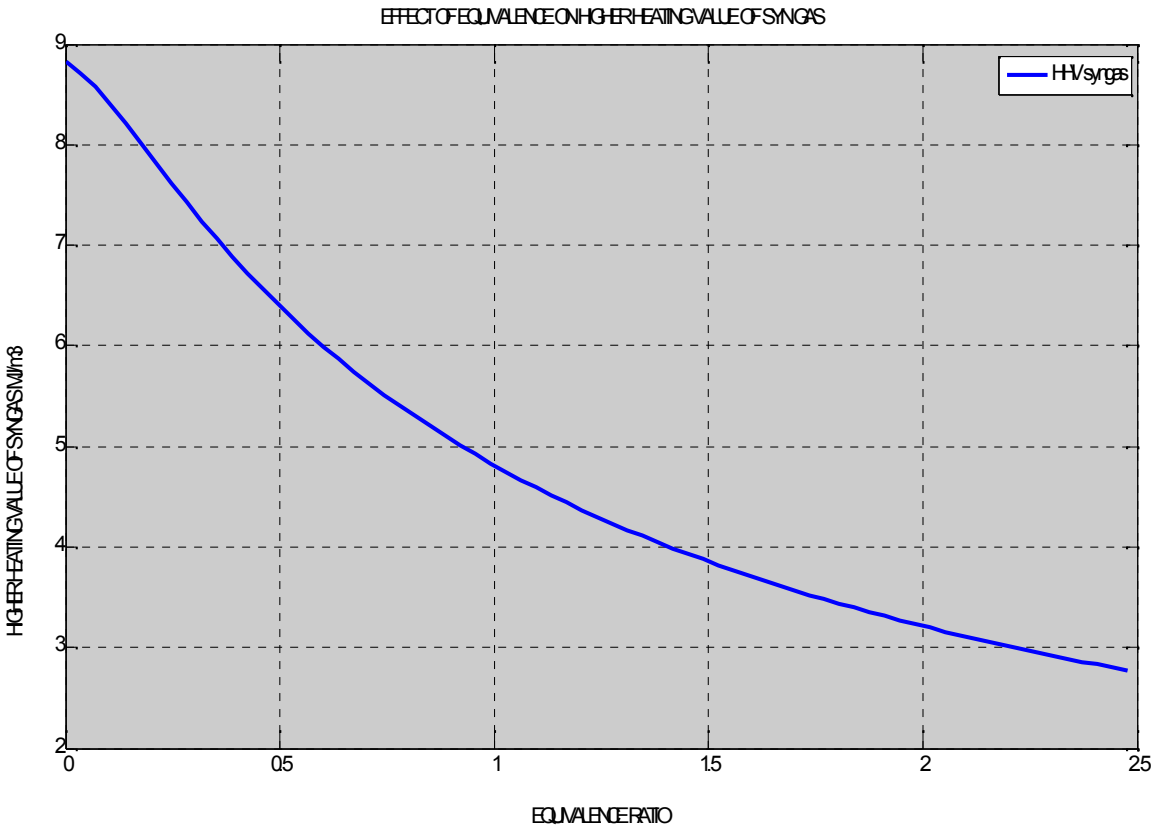

Figure 5.5 Effect of equivalence ratio on the HHV of syngas

5.7 Effect of Equivalence Ratio on Tar and Char Composition in Syngas

Many referenced literatures stated that the composition of tar should be below 10 mg/Nm^3 for normal function of the fluidized bed gasifiers. In the present study the tar composition below 2mg/Nm^3 for the equivalence ratio greater than 0.2 is obtained. This value is shown in the following figure.

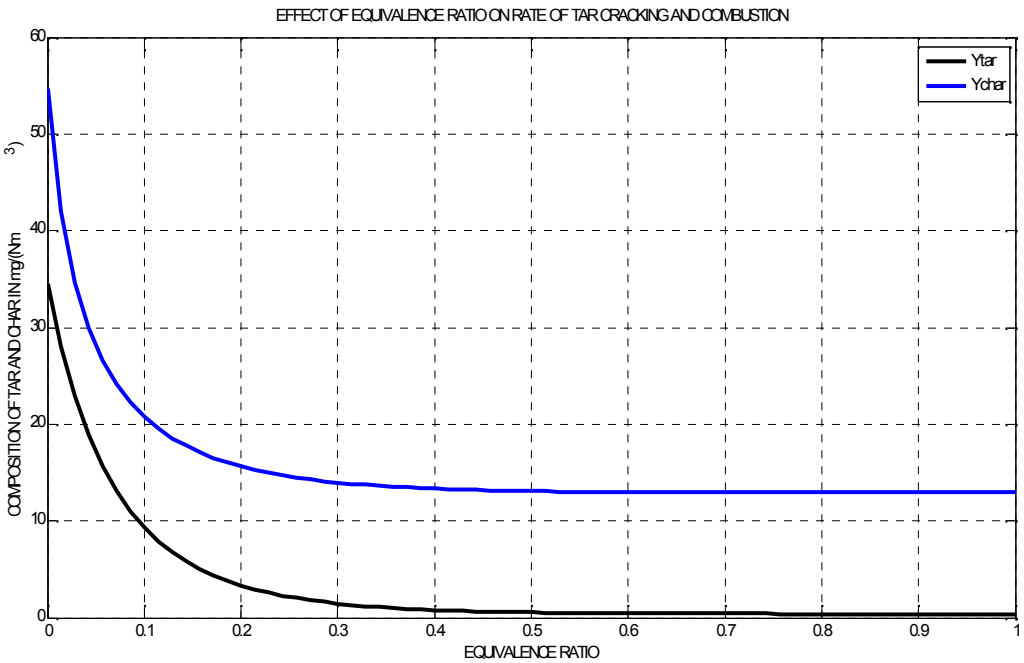

Figure 5.6 Effect of equivalence ratio on tar and char composition in the syngas

As shown from figure 5.6, tar and char concentration decreases with increase in ER, leading to trace formation of tar at ER of above 0.35. This is mainly due to two reasons: (i) higher temperature as a result of higher ER increases reaction rates of the chemical products; and (ii) high ER supplies additional oxygen for cracking of tar into lower hydrocarbons, CO_2 and H_2O.

Generally, the model predicts the amount of tar content in the produced gas. The effect of ER on tar content predicted by the model is presented in figure 5.6. As has been well established, an increase in ER promotes combustion of produced tar and thus reduces the tar content in the exit gas.

CHAPTER 6

SUMMARY, CONCLUSIONS AND RECOMMENDATIONS

6.1 Summary

Although biomass gasification is not a new concept by itself, current energy scenario and significant interests in renewable energy has spurred the industrial and academic research in this field. Proper utilization of biomass through gasification can increase the energy security and creates opportunities in the renewable energy sector.

Among many types of gasifiers, fluidized beds offer an excellent advantage over fixed bed gasifier in terms of scalability. On other hand, fixed beds are suited more for small-scale application. Through this simple mathematical and analytical model, a preliminary prediction of syngas composition, the design and basic sizing of a bubbling fluidized bed gasifier for saw dust were carried out. While using air as the gasifying agent, high amount of sensible energy is lost in heating the nitrogen from air. Although steam or oxygen gasification is possible, the cost associated with the process makes them economically unfeasible. Preventing heat losses from the gasifier by proper insulation can reduce air need to maintain the sustainable gasification temperature.

The yields of combustible gases tended to increase with increasing ER up to 0.25, which can be accounted for the enriched oxygen environment favoring the partial combustion of the carbonaceous materials. As ER is increased to greater than 0.25, the yield of these combustible gases is decreased, likely due to the oxidation of these gases to form CO_2 and H_2O. Generally, equivalence ratio plays an important role in determining the overall syngas quality. So, identifying and operating a gasifier in an optimal equivalence ratio can greatly increase the efficiency of the gasifier.

The effect of temperature has significant impact on overall gasification process. Higher temperature cannot be achieved without increasing equivalence ratio which in turn, maximizes quality of the syngas. Equilibrium temperature increases with increased ER up to a certain extent

or up to ER of 1.0. At ER > ~ 1.0, the effect of ER on equilibrium temperature is negligible, indicating that under these operating conditions the process tends to total combustion with excess air.

The type of biomass affects significantly the overall syngas composition and sometimes, also the operational issues in the biomass gasification plants. Even though, many pre-treatment processes exist to cure the biomass before feeding into the reactor, high ash content material is not desirable. High pressure gasification is very significant in decreasing the overall reactor size and increasing the quality of syngas from the gasifier. However, costs and maintenance problems can be a major issue to apply high pressure gasification process.

Tar content has remained one of the major issues in biomass gasification. Although primary or secondary tar treatment can be done to reduce the level of tar from the biomass gasifier, costs associated with the process must be considered. Increasing ER leads to a decrease in tar yield, leading to trace formation of tar at ER greater than 0.35.

In many literatures, the operating temperature for biomass gasification in fluidized bed gasifiers is in the range of 650 to 950^{o}C. But in this study, from the proposed model the operating temperature ranges of 592 to 985^{o}C is obtained. Interestingly, this temperature distribution agrees with most value ranges provided in many referenced literatures.

For the average composition of carbon, hydrogen, oxygen and ash in the saw dust, from the proposed model, the following syngas compositions with the corresponding amount of moisture content, operating temperature and equivalence ratio were obtained.

Table 6.1 Predicted syngas composition with the best quality

Inputs				**Outputs**						
%C	% H	% O	%Ash	H_2 (% vol.)	CO (% vol.)	CO_2 (% vol.)	CH_4 (% vol.)	Temp (^oC)	MC (%)	ER (-)
47.5	6.1	45.5	0.89	22.15	25.96	23.14	3.243	772	6.71	0.2478

So, the syngas with this composition have good quality and used for power generation and liquid-fuel synthesis. This is because the level of tar corresponding to the above optimum operating parameters is very small and its concentration is found to be 2mg/Nm^3.

6.2 Conclusions

This thesis describes a theoretical study on equilibrium modeling, its application in predicting syngas composition depending upon the change in various operating parameters. Although perfect chemical equilibrium conditions cannot be achieved in an actual gasification process, the proposed model generally predicts the syngas composition to a reasonable degree of accuracy. The effect of moisture content, equivalence ratio and temperature is also studied through this equilibrium model, which serves as an improvement tool in the field of gasifier design.

Additionally, basic design of the bubbling fluidized bed gasifier with easily available materials was successfully done to find the best quality syngas as a function of optimum operating parameters of the bubbling fluidized bed biomass gasifier. Though clear effect of one parameter alone could not be seen from the results, valuable information is provided about the syngas composition and temperature distribution inside the gasifier under variable operating conditions.

A discussion about tar content in syngas stream from the fluidized bed gasifier is important when it comes to the utilization of syngas for power generation and liquid-fuel synthesis from syngas. As expected, increasing the equivalence ratio generally led to decreased tar yield.

The comparison with results obtained from experimental tests of different literatures showed that the proposed model can be a useful tool when requiring a preliminary prediction of syngas

composition and the basic sizing of a fluidized bed gasifier. The successful result obtained from the proposed model stimulates the continuity of the research towards the development of this clean technology for the various agricultural residues and urban wastes in Ethiopia.

6.3 Recommendations

Future work should be done to develop a model that can accurately predict the syngas composition depending on the configuration setting of the gasifier. Steady-state modeling of the gasification process can be very useful for this purpose. With a steady-state model, the effect of secondary air which is automatically injected inside the gasifier can be more closely examined and validated. The steady state model can be also used to study the effect of external gas addition in greater detail and accuracy.

In a future work, it could be interesting to try to improve some of these models finding more empirical data for the composition of tar related to the temperature as well as other operating parameters, and to establish general equations from empirical data for the heating values of char and tar. It should be good to study the influence of other parameters such as the heating rate and the type of wood or biomass, to see if the temperature remains the main parameter. Thus, new models which include not only the temperature dependence should be built.

The major challenge of biomass gasification is related to the formation of tar with high amount. Although primary or secondary tar treatment is necessary to be done to reduce the level of tar from the biomass gasifier, costs associated with these process is very high. Hence, identification of cost-efficient tar removal techniques can be a major breakthrough in the field of biomass gasification and it is better to consider in future researches.

Finally, more species of biomass should be examined to evaluate the performance of the gasifier design and the characterization of tar and particulate impurities instead of using single feed stock.

References

[1] Gopal Gautam; Parametric Study of a Commercial-Scale Biomass Downdraft Gasifier: Experiments and Equilibrium Modeling, 2010

[2] G.W. Huber, K.Samolada, M.Vasalos, Synthesis of Transportation Fuels from Biomass: Chemistry, Catalysts, and Engineering, Chem Inform, 2006.

[3] R. Warnecke, Gasification of biomass: comparison of fixed bed and fluidized bed gasifier, Biomass and Bioenergy, 2000

http://www.tev.ntnu.no/MariaBarrio/publikasjoner/article%20gasifier.pdf

[4] A.V. Bridgewater, Renewable fuels and chemicals by thermal processing of biomass, Chemical Engineering Journal, (2003)

[5] P.C. Roy, A. Dutta, N. Chakra borty, Modelling of a downdraft biomass gasifier with finite rate kinetics in the reduction zone, International Journal of Energy Research, 2009.

[6] C.R. Altafini, P.R. Wander, R.M. Barretoa, Prediction of the working parameters of a wood waste gasifier through an equilibrium model, Energy Conversion and Management, 2003

[7] P.N. Sheth, B.V. Babu, Experimental studies on producer gas generation from wood waste in a downdraft biomass gasifier, Bioresource Technology, 2009.

[8] V. Skoulou, A. Zabaniotou, G. Stavropoulos, G. Sakelaropoulos, Syngas production from olive tree cuttings and olive kernels in a downdraft fixed-bed gasifier, International Journal of Hydrogen Energy, 2008

[9] J. Corella, J.M. Toledo, G. Molina, Calculation of the conditions to get less than 2 g tar/mn3 in a fluidized bed biomass gasifier, Fuel Processing Technology, 2006.

[10] A. van der Drift, Experimental fact-finding in CFB biomass gasification, Industrial & Engineering Chemistry Research, 2003.

[11] T. Riley, A novel biomass air gasification process for producing tar-free higher heating value fuel gas, Fuel Processing Technology, 2006.

[12] J. Saravanakumar, Effect of fuel properties on biomass combustion: Part I. Experiments--fuel type, equivalence ratio and particle size, Fuel, 2006.

[13] P.J. van den Enden, E.S. Lora, Design approach for a biomass fed fluidized bed gasifier using the simulation software CSFB, Biomass and Bioenergy, 2004.

[14] S.R.A. Kersten, W. Prins, Principles of a novel multistage circulating fluidized bed reactor for biomass gasification, Chemical Engineering Science, 2005.

[15] J. Wiman, A.E. Almstedt, Influence of pressure, fluidization velocity and particle size on the hydrodynamics of a freely bubbling fluidized bed, Chemical Engineering Science, 1998.

[16] I. Narvaez, J. Corella, A. Valin; Biomass gasification with air in an atmospheric bubbling fluidized bed. Effect of six operational variables on the quality of the produced raw gas, Industrial & Engineering Chemistry Research, 1996

http://www.carboconsult.com/fuel-compartment.asp

[17] Bridgewater AV. Computer modeling of fluidized bed gasifier. In: Ferrero GL, Maniatis K, Buekens A, eds. *Process and Gasification*. London, UK: Elsevier Applied Science; 1989.

[18] Watkinson AP. Biomass gasification in a circulating fluidized bed. *Biomass Bioenergy;* 2004

[19] S. Jarungthammachote, A. Dutta, Thermodynamic equilibrium model and second law analysis of a downdraft waste gasifier, Energy, 2007.

[20] A. Melger, J.F. Perez, H. Laget, A. Horillo, Thermo chemical equilibrium modeling of a gasifying process, Energy Conversion and Management, (59-67) 2007.

[21] J.M. Prins, Thermodynamic analysis of biomass gasification and torrefaction, in, Eindhoven University of Technology, 2005

[22] Bilodeau JF, The´rien N, Proulx P, Czernik S, Chornet E. A mathematical model of fluidized bed biomass gasification *Can J Chem Eng;* 1993.

[23] Kersten SRA. Biomass pyrolysis in a fluidized bed reactor. Part 1: Literature review and model simulations. *Ind Eng Chem Res;* 2005

[24] V.kumaran, Fluidized Bed Gasifier Design Report Public, (1-31) 2005

[25] Di Blasi C. Modeling of wood gasification in a countercurrent fixed-bed reactor AIChE J. 2004

[26]J. Ramírez, J.D. Martínez and S.L. Petro; Basic design of a fluidized bed gasifier for rice husk on a pilot scale, Latin American applied research, 299-306 (2007)

[27] Ramin Radmanesh, Jamal Chaouki, and Christophe Guy; Biomass Gasification in a Bubbling Fluidized Bed Reactor: Experiments and Modeling, Dept. of Chemical Engineering, 2006

[28] Wurzenberger JC. Thermal conversion of biomass: Comprehensive reactor and particle modeling. *AIChE J.* 2002.

[29] Bilbao R. Kinetics and modeling of gas formation in the thermal decomposition of powdery cellulose and pine sawdust. *Ind Eng Chem Res.* 1995

[30] Wolfinger MG, Tar cracking from fast pyrolysis of large beech wood particles. *J Anal Appl Pyrol*, 2002

http://www.btgworld.com/technologies/pyrolysis.html,

[31**]** *Howard W. Newton*, Fluidized-Bed Reactors Design, 3rd Edition, 1969

[32] Han, Kim. The reduction and control technology of tar during biomass gasification/pyrolysis: an overview. *Renewable Sustainable Energy Rev.;* 2008

[33] El-Rub, Bramer, G. Rapagna .Review of catalysts for tar elimination in biomass gasification processes. *Ind. Eng. Chem. Res.;* 2004

[34] Elizabeth Siemens Gusta, Tar elimination using dolomites during the gasification of pine sawdust, Chem. Eng'g University of Saskatchewan, 2008

[35] Ch. Charles, G. Sheba, Sc. Hurley, Y. Shao, Hanning, Catalytic Gasification of Pinewood Sawdust and Peat in a Pilot-scale Air-blown Fluidized Bed Gasifier,(1-8) 2009.

Appendix A

MATLAB Code for Syngas Equilibrium Modeling for Adiabatic Conditions

A.1 Main Program File

```
%MATLAB CODE FOR SYNGAS EQUILIBRIUM MODELING FOR ADIABATIC CONDITIONS
%THIS PROGRAM IS SET TO GIVE SYNGAS COMPOSITION IN DRY SYNGAS BASIS.IF FOR
%SOME REASON YOU WANT TO CHANGE, PLEASE MODIFY IN LINE 140 AND 141.
Format short
%disp ('elemental composition should be of the form [C, H, O, Ash]');
%ele_comp=input ('Enter elemental composition of biomass: ');
%disp ('Initial guess is of the form [H2 CO CO2 H2O CH4 3.76 N2] ')
xx0=[0.1,0.1,0.1,0.1,0.1,0.1]';
%%%%%%%%%%%%%%%%%%%%%%%%%%%%%%%%%%%%%%%%%%%%%%%%%%%%%%%%%%%%%%%%%%%%%%%%%%%%
%y=a*x1^4+b*x1^3+c*x1^2-d*x1-e;
ele_comp(1)=47.5;%Elemental composition of carbon in the feed stock
ele_comp(2)=6.11;%Elemental composition of hydrogen in the feed stock
ele_comp(3)=45.5;%Elemental composition of oxygen in the feed stock
Ash=0.89;        %Composition of ash in the feed stock (saw dust)
norm_1_C=ele_comp(1)/(12);%Normalization of carbon with its molecular mass
%Normalization of hydrogen with its molecular mass
norm_1_H=ele_comp(2)/(1.008);
norm_1_O=ele_comp(3)/(16); %Normalization of Oxygen with its molecular mass
X=norm_1_H/norm_1_C;       %Fraction of hydrogen wrt carbon
Y=norm_1_O/norm_1_C;       %Fraction of Oxygen wrt carbon
M_fs=25.0358;              %Mass flow rate of biomass kg/hr
ma=62.25;                  %Mass flow rate of air kg/hr
Mwa=137.28;                %Molecular mass of air kg/kmol
X2=ma/(4.76*Mwa);          %The amount of oxygen per kmol of biomass
m=0.061;                   %Moisture content
%T(1)=input('Enter the initial temperature(T(1)=');
T(1)=832;                 %The initial temperature
 rel=1; er=0.00001;iter=1;
 while (rel>er)
     i=iter;
```

```
    iter=iter+1;
%%%%%%%%%%%%%%%%%%%%%%%%%%%%%%%%%%%%%%%%%%%%%%%%%%%%%%%%%%%%%%%%%%%%%%%%%%%%
mw=((M_fs*m))/((18*(1-m))); %The amount of water per kmol of wood
T3=423.15;               %The assumed preheated air in let temperature in k
T5=298.15;               %Ambient temperature in k
T4=T3-T5;
%%%%%%%%%%%%%%%%%%%%%%%%%%%%%%%%%%%%%%%%%%%%%%%%%%%%%%%%%%%%%%%%%%%%%%%%%%%%
  k1(i)=(exp(7082.848/T(i)-6.567*log(T(i))+(7.466*10^(-3)/2)*T(i)- ...
    (2.164*10^(-6)/6)*T(i)^2+(0.701*10^(-5)/(2*(T(i)^2)))+32.541));
%%%%%%%%%%%%%%%%%%%%%%%%%%%%%%%%%%%%%%%%%%%%%%%%%%%%%%%%%%%%%%%%%%%%%%%%%%%%
k2(i)=exp((5870.53/T(i)+1.86*log(T(i))-2.7*10^(-4)*...
    T(i)-58200/(T(i)^2)-18.007));
%Substitute k1,k2,ER and mw values on the polynomial function and solve for
%%x1
ER=linspace(0,1,i); M_fs=12+X*1.008+Y*16;
for M=1:length(ER)
a(i)=8*k1(i).^2*k2(i);
b(i)=3*k1(i)*(2*k2(i)-1);
c(i)=k2(i)*k1(i)*(1.24-4*(1.025*ER(M)-mw));
d(i)=2*k2(i)*(mw+1.72);
e(i)=4*(1.54*1.025*ER(M)-2)*k2(i);
%p=a*x1^4+b*x1^3+c*x1^2-d*x1-e;
p=[a(i) b(i) c(i) d(i) e(i)];
r=roots(p);
y1=r';
if real(y1(1))>0 && imag(y1(1))==0
x1(i)=y1(1);
elseif  real(y1(2))>0 && imag(y1(2))==0
  x1(i)=y1(2);
elseif  real(y1(3))>0 && imag(y1(3))==0
    x1(i)=y1(3);
elseif  real(y1(4))>0 && imag(y1(4))==0
    x1(i)=y1(4);
else break;
end
x2(i)=-4*x1(i).^2*k1(i)-x1(i)+2.065-1.025*ER(M);
```

```
x3(i)=(3*x1(i)^2*k1(i)+x1(i)-2*1.025*ER(M)+2.065);
x4(i)=x1(i)+2*x2(i)+2*x3(i)-3*mw-1.235;
x5(i)=1.1025-x2(i)-x3(i);
Z=1:length(ER);
x6=[];
x6=[x6 1.025*ER(Z)];
%Then we have the following equation to determine the operating temperature
% Heat of formation of different compounds at 25 oC, kJ/kg mol
H_f_wood=-5111.12;H_f_H2O_g=-241.82;H_f_H2O_l=-285.830;H_f_CO2=-393.509;
H_vap=1000;H_f_CO=-110.525;H_f_CH4=-74.520;H_f_H2=0;H_f_O2=0;
H_f_N2=0;CP_O2=11.90;
%Specific heat capacity of different compounds as a function of temperature
%in (kJ/kg.K)
%%%%%%%%%%%%%%%%%%%%%%%%%%%%%%%%%%%%%%%%%%%%%%%%%%%%%%%%%%%%%%%%%%%%%%%%%%%
C1_H2O=32.24;C2_H2O=0.1923e-2;C3_H2O=1.055e-5;C4_H2O=-3.595e-9;
CP_H2O(i)=C1_H2O+C2_H2O*T(i)+C3_H2O*T(i)^2+C4_H2O*T(i)^3;
%%%%%%%%%%%%%%%%%%%%%%%%%%%%%%%%%%%%%%%%%%%%%%%%%%%%%%%%%%%%%%%%%%%%%%%%%%%
C1_H2=29.11;C2_H2=-0.1916e-2;C3_H2=0.4003e-5;C4_H2=-0.8704e-9;
CP_H2(i)=C1_H2+C2_H2*T(i)+C3_H2*T(i)^2+C4_H2*T(i)^3;
%%%%%%%%%%%%%%%%%%%%%%%%%%%%%%%%%%%%%%%%%%%%%%%%%%%%%%%%%%%%%%%%%%%%%%%%%%%
C1_CO=28.16;C2_CO=0.1675e-1;C3_CO=0.5372e-5;C4_CO=-2.222e-9;
CP_CO(i)=C1_CO+C2_CO*T(i)+C3_CO*T(i)^2+C4_CO*T(i)^3;
%%%%%%%%%%%%%%%%%%%%%%%%%%%%%%%%%%%%%%%%%%%%%%%%%%%%%%%%%%%%%%%%%%%%%%%%%%%
C1_CO2=22.26;C2_CO2=5.981e-2;C3_CO2=-3.501e-5;C4_CO2=-7.469e-9;
CP_CO2(i)=C1_CO2+C2_CO2*T(i)+C3_CO2*T(i)^2+C4_CO2*T(i)^3;
%%%%%%%%%%%%%%%%%%%%%%%%%%%%%%%%%%%%%%%%%%%%%%%%%%%%%%%%%%%%%%%%%%%%%%%%%%%
C1_CH4=19.89;C2_CH4=5.204e-2;C3_CH4=1.269e-5;C4_CH4=-11.01e-9;
CP_CH4(i)=C1_CH4+C2_CH4*T(i)+C3_CH4*T(i)^2+C4_CH4*T(i)^3;
%%%%%%%%%%%%%%%%%%%%%%%%%%%%%%%%%%%%%%%%%%%%%%%%%%%%%%%%%%%%%%%%%%%%%%%%%%%
C1_N2=28.90;C2_N2=-0.1571e-2;C3_N2=-0.8081e-5;C4_N2=-2.873e-9;
CP_N2(i)=C1_N2+C2_N2*T(i)+C3_N2*T(i)^2+C4_N2*T(i)^3;
%%%%%%%%%%%%%%%%%%%%%%%%%%%%%%%%%%%%%%%%%%%%%%%%%%%%%%%%%%%%%%%%%%%%%%%%%%%
T(i+1)=T(i)+(H_f_wood+mw*(H_f_H2O_l+H_vap)+H_f_O2+3.76*1.025*ER(M)*...
    H_f_N2+T4*(1.025*ER(M)*CP_O2+3.76*1.025*ER(M)*CP_N2(i))-x1(i)*...
    H_f_H2+x2(i)*H_f_CO+x3(i)*H_f_CO2+x4(i)*H_f_H2O_g+x5(i)*H_f_CH4)/...
  ((x1(i)*CP_H2(i)+x2(i)*CP_CO(i)+x3(i)*CP_CO2(i)+x4(i)*CP_H2O(i)+x5(i)*...
```

```
  CP_CH4(i)+3.76*1.025*ER(M)*CP_N2(i)));
end
    rel(i)=abs(T(i+1)-T(i))/abs(T(i+1));
    T(i)=T(i+1);
    T1=(T-273.15);
 end
sol_final=[];
sol_temp=[x1;x2;x3;x4;x5;x6];
%%%%%%%%%%%%%%%%%%Continued below%%%%%%%%%%%%%%%%%%%%%%%%%%%%%%%%%%%%%%%%%%%%
sol_final=[sol_final sol_temp];
%%%%%%%%%%%%%%%%%%%%%%%%%%%%%%%%%%%%%%%%%%%%%%%%%%%%%%%%%%%%%%%%%%%%%%%%%%%%%%%
M_fs=12+X*1.008+Y*16;
Er=[];
for E=1:length(ER)
Er=[Er ((ma)*1.5*4.76*1.025*ER(E)*100/(M_fs))/((8.89*ele_comp(1))+(26.5*...
    ele_comp(2))+(3.3*ele_comp(3)))];
end
%%%%%%%%%%%%%%%%%%%%%%%%%%%%%%%%%%%%%%%%%%%%%%%%%%%%%%%%%%%%%%%%%%%%%%%%%%%%%%%
%multiplying ER with 3.76 to get correct N2 mols
p=length(ER);frac_N2=[];
for l=1:p
frac_N2=[frac_N2 sol_final(6,l)*3.76];
end
final_comp=[sol_final(1:5,1:p);frac_N2];
%%%%%%%%%%%%%%%%%%%%%%%%%%%%%%%%%%%%%%%%%%%%%%%%%%%%%%%%%%%%%%%%%%%%%%%%%%%%%%%
your_rep=input('Do you want to find syngas composition in dry syngas
basis(y/n): ','s');
your_rep='y';
if your_rep=='n';
%finding total amount of product gas for each moisture contents
total_frac_m=[];
for n=1:p
total_frac_m=[total_frac_m sum(final_comp(1:6,n))];
end
total_frac_m; %sum of all product gases
else
```

```
%%%%%%%%%%%%%%%%%%%%%%%%%%%%%%%%%%%%%%%%%%%%%%%%%%%%%%%%%%%%%%%%%%%%%%%%%%%%%%%
%finding total amount of product gas on dry basis for each moisture contents
dry_final_comp=final_comp;
dry_final_comp(4,:)=[];
total_frac_m=[];
for n=1:p
total_frac_m=[total_frac_m sum(dry_final_comp(1:5,n))];
end
total_frac_m;
final_comp=dry_final_comp;
end
%%%%%%%%%%%%%%%%%%%%%%%%%%%%%%%%%%%%%%%%%%%%%%%%%%%%%%%%%%%%%%%%%%%%%%%%%%%%%%%
%expressing all the components in molar fraction or volumetric fraction
final_frac_comp=[];
for MM=1:length(total_frac_m)
final_frac_m=[];
if your_rep=='y'
l_in=length(xx0)-1;
else
l_in=length(xx0);
end
for NN=1:l_in
final_frac_m=[final_frac_m;final_comp(NN,MM)/total_frac_m(MM)];
end
final_frac_comp=[final_frac_comp final_frac_m];
end
for j=1:length(T1)-1
    T2(j)=T1(j);
end
x=final_frac_comp'*100;Z=T2';
H2=final_frac_comp(1,:);    %volumetric fraction of Hydrogen
CO=final_frac_comp(2,:);    %volumetric fraction of Carbon monoxide
CO2=final_frac_comp(3,:);   %volumetric fraction of Carbon dioxide
CH4=final_frac_comp(4,:);   %volumetric fraction of Methane
N2=final_frac_comp(5,:);    %volumetric fraction of Nitrogen
```

```
HHVH2=12.76;                %HHV of Hydrogen in MJ/m3
HHVCO=12.6;                 %HHV of Carbon monoxide in MJ/m3
HHVCH4=39.8;                %HHV of Methane in MJ/m3
%HHV of the biomass was calculated by using results from ultimate analysis.
HHV_biomass = 33823*ele_comp(1)+144249*...
    ((8*ele_comp(2)-ele_comp(3))/8)+9418*S; %HHV of biomass kJ/kg
LHV_syngas=0.1263*CO+0.358*CH4+0.1079*H2;   %LHV of syngas MJ/m3
%The volumetric content of syngas constituents multiplied by their
%individual higher heating value (HHV) gave the overall higher heating
HHV_syngas =(H2*HHVH2+CO*HHVCO+CH4*HHVCH4);%HHVsyngas is the heating value of
syngas
den_air=1.171;     %Density of air Kg/m3
Uf=0.34;           %Fluidization velocity during the gasification in m/s
A=0.12566;         %Cross-sectional area of the reactor in m2
Tb=T2+47;          %The bubbling temperature
d=Tb-T2;c=Tb.^4-T2.^4;
dp=0.08505*10^-3;      %Diameter of the bubbling particle
d_fs=578*10^-6;        %Diameter of the saw dust particle
ds=385*10^-6;          %Diameter of the sand particle
Cp =1112.0+4.85*(T2-273.15);%Wood specific heat in J/(kg.K)
des_par=2650;              %Density of the sand particle kg/m3
dens_gas=0.353;            %Density of the gas kg/m3
mue=7.45e-3;               %Dynamic viscosity of wood particle [kg/ms]
Kw=0.065;                  %Thermal conductivity of wood particle [W/m K]
Pr=mue.*Cp/Kw;             %prandtl number
Re=5.7;                    %Rayleigh Number
h_conv=(2+0.6*Re^0.5 *Pr.^(1/3))/dp;%The convection heat transfer coefficient
Den_w=360;                          %Density of the wood in kg/m3
Ep=0.95;                            %Emissivity for wood particles
E_fb=0.8;                           %Effective emissivity
np=5.0;
t=linspace(0,1,71);                 %Elapsed time in second
for G=1:length(t)
    t_g=1*t(G);                     %Time step in second
end
Sigma=5.67*10^ (-8);            %Stephan–Boltzmann constant in W/(m^2 K^4)
```

```
Vp=1.02*10^2;                    %The volume of the particle in mm^3
q=(1+np*ds/d_fs)^2;
E_rad = 1/Ep +1/(q*(1/E_fb -1)); %Radiative heat transfer coefficient
 Hi=((h_conv*A.*(d)).*t_g./(Den_w.*Cp)+ ...
    (sigma*E_rad*A.*(c)).*t_g./(Den_w.*Cp))*100;
%Rate of heat transfer kJ/kg of feed stock
T6=5.6./(((h_conv*A.*(d)).*t_g./(Den_w.*Cp.*Vp)+ ...
    (sigma*E_rad*A.*(c)).*t_g./(Den_w.*Cp.*Vp)));
%%%%%%%%%%%%%%%%%%%%%%%%%%%%%%%%%%%%%%%%%%%%%%%%%%%%%%%%%%%%%%%%%%%%%%%%%%%%
%%%%%%%%%%%%%%%%%%%%%%Plots of different parameters%%%%%%%%%%%%%%%%%%%%%%
   plot(T2,H2,'b-',T2,CO,'k-',T2,CO2,'k-*',T2,CH4,'r-',T2,N2,'g-
','linewidth',3)
   xlabel('OPERATING TEMPERATURE (degree celicius)')
   ylabel('FRACTIONAL COMPOSITION OF SYNGAS (mol)')
   title('EFFECT OF OPERATING TEMPERATURE ON SYN GAS COMPOSITION')
   legend('H2','CO','CO2','CH4','N2')
  gtext('H2');gtext('CO');gtext('CO2');gtext('CH4');gtext('N2');
   grid on
   pause
clf
plot(Er,H2,'b-',Er,CO,'k-',Er,CO2,'k-*',Er,CH4,'r-',Er,N2,'g-','linewidth',3)
xlabel('EQUIVALENCE RATIO')
ylabel('FRACTIONAL COMPOSITION 0F SYNGAS (mol)')
title('EFFECT OF EQUIVALENCE RATIO ON SYN GAS COMPOSITION')
legend('H2','CO','CO2','CH4','N2')
gtext('H2');gtext('CO');gtext('CO2');gtext('CH4');gtext('N2');
grid on
  pause
clf
   plot(Er,T2,'k-','linewidth',3)
   xlabel('EQUIVALENCE RATIO')
   ylabel('OPERATING TEMPERATURE (degree celicius)')
   title('EFFECT OF EQUIVALENCE RATIO ON OPERATING TEMPERATURE')
   grid on
    pause
 clf
```

```
plot(M_Cont,H2,'b-',M_Cont,CO,'k-',M_Cont,CO2,'k-*',M_Cont,CH4,'r
',M_Cont,N2,'g-','linewidth',3)
   xlabel('MOISTURE CONTENT (% wet basis)')
   ylabel('FRACTIONAL COMPOSITION OF SYNGAS (mol)')
   title('EFFECT OF MOISTURE CONTENT ON SYN GAS COMPOSITION')
   legend('H2','CO','CO2','CH4','N2')
   gtext('H2');gtext('CO');gtext('CO2');gtext('CH4');gtext('N2');
   grid on
    pause
clf
   plot(Er,HHV_syngas ,'linewidth',3)
   xlabel('EQUIVALENCE RATIO')
   ylabel('HIGHER HEATING VALUE OF SYNGAS MJ/m3')
   title('EFFECT OF EQUIVALENCE ON HIGHER HEATING VALUE OF SYN GAS')
   legend('HHV syngas')
   grid on
   pause
clf
   plot(t,T6,'k-*','linewidth',3)
   xlabel('Time (sec)')
   ylabel('Temperature (°C)')
   title('RATE OF HEAT TRANSFER BY CONVECTION AND RADIATION MODE')
   legend('Heat transfer by conv and rad mode')
   grid on
 %END OF THE PROGRAM
```

Appendix B

Syngas Composition from MATLAB Simulation

Table B.1 Syngas Composition with their respective, Operating Temperature, Moisture Content and Equivalence Ratio from MATLAB Simulation

Operating Temp (^oC)	***H_2 (% vol.)***	***CO (% vol.)***	***CO_2 (% vol.)***	***CH_4 (% vol.)***	***N_2 (% vol.)***	***Moisture Content (%)***	***ER (-)***
592.0848	57.4600	1.8897	28.0872	12.5631	0	0	0
623.0241	47.3770	12.0635	28.0558	9.0819	3.4219	1.0166	0.0354
652.0188	40.6099	18.3650	27.5567	6.8901	6.5784	2.0127	0.0708
679.2636	36.0131	22.0920	26.8641	5.5016	9.5293	2.9889	0.1062
704.8669	32.7841	24.2033	26.1131	4.5977	12.3018	3.9459	0.1416
728.8955	30.4160	25.3218	25.3626	3.9868	14.9128	4.8842	0.1770
751.3973	28.6011	25.8306	24.6362	3.5570	17.3752	5.8043	0.2124
772.4138	27.1525	25.9621	23.9421	3.2426	19.7007	6.7068	0.2478
791.9854	25.9549	25.8586	23.2825	3.0040	21.9000	7.5922	0.2832
810.1550	24.9357	25.6082	22.6568	2.8166	23.9827	8.4609	0.3186
826.9693	24.0474	25.2666	22.0633	2.6651	25.9576	9.3135	0.3540
842.4793	23.2584	24.8696	21.5001	2.5393	27.8327	10.1503	0.3894
856.7399	22.5470	24.4403	20.9650	2.4324	29.6153	10.9718	0.4248
869.8102	21.8979	23.9941	20.4561	2.3399	31.3121	11.7784	0.4602
881.7521	21.2999	23.5412	19.9716	2.2584	32.9290	12.5706	0.4956
892.6302	20.7448	23.0883	19.5097	2.1857	34.4716	13.3486	0.5309
902.5105	20.2263	22.6400	19.0689	2.1200	35.9448	14.1129	0.5663
911.4594	19.7396	22.1994	18.6477	2.0601	37.3532	14.8639	0.6017
919.5435	19.2809	21.7682	18.2449	2.0050	38.7010	15.6018	0.6371
926.8282	18.8469	21.3478	17.8593	1.9540	39.9920	16.3271	0.6725
933.3773	18.4352	20.9388	17.4898	1.9064	41.2297	17.0400	0.7079
939.2523	18.0437	20.5417	17.1354	1.8620	42.4174	17.7408	0.7433

944.5120	17.6704	20.1564	16.7951	1.8201	43.5580	18.4299	0.7787
949.2121	17.3140	19.7830	16.4682	1.7806	44.6542	19.1076	0.8141
953.4050	16.9730	19.4213	16.1538	1.7432	45.7087	19.7740	0.8495
957.1398	16.6463	19.0710	15.8512	1.7077	46.7237	20.4296	0.8849
960.4616	16.3329	18.7319	15.5599	1.6739	47.7015	21.0746	0.9203
963.4125	16.0319	18.4035	15.2791	1.6416	48.6440	21.7092	0.9557
966.0308	15.7424	18.0855	15.0083	1.6108	49.5531	22.3337	0.9911
968.3516	15.4637	17.7776	14.7469	1.5813	50.4305	22.9483	1.0265
970.4067	15.1952	17.4793	14.4946	1.5530	51.2780	23.5532	1.0619
972.2251	14.9362	17.1904	14.2507	1.5258	52.0969	24.1487	1.0973
973.8328	14.6863	16.9104	14.0149	1.4996	52.8888	24.7350	1.1327
975.2532	14.4449	16.6389	13.7869	1.4744	53.6549	25.3123	1.1681
976.5075	14.2115	16.3757	13.5661	1.4501	54.3965	25.8809	1.2035
977.6145	13.9858	16.1205	13.3524	1.4267	55.1147	26.4408	1.2389
978.5910	13.7673	15.8728	13.1452	1.4041	55.8106	26.9923	1.2743
979.4520	13.5557	15.6324	12.9444	1.3822	56.4853	27.5357	1.3097
980.2110	13.3506	15.3990	12.7497	1.3610	57.1397	28.0710	1.3451
980.8797	13.1517	15.1723	12.5607	1.3405	57.7747	28.5984	1.3805
981.4688	12.9588	14.9521	12.3773	1.3207	58.3911	29.1182	1.4159
981.9876	12.7716	14.7380	12.1992	1.3014	58.9898	29.6304	1.4513
982.4444	12.5897	14.5299	12.0261	1.2828	59.5716	30.1353	1.4867
982.8464	12.4131	14.3275	11.8578	1.2646	60.1370	30.6331	1.5221
983.2003	12.2413	14.1305	11.6943	1.2470	60.6868	31.1237	1.5574
983.5118	12.0743	13.9389	11.5351	1.2299	61.2217	31.6075	1.5928
983.7858	11.9119	13.7523	11.3803	1.2133	61.7422	32.0845	1.6282
984.0268	11.7538	13.5706	11.2295	1.1971	62.2489	32.5550	1.6636
984.2389	11.5999	13.3936	11.0827	1.1814	62.7424	33.0189	1.6990
984.4254	11.4499	13.2212	10.9397	1.1661	63.2231	33.4765	1.7344
984.5895	11.3039	13.0530	10.8003	1.1512	63.6916	33.9279	1.7698
984.7337	11.1615	12.8891	10.6645	1.1366	64.1483	34.3732	1.8052

984.8606	11.0227	12.7292	10.5320	1.1224	64.5937	34.8126	1.8406
984.9722	10.8873	12.5732	10.4027	1.1086	65.0281	35.2461	1.8760
985.0703	10.7552	12.4210	10.2766	1.0952	65.4520	35.6739	1.9114
985.1565	10.6263	12.2724	10.1536	1.0820	65.8657	36.0961	1.9468
985.2324	10.5005	12.1273	10.0334	1.0692	66.2697	36.5127	1.9822
985.2991	10.3776	11.9855	9.9160	1.0566	66.6642	36.9240	2.0176
985.3577	10.2575	11.8471	9.8014	1.0444	67.0496	37.3299	2.0530
985.4092	10.1403	11.7118	9.6894	1.0325	67.4261	37.7307	2.0884
985.4545	10.0256	11.5795	9.5799	1.0208	67.7942	38.1264	2.1238
985.4944	9.9136	11.4502	9.4729	1.0094	68.1540	38.5171	2.1592
985.5294	9.8040	11.3237	9.3682	0.9982	68.5059	38.9029	2.1946
985.5602	9.6968	11.2000	9.2658	0.9873	68.8501	39.2839	2.2300
985.5872	9.5919	11.0790	9.1656	0.9766	69.1868	39.6601	2.2654
985.6110	9.4893	10.9605	9.0676	0.9661	69.5164	40.0317	2.3008
985.6319	9.3889	10.8446	8.9717	0.9559	69.8389	40.3988	2.3362
985.6503	9.2906	10.7311	8.8777	0.9459	70.1548	40.7614	2.3716
985.6665	9.1943	10.6199	8.7857	0.9361	70.4640	41.1196	2.4070
985.6807	9.1000	10.5110	8.6956	0.9265	70.7669	41.4735	2.4424
985.6931	9.0076	10.4043	8.6073	0.9171	71.0637	41.8232	2.4778

Appendix C

Program to Determine the Composition of Tar and Char

```
%Program to determine the composition of tar and char wrt equivalence ratio
ele_comp(1)=47.5;  %Elemental composition of carbon in the feed stock
ele_comp(2)=6.11;  %Elemental composition of hydrogen in the feed stock
ele_comp(3)=45.5;  %Elemental composition of oxygen in the feed stock
Ash=0.89;          %Composition of ash in the feed stock
norm_1_C=ele_comp(1)/(12); %Normalization of carbon with its molecular mass
%Normalization of hydrogen with its molecular mass
norm_1_H=ele_comp(2)/(1.008);
norm_1_O=ele_comp(3)/(16); %Normalization of Oxygen with its molecular mass
X=norm_1_H/norm_1_C; Y=norm_1_O/norm_1_C;
M_fs=25.0358;              %Mass flow rate of biomass kg/hr
ma=62.25;                  %Mass flow rate of air kg/hr
Mwa=137.28;                %Molecular mass of air kg/kmol
X2=ma/(4.76*Mwa);          %The amount of oxygen per kmol of biomass
m=0.061;                   %Moisture content
%T(1)=input('Enter the initial temperature(T(1)=');
T(1)=832;
 rel=1;
 er=0.00001;
 iter=1;
 while (rel>er)
     i=iter;
    iter=iter+1;
mw=((M_fs*m))/((18*(1-m)));%The amount of water per kmol of wood
T3=423.15;         %The assumed preheated air in let temperature in k
T5=298.15;         %Ambient temperature in k
T4=T3-T5;
 k1(i)=(exp(7082.848/T(i)-6.567*log(T(i))+(7.466*10^(-3)/2)*T(i)- ...
    (2.164*10^(-6)/6)*T(i)^2+(0.701*10^(-5)/(2*(T(i)^2)))+32.541));
 k2(i)=exp((5870.53/T(i)+1.86*log(T(i))-2.7*10^(-4)*...
    T(i)-58200/(T(i)^2)-18.007));
%Substitute k1, k2, ER and mw values on the polynomial function
```

```
%and solve for x1
ER=linspace(0,1,i);        %%Equivalence ratio
M_fs=12+X*1.008+Y*16;      %Mass flow rate of feed stock (kg/hr)
for M=1:length(ER)
a(i)=8*k1(i).^2*k2(i);
b(i)=3*k1(i)*(2*k2(i)-1);
c(i)=k2(i)*k1(i)*(1.24-4*(1.025*ER(M)-mw));
d(i)=2*k2(i)*(mw+1.72);
e(i)=4*(1.54*1.025*ER(M)-2)*k2(i);
%p=a*x1^4+b*x1^3+c*x1^2-d*x1-e;
p=[a(i) b(i) c(i) d(i) e(i)];
y1=roots(p);
if y1(1,:)>0
x1(i)=y1(1,:);
end
if y1(2,:)>0
  x1(i)=y1(2,:);
end
if y1(3,:)>0
    x1(i)=y1(3,:);
end
if y1(4,:)>0
    x1(i)=y1(4,:);
else
   break
end
if x1(i)>0
x2(i)=-4*x1(i).^2*k1(i)-x1(i)+2.065-1.025*ER(M);
x3(i)=(3*x1(i)^2*k1(i)+x1(i)-2*1.025*ER(M)+2.065);
x4(i)=x1(i)+2*x2(i)+2*x3(i)-3*mw-1.235;
x5(i)=1.1025-x2(i)-x3(i);
else
   break
end
Z=1:length(ER);
x6=[];
```

```
x6=[x6 1.025*ER(Z)];
%Then we have the following equation to determine the operating temperature
% Heat of formation of different compounds at 25 oC, kJ/kg mol
H_f_wood=-5111.12; H_f_H2O_g=-241.82; H_f_H2O_l=-285.830;H_f_CO2=-393.509;
H_vap=1000;H_f_CO=-110.525;H_f_CH4=-74.520;H_f_H2=0;H_f_O2=0;
H_f_N2=0;CP_O2=11.90;
%Specific heat capacity of different compounds as a function of temperature
%in (kJ/kg.K)
C1_H2O=32.24;C2_H2O=0.1923e-2;C3_H2O=1.055e-5;C4_H2O=-3.595e-9;
CP_H2O(i)=C1_H2O+C2_H2O*T(i)+C3_H2O*T(i)^2+C4_H2O*T(i)^3;
%%%%%%%%%%%%%%%%%%%%%%%%%%%%%%%%%%%%%%%%%%%%%%%%%%%%%%%%%%%%%%%%%%%%%%%%%%%
C1_H2=29.11;C2_H2=-0.1916e-2;C3_H2=0.4003e-5;C4_H2=-0.8704e-9;
CP_H2(i)=C1_H2+C2_H2*T(i)+C3_H2*T(i)^2+C4_H2*T(i)^3;
%%%%%%%%%%%%%%%%%%%%%%%%%%%%%%%%%%%%%%%%%%%%%%%%%%%%%%%%%%%%%%%%%%%%%%%%%%%
C1_CO=28.16;C2_CO=0.1675e-1;C3_CO=0.5372e-5;C4_CO=-2.222e-9;
CP_CO(i)=C1_CO+C2_CO*T(i)+C3_CO*T(i)^2+C4_CO*T(i)^3;
%%%%%%%%%%%%%%%%%%%%%%%%%%%%%%%%%%%%%%%%%%%%%%%%%%%%%%%%%%%%%%%%%%%%%%%%%%%
C1_CO2=22.26;C2_CO2=5.981e-2;C3_CO2=-3.501e-5;C4_CO2=-7.469e-9;
CP_CO2(i)=C1_CO2+C2_CO2*T(i)+C3_CO2*T(i)^2+C4_CO2*T(i)^3;
%%%%%%%%%%%%%%%%%%%%%%%%%%%%%%%%%%%%%%%%%%%%%%%%%%%%%%%%%%%%%%%%%%%%%%%%%%%
C1_CH4=19.89;C2_CH4=5.204e-2;C3_CH4=1.269e-5;C4_CH4=-11.01e-9;
CP_CH4(i)=C1_CH4+C2_CH4*T(i)+C3_CH4*T(i)^2+C4_CH4*T(i)^3;
%%%%%%%%%%%%%%%%%%%%%%%%%%%%%%%%%%%%%%%%%%%%%%%%%%%%%%%%%%%%%%%%%%%%%%%%%%%
C1_N2=28.90;C2_N2=-0.1571e-2;C3_N2=-0.8081e-5;C4_N2=-2.873e-9;
CP_N2(i)=C1_N2+C2_N2*T(i)+C3_N2*T(i)^2+C4_N2*T(i)^3;
%%%%%%%%%%%%%%%%%%%%%%%%%%%%%%%%%%%%%%%%%%%%%%%%%%%%%%%%%%%%%%%%%%%%%%%%%%%
T(i+1)=T(i)+(H_f_wood+mw*(H_f_H2O_l+H_vap)+H_f_O2+3.76*...
    1.025*ER(M)*H_f_N2+T4*(1.025*ER(M)*CP_O2+3.76*1.025*ER(M)*CP_N2(i))- ...
x1(i)*H_f_H2+x2(i)*H_f_CO+x3(i)*H_f_CO2+x4(i)*H_f_H2O_g+x5(i)*H_f_CH4)/...
  ((x1(i)*CP_H2(i)+x2(i)*CP_CO(i)+x3(i)*CP_CO2(i)+x4(i)*CP_H2O(i)+x5(i)*...
  CP_CH4(i)+3.76*1.025*ER(M)*CP_N2(i)));
end
    rel(i)=abs(T(i+1)-T(i))/abs(T(i+1));
    T(i)=T(i+1);
 end
T2=(T-273.15);                          %The operating temperature in ºC
```

```
Z=((T2+273.15)-833)/160;                %Z is a dimensionless temperature
Ytar=-2.8025./(1-1112.345*exp(-(912*0.08*...
    (T2-273.15))))+45.69*exp(-Z);        %Composition of tar in the syn gas
C_tar=54.5./(1+exp(-54.5*0.0024.*(T-273.15)));%Composition of C in the tar
H_tar=6.5.*exp(-0.0077*(T-273.15));          %Composition of H in the tar
O_tar=39.*exp (-0.0012*(T-273.15));          %Composition of O in the tar
Ychar=5./(1-1.25*exp(-(5*0.0002*...
    (T2-273.15))));                      %composition of char in the syn gas
C_char=98./(1+exp(-98*0.00035*(T2-273)));%composition of Carbon in the char
H_char=53.*exp(-0.00177*(T2-273));       %composition of Hydrogen in the char
O_char=25.*exp(-0.0027*(T2-273));        %composition of oxygen in the char
   plot(ER, Ytar(1:71),'k-',ER, Ychar(1:71),'b-','linewidth',3)
   xlabel('EQUIVALENCE RATIO')
   ylabel('RATE OF TAR CRACKING AND COMBUSTION IN kg/(m^3 s)')
   title('EFFECT OF EQUIVALENCE RATIO ON COMPOSITION OF TAR AND CHAR')
legend('Ytar', 'Ychar')
   grid on
   %End of the program
```

Appendix D

Workshop and Assembly Drawing of the Fluidized Bed Biomass Gasifier

In chapter four, the basic design of the bubbling fluidized bed gasifier which includes the mathematical analysis with some systematical sketches and supporting diagrams are performed.

But the workshop and the complete assembly drawing of the system as a whole are described in appendix D and shown below.